

12-1-2014

New early Miocene 40Ar/39Ar ages for Nakwai, northwest Kenya, Africa, and Paleontological analysis of Meroehyrax kyongoi dentition

Dawn Elena Reynoso
University of Nevada, Las Vegas, pape@unlv.nevada.edu

Follow this and additional works at: <https://digitalscholarship.unlv.edu/thesesdissertations>



Part of the [Geochemistry Commons](#), [Geology Commons](#), and the [Paleontology Commons](#)

Repository Citation

Reynoso, Dawn Elena, "New early Miocene 40Ar/39Ar ages for Nakwai, northwest Kenya, Africa, and Paleontological analysis of Meroehyrax kyongoi dentition" (2014). *UNLV Theses, Dissertations, Professional Papers, and Capstones*. 2290.

<https://digitalscholarship.unlv.edu/thesesdissertations/2290>

This Thesis is protected by copyright and/or related rights. It has been brought to you by Digital Scholarship@UNLV with permission from the rights-holder(s). You are free to use this Thesis in any way that is permitted by the copyright and related rights legislation that applies to your use. For other uses you need to obtain permission from the rights-holder(s) directly, unless additional rights are indicated by a Creative Commons license in the record and/or on the work itself.

This Thesis has been accepted for inclusion in UNLV Theses, Dissertations, Professional Papers, and Capstones by an authorized administrator of Digital Scholarship@UNLV. For more information, please contact digitalscholarship@unlv.edu.

NEW EARLY MIOCENE $^{40}\text{AR}/^{39}\text{AR}$ AGES FOR NAKWAI, NORTHWEST KENYA, AFRICA, AND
PALEONTOLOGICAL ANALYSIS OF *MEROËHYRAX KYONGOI* DENTITION

by

Dawn E. Reynoso

Bachelor of Science in Earth Science
University of Nevada, Las Vegas
2011

A thesis submitted in partial fulfillment
of the requirements for the

Master of Science - Geoscience

Department of Geoscience
College of Sciences
The Graduate College

University of Nevada, Las Vegas
December 2014

Copyright by Dawn E. Reynoso, 2015

All Rights Reserved

We recommend the thesis prepared under our supervision by

Dawn Elena Reynoso

entitled

**New Early Miocene 40AR/39AR Ages for Nakwai, Northwest Kenya,
Africa and Paleontological Analysis of Meroehyrax Kyongoi Dentition**

is approved in partial fulfillment of the requirements for the degree of

Master of Science - Geoscience

Department of Geoscience

Terry L. Spell, Ph.D., Committee Chair

Stephen M. Rowland, Ph.D., Committee Member

John W. Kappelman, Ph.D., Committee Member

Brett R. Riddle, Ph.D., Graduate College Representative

Kathryn Hausbeck Korgan, Ph.D., Interim Dean of the Graduate College

December 2014

ABSTRACT

New Early Miocene $^{40}\text{Ar}/^{39}\text{Ar}$ ages for Nakwai, northwest Kenya, Africa, and Paleontological

Analysis of *Meroëhyrax kyongoi* dentition

by

Dawn E. Reynoso

Dr. Terry L. Spell, Committee Chair
Associate Professor of Geology
University of Nevada, Las Vegas

Nakwai is a fossiliferous region in the Turkana Basin of northwestern Kenya. Until recently the only ages for the Nakwai formation were based on biostratigraphic correlation with Losodok; a late Oligocene site located to the north of Nakwai. The new $^{40}\text{Ar}/^{39}\text{Ar}$ ages in this study range from 23 Ma to 15 Ma and constrain the upper portions of the Nakwai section to the early Miocene. These ages make it the only securely dated fossil locality in the region that represents the earliest Miocene; all of the other early Miocene fossil localities date back to ~20 Ma or younger. The time period following the Oligocene – Miocene boundary is crucial for understanding the dynamics and timing of the great faunal transition that happened between the endemic fauna of island Afro-Arabia as it made contact with Eurasia and brought many of the animals into Africa that we associate with the continent today. These new dates help constrain the timing of this transitional event, which was previously thought to have been at, or near the Oligocene – Miocene boundary.

Hyracoidea is a group of mammals native to Africa, which were very diverse throughout the early Cenozoic. During the late Oligocene and early Miocene some species of hyracoid appear to be developing hypsodont and selenodont features in their cheek teeth. Dental features such as hypsodonty were long thought to have evolved in response to an increase in

silica-rich C4 grasses. However, in Africa these grasses did not arrive until the Late Miocene. The species *Meroëhyrax kyongoi*, which has been recovered from Nakwai, is a member of the Pliohyracidae family; which has been described as having these dental features. Dental measurements from *Meroëhyrax kyongoi* along with two younger species of Pliohyracidae were compared to try to assess the changes in these features through time. The degree of hypsodonty was also established within these taxa by determining a Hypsodonty Index (HI) for each specimen. These dental data suggest that, although tooth size does increase through time, the degree of hypsodonty remains relatively constant. When compared to other hypsodont herbivores, the HI of these hyracoids does not indicate true hypsodonty.

ACKNOWLEDGMENTS

I have many people that I would like to thank for their help along the way but first and foremost I would like to thank Dr. Terry L. Spell, my advisor and committee chair, for his guidance, and never ending understanding and support. I knew throughout the process that no matter what was happening he would be there to back me up or to offer me advice and I could not have asked for a better advisor. Funding for this project was largely provided by the Nevada Isotope Geochronology Laboratory (NIGL), without which I know this project would not have been possible, and I am extremely grateful. I would also like to thank the UNLV Geoscience Department for the Bernada French Scholarship and the Edwards & Olswang Geology Scholarship. I am grateful to the UNLV Graduate College for the UNLV Graduate Access Grant and the Patricia J. Sastaunik Graduate Scholarship.

I would like to thank the rest of my committee members: Dr. Steve Rowland for being a great teacher and for having an enthusiasm for knowledge that is extremely contagious, Dr. John Kappelman for talking me and my advisor onto the project and being a fantastic guide while in the field, and Dr. Brett Riddle for introducing me to the world of mammalogy and challenging me to look at things from another perspective. I would especially like to thank Dr. Tab D. Rasmussen for allowing me and Dr. Spell to join his team of researchers, for giving me a paleontological project in addition to the isotopic dating project, and for teaching me everything I needed to know about hyrax teeth even though he was under the weather. I want to thank Kathy Zanetti for her help and guidance in the NIGL lab with the processing, packaging, and analyzing of my samples. I greatly appreciate Dr. Josh Bonde for being such a great friend and mentor; I know I can always count on him if I have a question or if I just need to pass some time. I would also like to say thank you to Dr. Tony Friscia for being a great help while in the field and for always being willing to answer my questions. Of course without my family's support I'm not

sure what I would do; thank you to my beautiful daughter Megan, and my husband Jason, my dad Steve Pape and his wife Lisa, my mom Lori Foell, my Aunt Kathy, and everyone one else who has been behind me for this process.

I also owe a huge amount of thanks to the following people for their help in the field, at school, in the lab, in the office, and for their moral support: Dr. Aubrey Bonde, Kati Gibler, Dr. Ellen Miller, Dr. Neil Tabor, Dr. Elizabeth Gierlowski-Kordesch, Dr. Rod Metcalf, Dr. Pamela Burnley, Dr. Michael Wells, all of my fantastic professors, fellow members of the Dead Lizard Society, all of my fellow Geoscience Department students, the office staff including Liz Smith and Maria Figueroa (who takes such great care of all of us in the Geoscience Department), and our Kenyan field companions Samuel, Mathwe, Francis, Joseph, Nicholas, Victoria, Bonaventure and Boniface.

TABLE OF CONTENTS

ABSTRACT.....	i
ACKNOWLEDGMENTS.....	v
LIST OF TABLES.....	viii
LIST OF FIGURES.....	ix
CHAPTER 1 INTRODUCTION.....	1
CHAPTER 2 BACKGROUND.....	6
GEOLOGIC SETTING.....	6
PREVIOUS WORK.....	7
CHAPTER 3 METHODS.....	10
⁴⁰ AR/ ³⁹ AR DATING.....	10
PALEONTOLOGICAL METHODS.....	14
CHAPTER 4 RESULTS.....	17
⁴⁰ AR/ ³⁹ AR DATING.....	17
PALEONTOLOGY.....	33
CHAPTER 5 DISCUSSION.....	45
CHAPTER 6 CONCLUSIONS.....	52
APPENDIX A ⁴⁰ AR/ ³⁹ AR DATA TABLES.....	54
APPENDIX B PALEONTOLOGICAL TABLES AND FIGURES.....	62
REFERENCES.....	74
CURRICULUM VITAE.....	78

LIST OF TABLES

TABLE 1 $^{40}\text{Ar}/^{39}\text{Ar}$ AGES FOR THE SAMPLES THAT WERE ANALYZED FROM NAKWAI.....18

TABLE 2 CORRELATION COEFFICIENTS (R) AND SIGNIFICANCE (P) FOR MESIODISTAL (MD) LENGTH TO MESIAL WIDTH (MW), DISTAL WIDTH (DW), AND AVERAGE WIDTH (AVGW) OF THE LOWER MOLARS FROM *M. KYONGOI*, *M. BATEAE*, AND *P. NGORORAENSIS*.....38

LIST OF FIGURES

FIGURE 1 COMPARISON OF HYPSONDONTY BETWEEN *MEROËHYRAX SPP.* WHICH IS DESCRIBED AS HAVING HYPSONDONT MOLARS AND *BRACHYHYRAX SPP.* WHICH HAS BRACHYDONT MOLARS.....3

FIGURE 2 THE DIVERSITY OF THE DIFFERENT FAMILIES OF HYRACOIDS THROUGH TIME.....4

FIGURE 3 MAP OF WEST TURKANA, NORTHWESTERN KENYA, SHOWING THE LOCATION OF NAKWAI AND OTHER FOSSIL LOCALITIES.....7

FIGURE 4 MAP OF NAKWAI AREA SHOWING APPROXIMATE TURKANA OLIGOCENE PROJECT (TOP) SECTIONS AND SAMPLE NAMES AND LOCATIONS WITHIN EACH TOP SECTION.....11

FIGURE 5 PHOTOS OF *MEROËHYRAX KYONGOI* MAXILARY FRAGMENTS CONTAINING AN UPPER RIGHT M1 AND A MANDIBLE FRAGMENT WITH A LOWER RIGHT M3.....16

FIGURE 6 $^{40}\text{Ar}/^{39}\text{Ar}$ AGE SPECTRUM FOR SAMPLE DRT-15; PLATEAU STEPS HAVE BOLD OUTLINES.....20

FIGURE 7 $^{40}\text{Ar}/^{39}\text{Ar}$ AGE SPECTRUM FOR SAMPLE DRT-18.....21

FIGURE 8 $^{40}\text{Ar}/^{39}\text{Ar}$ AGE SPECTRUM FOR SAMPLE DRT-06; PLATEAU STEPS HAVE BOLD OUTLINES.....22

FIGURE 9 $^{40}\text{Ar}/^{39}\text{Ar}$ AGE SPECTRUM FOR SAMPLE DRT-10.....23

FIGURE 10 $^{40}\text{Ar}/^{39}\text{Ar}$ AGE SPECTRUM FOR DRT-04 BASALT GROUNDMASS.....24

FIGURE 11 $^{40}\text{Ar}/^{39}\text{Ar}$ AGE SPECTRUM OF JK004 WITH PLATEAU SEGMENT.....25

FIGURE 12 $^{40}\text{Ar}/^{39}\text{Ar}$ AGE SPECTRUM FOR SAMPLE DRT-23.....26

FIGURE 13 $^{40}\text{Ar}/^{39}\text{Ar}$ AGE SPECTRUM FOR DRT-08.....27

FIGURE 14 CUMULATIVE PROBABILITY PLOT OF DRT-09 CRYSTAL POPULATION, 10 OUT OF 10 FUSIONS.....28

FIGURE 15 CUMULATIVE PROBABILITY PLOT SHOWING THE AGE DISTRIBUTION FOR ALL SINGLE CRYSTAL FUSIONS IN DRT-20.....	30
FIGURE 16 CUMULATIVE PROBABILITY PLOT FOR THE DISTRIBUTION OF THE YOUNGER AGE POPULATION FROM DRT-13.....	32
FIGURE 17 UPPER MOLAR SIZE WITH <i>M. KYONGOI</i> (BLUE MARKER) COMPARED TO <i>P. NGORORAENSIS</i> (YELLOW MARKER): (A) FIRST MOLAR (M1), (B) SECOND MOLAR (M2), AND (C) THIRD MOLAR (M3).....	34
FIGURE 18 LOWER MOLAR SIZE WITH <i>M. KYONGOI</i> (BLUE MARKER) COMPARED AGAINST <i>M. BATEAE</i> (GREEN MARKER) AND <i>P. NGORORAENSIS</i> (YELLOW MARKER): (A) FIRST MOLAR (M1), (B) SECOND MOLAR (M2), AND (C) THIRD MOLAR (M3).....	35
FIGURE 19 UPPER MESIODISTAL LENGTH (MD) WITH (A) MESIAL WIDTH (MW), (B) DISTAL WIDTH (DW), AND (C) AVERAGE WIDTH (AVGW) OF <i>M. KYONGOI</i> (BLUE MARKER) AND <i>P. NGORORAENSIS</i> (YELLOW MARKER).....	37
FIGURE 20 UPPER MOLAR MESIODISTAL LENGTH (MD) COMPARED TO THE THREE CROWN HEIGHT MEASUREMENTS.....	39
FIGURE 21 LOWER MOLAR MESIODISTAL LENGTH (MD) COMPARED TO THE THREE CROWN HEIGHT MEASUREMENTS.....	40
FIGURE 22 HYPSONDONTY INDEX OF THE LOWER MOLARS USING THE PROTOCONID HEIGHT (PH) AS THE MEASUREMENT FOR HEIGHT OF THE CROWN.....	43
FIGURE 23 HYPSONDONTY INDEX OF THE LOWER MOLARS, SEPARATED BY TOOTH NUMBER, USING THE METACONID HEIGHT (MH) AS THE MEASUREMENT FOR HEIGHT OF THE CROWN.....	44
FIGURE 24 GENERALIZED STRATIGRAPHIC COLUMN OF NAKWAI.....	49

CHAPTER 1

INTRODUCTION

Nakwai is located in the Turkana Basin of northwestern Kenya. The Turkana Basin is a hydrographic sedimentary basin that is part of the East African Rift System (Feibel, 2011). The oldest sediments in the region are Cretaceous in age and are preserved with other Turkana Basin sediments from Paleogene through Quaternary age (Boschetto et al., 1992; Brown and McDougall, 2011; Feible, 2011). Afro-Arabia was an isolated island continent during much of the time the basin was forming but during the African Mid-Tertiary Event (AMTE, name proposed by Rasmussen and Gutierrez, 2009) near the Oligocene-Miocene boundary (i.e., approximately 23 Ma) Africa made continental contact with Eurasia (Kappelman et al., 2003; Leakey et al., 2011; Rasmussen and Gutierrez, 2009). This is a significant period in time because the fossil record in this region could record the biotic interchange between Afro-Arabia and Eurasia.

In 1987 a researcher from a team lead by the Leakeys discovered a rich fossil locality in northwest Kenya that became known as Benson's site (Gutierrez, 2011). During the mid 2000's, researchers returned to Benson's site and found several more fossil localities nearby, eventually referring to the area as Nakwai (Gutierrez, 2011; Rasmussen and Gutierrez, 2009). The faunal assemblage from Nakwai is broadly comparable to the faunal assemblage at Losodok (known as Lothidok in some publications) (Gutierrez, 2011; Leakey et al., 2011; Rasmussen and Gutierrez, 2009), which lies approximately 90 km north of Nakwai. The K/Ar ages of the Losodok fauna used by Rasmussen and Gutierrez (2009) for faunal correlations came from the age constraints of the Late Oligocene fossiliferous Eragaleit beds (Boschetto et al., 1992; Brown and McDougall, 2011; Rasmussen and Gutierrez, 2009).

There are few fossiliferous sites in the Turkana Basin known from the Oligocene-Miocene boundary; the Eragaleit beds of Losodok are dated between 24 and 27 Ma and the

majority of early Miocene sites are between 17-20 Ma (Werdelin, 2010), making them latest early Miocene (Boschetto et al., 1992; Leakey et al., 2011). Samples of basalts and volcanoclastic material were collected for this study during the 2012 field season for $^{40}\text{Ar}/^{39}\text{Ar}$ dating. These samples constrain the age of the upper portion of the Nakwai section to the earliest Miocene (22.85 Ma – 14.39 Ma). Nakwai being earliest Miocene will help to fill in the temporal gap between the late Oligocene sites, like Losodok, and other early Miocene sites. Further study of the fauna at Nakwai will give valuable information for understanding the dynamics of the faunal transition by offering the first glimpse of the interactions between the endemic fauna and the Eurasian immigrants; it will ultimately help to further constrain the timing of the geographical contact.

Many modern herbivores have high crowned or hypsodont cheek teeth with highly variable patterns of enamel and dentine on the occlusal or grinding surfaces (Figure 1 (a-d); Feldhamer et. al., 2007). Selenodonty refers to a specific pattern of cusps on the occlusal surface where the enamel forms continuous crescent shaped ridges; deer are one of the many modern mammals that have this form of cheek teeth (Figure 1 (e-f); Feldhamer et. al., 2007). The most widely accepted hypothesis for the evolution of hypsodonty in mammals has been linked to the increase of silica-rich C4 grasses (Strömberg, 2006). Endemic animals of Africa had evolved in isolation prior to the continental contact with Eurasia during the Late Oligocene; this includes mammals from the order Hyracoidea which have been recovered from Nakwai (Gutierrez, 2011; Leakey et al., 2011). This group is of interest because initial observations of the Nakwai specimens suggested that many species of hyracoids had evolved characteristics of hypsodonty and selenodonty in the absence of silica-rich C4 grasses (Rasmussen and Simons, 1988; Gutierrez, 2011). Silica-rich grasses were not widespread in Africa until the late Miocene, and the preliminary results of carbon isotope analysis among the Nakwai mammals suggest that

there is no signature of C4 grasses present (Bobe, 2006; T. Rasmussen, personal communication, 2012). The presence of these traits contradicts the hypothesis that hypsodonty is a feature that evolved in response to an increase of C4 grasses in an herbivorous diet and suggests that this is not the sole evolutionary driver for an increase in hypsodonty. Some other factors that have been suggested previously are related more to feeding behaviors and environmental factors that have the potential to increase the amount of abrasive material ingested unintentionally by the animal (Bargo et al., 2006; Janis, 1979, 1988; Williams and Kay, 2011).

Figure 1

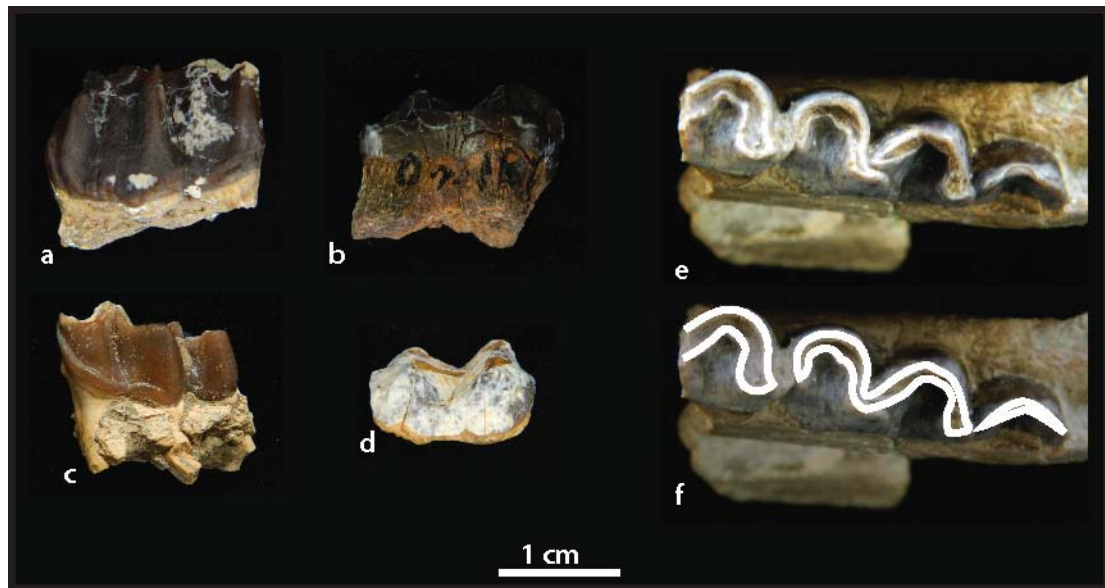


Figure 1: Comparison of hypsodonty between *Meroëhyrax* spp. which is described as having hypsodont molars and *Brachyhyrax* spp. which has brachydont molars. (a) *Meroëhyrax kyongoi* upper left M3, (c) *Meroëhyrax bateae* lower left m3, *Brachyhyrax* (b) upper left M and (d) lower right m. Selenodonty is illustrated on lower right m3 of *Paraplioxyrax ngororaensis*; (e) clear view of occlusal surface (f) occlusal surface with crescent shaped ridges outlined in white.

Meroëhyrax and other closely related hyracoids were apparently evolving features of hypsodonty and selenodonty in their dentition prior to the arrival and expansion of these C4 grasses. *Meroëhyrax kyongoi*, a species found in Nakwai and Losodok, is a member of the family Plioxyracidae, and all members of this family have all been formally described as having hypsodont cheek teeth, although not to the extreme extent of more traditional examples of

hypsoodonty such as horses (Rasmussen and Gutierrez, 2009). Similar to *Meroëhyrax*, members of other hyracoid families, such as the genus *Selenohyrax* and *Antilohyrax* from the Oligocene of Fayum, Egypt, had developed features of selenodonty prior to the arrival and expansion of C4 grasses (Rasmussen and Simons, 1988, 2000; Gutierrez, 2011). For this study dental measurements were made for *Meroëhyrax kyongoi* and for two other closely related pliohyracids from the early to mid Miocene.

Figure 2

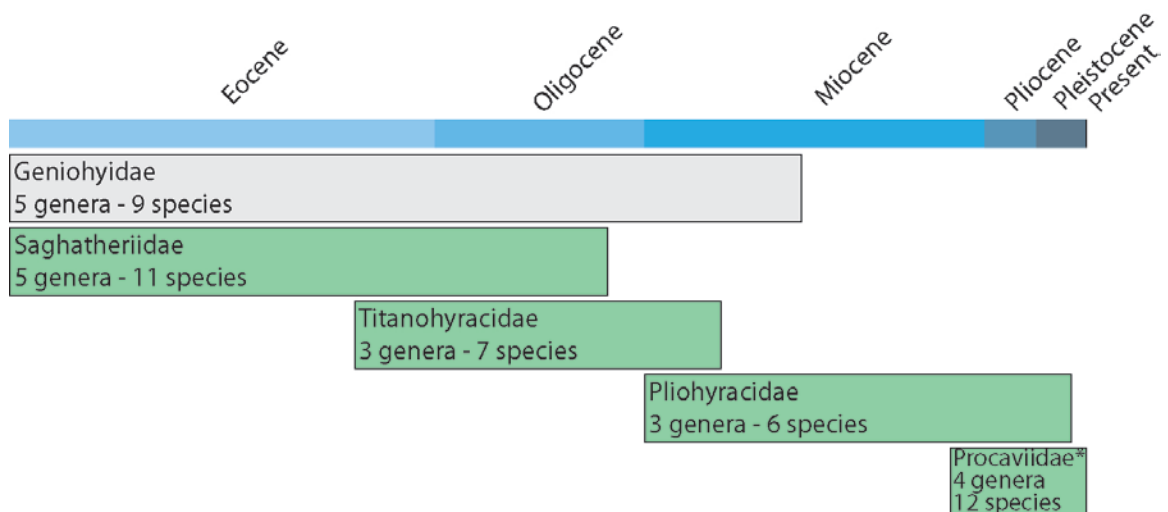


Figure 2: The diversity of the different families of hyracoids through time. Families with genera that have been described as having hypsoodont or selenodont cheek teeth are shown in green. Other hyracoids have been formally described from the late Oligocene of Egypt but the placement within an existing family has not been determined. *Procaviidae is the only family with extant species, accounting for seven of the 12 species representing three of the four genera.

The hyracoid lineage is composed of the following five families: Geniohyidae, Saghatheriidae, Titanohyracidae, Pliohyracidae and Procaviidae which is the only family with extant members (Rasmussen and Gutierrez, 2010). It is important to note that until the formal taxonomy was constructed by Rasmussen and Gutierrez (2010) that Geniohyidae, Saghatheriidae and Titanohyracidae were considered subfamilies of Pliohyracidae. Hyracoids first appear in the fossil record during the Eocene and were a very diverse group through the early Miocene (Figure 2). Following the AMTE the diversity of hyraxes decreased drastically.

This drastic taxonomic decrease has been attributed to the arrival of artiodactyls which were competing for resources with the hyraxes (Leakey et al., 2011).

CHAPTER 2

BACKGROUND

Geologic Setting

The Nakwai fossil locality of northwestern Kenya is located in the Turkana Basin west of Lake Turkana (Figure 2). The Turkana Basin formed during the initial phases of extension in the East African Rift System (Ducrocq et al., 2010) and is situated between the Ethiopian and Kenyan domes (Feible, 2011). The sedimentary sequences in this region rest on Pan African Neo-Proterozoic to Cambrian metamorphic basement which was likely exhumed in the Cenozoic during the formation of the Main Ethiopian Rift and the Kenya Rift (Feible, 2011; Brown and McDougall, 2011). The preserved sediments of the Turkana Basin capture a wide range of ages, the oldest are Paleogene and the youngest are Pleistocene being the youngest (Boschetto et al., 1992; Brown and McDougall, 2011; Feible, 2011).

Until recently the geology at Nakwai was unstudied. Currently this section is being formally described by a team of researchers from Washington University, Southern Methodist University, The University of Nevada Las Vegas, and the University of Texas at Austin. These fossiliferous sedimentary sequences rest on metamorphic basement and are unconformably capped by basalts. The sediments at Nakwai consist predominantly of siltstones, mudstones, and sandstones with a few localized carbonate lake sediments. A few of the mudstones are volcanoclastic in nature and are distinguished from other mudstones in the area by an abundance of amphiboles. There are also several primary ash fall tuffs and a few reworked ash units in the lower portion of the section.

Figure 3

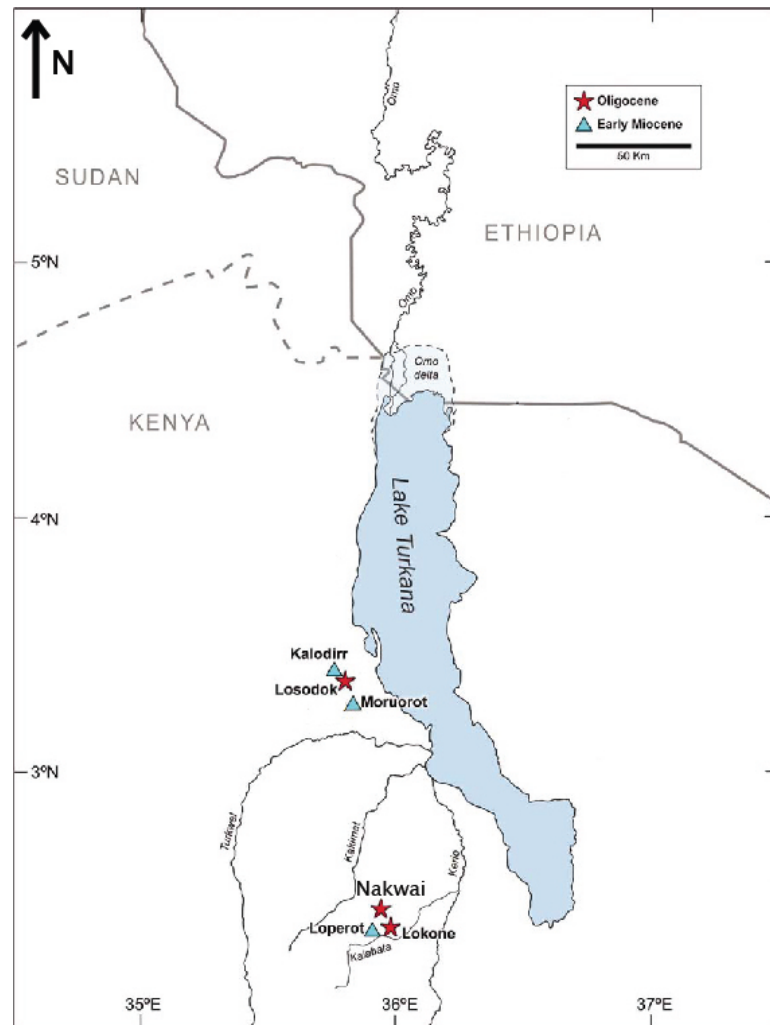


Figure 3: Map of West Turkana, northwestern Kenya showing the location of Nakwai and other fossil localities. Map modified from Leakey et al., 2011.

Previous Work

Much of the research in this region focuses on early primate and human evolution. The Leakey family has been conducting research in the region for decades, and in 1987 Meave Leakey led a team of researchers to the Nakwai area. One member of the Leakey's research team, Benson Kyongo, discovered a rich fossil locality on that trip, later called Benson's site. It was the first of many found at Nakwai (Gutierrez, 2011). Since the discovery of Benson's site, a few researchers have returned to study the area. D. Tab Rasmussen and a few colleagues went

to Benson's site in 2007 to investigate and to conduct a paleontological survey of the surrounding area. This visit resulted in the discovery of numerous other fossil localities in the Nakwai area (Gutierrez, 2011; Rasmussen and Gutierrez, 2009). These rich fossil localities were the basis for the Turkana Oligocene Project (TOP). TOP was funded by the National Science Foundation, with the goal of formally describing the geology and continuing the analysis of the Nakwai fauna with an emphasis on its primates.

There have been only a few publications to date on the Nakwai area because work is ongoing, but other locations that have been correlated with Nakwai or are thought to be contemporaneous have been studied more extensively. North of Nakwai, across the Turkwell River is the Losodok Range, a region with numerous fossil localities (Boschetto et al., 1992; Leakey et al., 2011). Losodok is a late Oligocene fossil locality that was discovered in the 1930s (Figure 3; Gutierrez, 2011). The fossils of Losodok were collected from the Eragaleit Beds and the ages were constrained using isotopic dates obtained by conventional K/Ar dating of interbedded Kalakol basalts. These dates set older and younger age limits of 27.5 Ma and 24.2 Ma, respectively (Boschetto et al., 1992; Leakey et al., 2011). The faunal correlations of Rasmussen and Gutierrez (2009) suggested that the Nakwai fauna was similar in age to the fauna at Losodok, thus potentially adding another late Oligocene fossil locality to those known from the Turkana Basin (Gutierrez, 2011; Rasmussen and Gutierrez, 2009). The age of the entire Losodok Formation is well constrained; the Eragaleit beds are stratigraphically the lowest fossil-bearing unit in a succession that also contains the early Miocene fossil localities of Moruorot and Kalodirr (17.5 – 16.8 Ma, Figure 3) (Boschetto et al., 1992; Brown and McDougall, 2011; Leakey et al., 2011).

Other fossil sites located near Nakwai include the late Oligocene Lokone fossil locality to the southeast and the early Miocene Loperot locality to the southwest (Figure 3) (Ducrocq et al.,

2010; Leakey et al., 2011). The age of the Lokone fossils have not been constrained by isotopic dating methods, however biostratigraphic correlations suggest that it is late Oligocene (Ducrocq et al., 2010; Leakey et al., 2011). Loperot is reported to be early Miocene, with K/Ar ages ranging from 17.5 – 13.9 Ma for the overlying basalts (Baker, 1971; Boschetto et al., 1992; Brown and McDougall, 2011; Leakey et al., 2011).

CHAPTER 3

METHODS

$^{40}\text{Ar}/^{39}\text{Ar}$ Dating

Samples for $^{40}\text{Ar}/^{39}\text{Ar}$ dating were collected from Nakwai during the 2012 field season. These samples were collected from several locations within the measured sections. The sections where samples were collected include: Turkana Oligocene Project (TOP) 1, TOP 8, TOP 46, TOP 64/65, TOP 69, TOP 80, and TOP 106 (Figure 4). Three different lithologies were sampled, including basalt, air fall tuff, and volcanoclastic siltstone and mudstone, with the latter containing visible amphibole crystals. Of the three lithologies collected, 17 were basalts, seven were air fall tuffs, and two were volcanoclastic siltstones/mudstones.

Figure 4

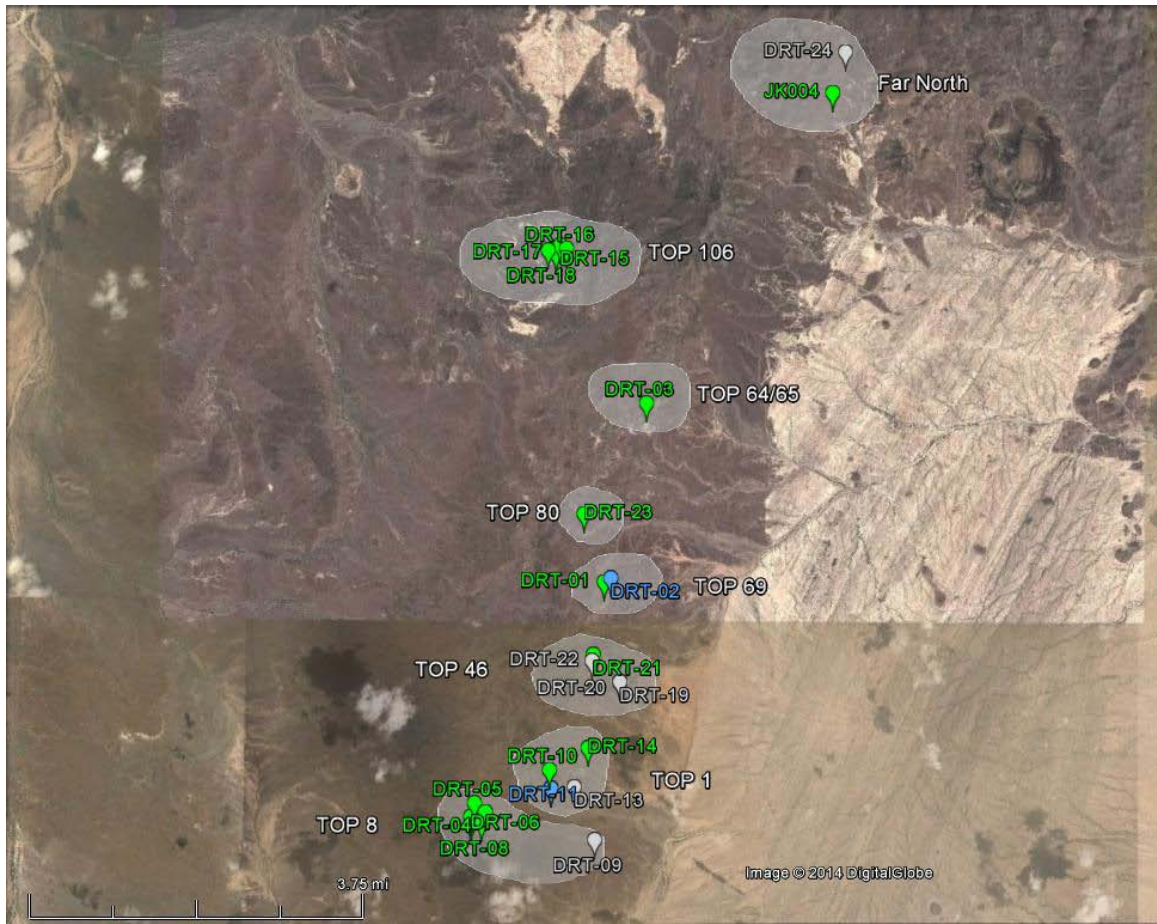


Figure 4: Map of the Nakwai area showing approximate Turkana Oligocene Project (TOP) sections and sample names and locations within each TOP section. Basalts are in green, air fall tuffs in gray, and volcaniclastic mudstones in blue. This map is modified from a Google Earth image.

A thin section was made for each of the 17 basalt samples. Each thin section was visually inspected for the presence of glass or alteration in the groundmass; samples with glass or alteration were deemed unlikely to produce reliable data. Samples were chosen based on the stratigraphic importance of the sample and how likely the sample was to yield reliable data. Of the 17 original basalt samples, eight were chosen for dating: DRT-04, DRT-06, DRT-08, DRT-10, DRT-15, DRT-18, DRT-23, and JK004. These samples were broken into rock chips using a Braun Chipmunk, then crushed using a Bico Pulverizer before being sieved into 106-300 μm , 300-600 μm , and 600-1180 μm size fractions. Approximately 100 mg of holocrystalline

groundmass, free of phenocryst fragments, was picked from the 300-600 μm size fraction of each sample. The groundmass was then washed in an ultrasonic bath of dilute nitric acid (5%) to reduce atmospheric contamination and to remove trace amounts of alteration products, and then rinsed with acetone. The nitric acid bath and acetone rinse was repeated with samples where more alteration products were present.

The seven air fall tuffs were broken into rock chips using the Braun Chipmunk and then crushed using a Bico Pulverizer. Each of the seven crushed samples was sieved into 106-300 μm , 300-600 μm , and 600-1180 μm size fractions. Each size fraction was visually inspected for datable sanidine crystals. Sample DRT-12 did not yield enough crystals to make it suitable for dating. Single crystals of sanidine in the 106-300 μm , 300-600 μm size fractions were handpicked from the following samples: DRT-09, DRT-11, DRT-13, DRT-19, DRT-20, DRT-22, and DRT-24. The single sanidine crystals were washed using dilute hydrofluoric acid (5%) for three minutes and then rinsed with acetone. The sanidines were then washed in an ultrasonic bath of acetone until they were free of any remaining volcanic glass and matrix.

The two volcanoclastic siltstone/mudstone samples were broken into rock chips using the Braun Chipmunk and then processed by the Bico Pulverizer until crushed. Each crushed sample was sieved into 106-300 μm , 300-600 μm , and 600-1180 μm size fractions. Single amphibole crystals were handpicked from the 300-600 μm and 600-1180 μm size fractions of samples DRT-02 and DRT-11. An abundance of amphiboles was discovered and collected from sample DRT-22 as it was being processed for single sanidine crystals. Once picked, the amphiboles were washed in an ultrasonic bath of acetone until the adhering matrix was removed. For some samples the ultrasonic bath treatment had to be repeated several times.

All of the samples were wrapped in aluminum foil, packed into fused silica tubes with fluence monitors, optical grade CaF_2 , and synthetic K-glass. They were then loaded into an

aluminum container for irradiation. The irradiation package was sent to the U.S. Geological Survey TRIGA Reactor in Denver, CO where it was irradiated for seven hours. The fluence monitor used for age calculation was the Fish Canyon Tuff sanidine which has an age of 28.2 Ma (Renne et al., 1998).

All $^{40}\text{Ar}/^{39}\text{Ar}$ analyses were conducted at the Nevada Isotope Geochronology Laboratory (NIGL) located at the University of Nevada Las Vegas. Bulk samples of basalt groundmass were analyzed using the step heating method in a furnace. The single sanidines from the air fall tuffs were analyzed using single crystal laser fusion with a 20W CO_2 laser. The amphiboles that were handpicked from the volcanoclastic siltstones/mudstones were analyzed in bulk by step heating in a furnace. Once the gas was released from the samples it went through a purification process using three GP-50 SAES getters to remove any reactive gases before the gas sample was allowed to expand into the MAP-215 50 noble gas mass spectrometer. The mass spectrometer sensitivity was $\sim 6 \times 10^{-17} \text{ mol mV}^{-1}$ and the data reduction and age calculations were performed using LabSpec software. The fluence monitors, CaF_2 , and K-glass fragments were analyzed using single crystal laser fusion using a 20W CO_2 laser. Repeated analysis of CaF_2 and K-glass fragments allowed for the determination of the Ca and K correction factors.

All ages are reported at the 1σ uncertainty level with the criteria for age calculations as follows. Plateau ages are defined as a segment of an age spectrum that consists of a minimum of three contiguous steps that overlap at $\pm 2\sigma$ uncertainty and account for $>50\%$ of ^{39}Ar released. The total gas age is a weighted calculation based on the amount of ^{39}Ar released in each step, and the weighted mean age follows the criteria established by Wendt and Carl (1991) for determining the mean square of weighted deviates (MSWD). For samples with MSWD values that are too high the largest contributor to an unacceptable MSWD value or outlier is omitted from the weighted mean; this process is then repeated until an acceptable MSWD value

has been achieved. A final age calculation is based on the refined analyses (Wendt and Carl, 1991). Each data set was also checked for a valid inverse isochron which is based on the MSWD criteria of Wendt and Carl (1991). Each isochron was examined to determine the effects of excess argon.

Paleontological Methods

Specimens of *Meroëhyrax kyongoi* were collected by D.T. Rasmussen and his team during the 2007-2009 field seasons from several of the TOP sections (Figure 3) within the Nakwai area. The specimens were catalogued in the field and are currently housed in the National Museums of Kenya in Nairobi. Some additional specimens are included in this study, which were collected earlier. These specimens include the *Meroëhyrax kyongoi* holotype (KNM-NW 22558A), collected during an earlier survey of the Nakwai area by Benson Kyongo in 1987 (Rasmussen and Gutierrez, 2009). Specimens included in this study consist of both upper and lower molars, with the majority of specimens being isolated teeth.

The *Meroëhyrax bateae* specimens included in this study were collected from a site on Rusinga Island which is located in the northeastern part of Lake Victoria in Kenya. *Meroëhyrax bateae* is the type specimen for the genus *Meroëhyrax*, first described by Whitworth in 1954 (Pickford and Fischer, 1987; Rasmussen and Gutierrez, 2010). These specimens are currently housed in the National Museums of Kenya in Nairobi. Only two specimens of *Meroëhyrax bateae* were available for this study, a single lower left M3 and a mandibular fragment that contains a lower left M1 and M2.

Paraplioxyrax ngororaensis was first described by Pickford and Fischer (1987). The specimens that are included in this study were collected by Pickford and his team between the years 1969 and 1975 from Ngorora, Kenya (Pickford and Fischer, 1987). These specimens are

also housed in the National Museums of Kenya in Nairobi. These specimens include both upper and lower molars, many of which were found intact in mandibular or maxillary fragments.

Measurements of mesiodistal length, mesial width and distal width were made on all specimens. Three additional measurements of crown height were made on *Meroëhyrax kyongoi*, *Meroëhyrax bateae* and *Parapliohyrax ngororaensis*. Measurements are illustrated in Figure 5. All dental measurements were made using digital calipers and are presented in millimeters.

Standard measurements for mesiodistal length (MD, Figure 5a and d) were taken along the midline between the buccal and lingual side of the tooth. Mesial and distal width measurements were taken between the buccal and lingual sides of the tooth. Mesial width (MW, Figure 5a and d) was the greatest length across the paracone (not including parastyle) and protocone (upper) or trigonid (lower). Distal width (DW, Figure 5a and d) was the greatest length across the metacone (not including metastyle) and hypocone (upper) or talonid basin (lower).

Crown height includes three separate measurements of the length between the base of the enamel and the crown of the tooth; these measured features differ between the upper and lower teeth. The location of these measurements was determined specifically for this study because there is no standard for crown height measurement in hyracoids (T. Rasmussen personal communication, 2013). Crown height of the upper teeth was measured from the base of the enamel to the maximum height of the protocone (PH), paracone (PaH), and the notch in the center of the median lingual cleft (protocone hypocone valley, PHV; Figure 5b and c). Crown height of the lower teeth was taken from the base of the enamel to the maximum height of the metaconid (MH), protoconid (PH), and the center of the talonid basin where it drains onto the lingual edge (TB; Figure 5e and f). Bivariate plots were used to compare the dental measurements to establish differences in tooth size and the degree of hypsodonty in the three

species. Following Janis (1988), the hypsodonty index (HI) was determined for specimens that were unworn to moderately worn in order to directly compare the crown height between species.

Figure 5

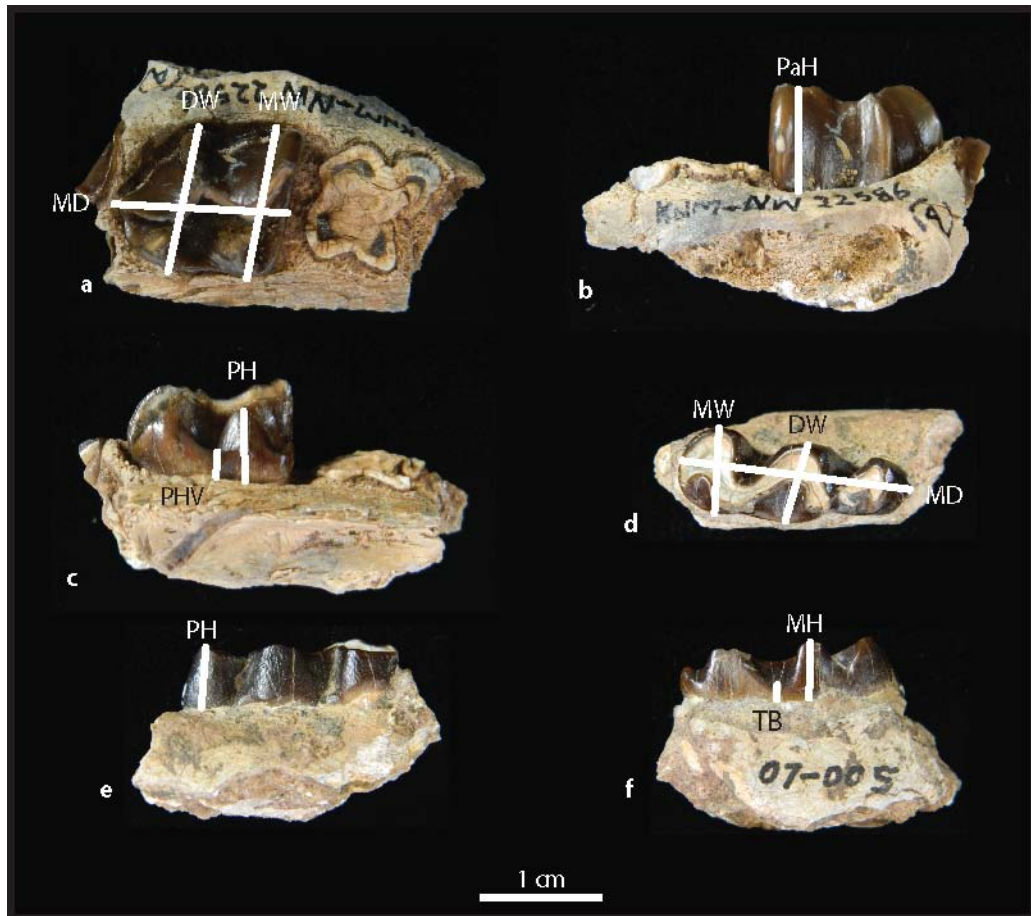


Figure 5: Photos of *Meroëhyrax kyongoi* maxillary fragment containing an upper right M1 and a mandible fragment with a lower right m3. Length and width measurements for upper (a) and lower (d) teeth: mesiodistal length (MD), mesial width (MW) and distal width (DW). Upper tooth crown height: (b) paracone height (PaH), (c) protocone height (PH) and (c) paracone-hypocone valley (PHV). Lower tooth crown height: (e) protoconid height (PH), (f) metaconid height (MH) and (f) talonid basin (TB).

CHAPTER 4

RESULTS

$^{40}\text{Ar}/^{39}\text{Ar}$ Dating

A total of 19 samples were analyzed using the $^{40}\text{Ar}/^{39}\text{Ar}$ isotopic dating method. Both furnace step heating and single crystal laser fusion analyses were utilized. Three of the samples that were analyzed did not yield usable data and will not be discussed. They are DRT-02 amphibole, DRT-11 amphibole, and DRT-22 amphibole. Of the 15 remaining samples, 12 were collected within sedimentary sections that were previously measured as a part of the Turkana Oligocene Project (TOP), and they define the upper and lower age limits of the Nakwai succession. Sample DRT-09 was collected from an ash flow tuff from a unit near the middle of the sedimentary succession. The stratigraphically lowest sample, DRT-13, provides a maximum dated age of 22.85 ± 0.22 Ma but the sedimentary sequence continues some 180 m below this level (Table 1). This sedimentary sequence is unconformably capped by basalt DRT-08 with an age of 17.02 ± 0.14 Ma (Table 1). The TOP 106 section is separated from the main sedimentary succession and is stratigraphically younger than the main succession. It is constrained between DRT-18 with an older age of 15.64 ± 0.07 Ma, and sample DRT-15 and its younger age of 14.39 ± 0.61 Ma (Table 1).

Table 1

Sample Name	Material	Far North	TOP 106	TOP 80	TOP 46	TOP 1	TOP 8
DRT-15	Basalt Groundmass		14.39 ± 0.61^1				
DRT-18	Basalt Groundmass		15.64 ± 0.07^2				
DRT-06	Basalt Groundmass						16.14 ± 0.13^1
DRT-10	Basalt Groundmass					16.15 ± 0.07^2	
DRT-04	Basalt Groundmass						16.78 ± 0.10^2
JK004	Basalt Groundmass	16.91 ± 0.32^1					
DRT-23	Basalt Groundmass			16.97 ± 0.14^1			
DRT-08	Basalt Groundmass						17.02 ± 0.14^1
DRT-09	Sanidine						20.89 ± 0.15^3
DRT-22	Sanidine				$*23.01 \pm 0.48^3$		
DRT-20	Sanidine				$*23.01 \pm 0.25^3$		
DRT-11	Sanidine					503.72 ± 11.48^4	
DRT-13	Sanidine					22.85 ± 0.22^3	
DRT-24	Sanidine	423.22 ± 73.27^4					
DRT-19	Sanidine				469.12 ± 51.06^4		

¹ Plateau Age, ² Total Gas Age, ³ Weighted Mean Age, and ⁴ Mean Age

*Sample yielded very few viable analyses; therefore, ages obtained are used as supporting data.

Table 1: ⁴⁰Ar/³⁹Ar ages for the samples that were analyzed from Nakwai. Uncertainties are recorded to $\pm 1 \sigma$. Samples are arranged in stratigraphic order and by field location from North (left) to South (right).

For sample DRT-15 basalt groundmass was collected from above the fossiliferous carbonate unit in the TOP 106 section and was analyzed by step heating. Analysis of the first five steps in the heating schedule showed that the sample released a very small amount of gas, essentially making them a blank analysis. These steps were omitted from the final data set because they make the age calculations unreliable. The total gas age for the remaining steps is 12.96 ± 0.60 Ma (Table 1, Appendix A). The plateau age for this sample of 14.39 ± 0.61 Ma is based on steps 2-5 of the age spectrum and accounts for 97% of the total ^{39}Ar released (Figure 6). The isochron, although statistically valid, is not considered reliable due to the low number of data points and the placement of two of the data points being clustered together essentially forming a single data point. The plateau age of 14.39 ± 0.61 Ma is considered the most reliable age for sample DRT-15 (Table 1).

Figure 6

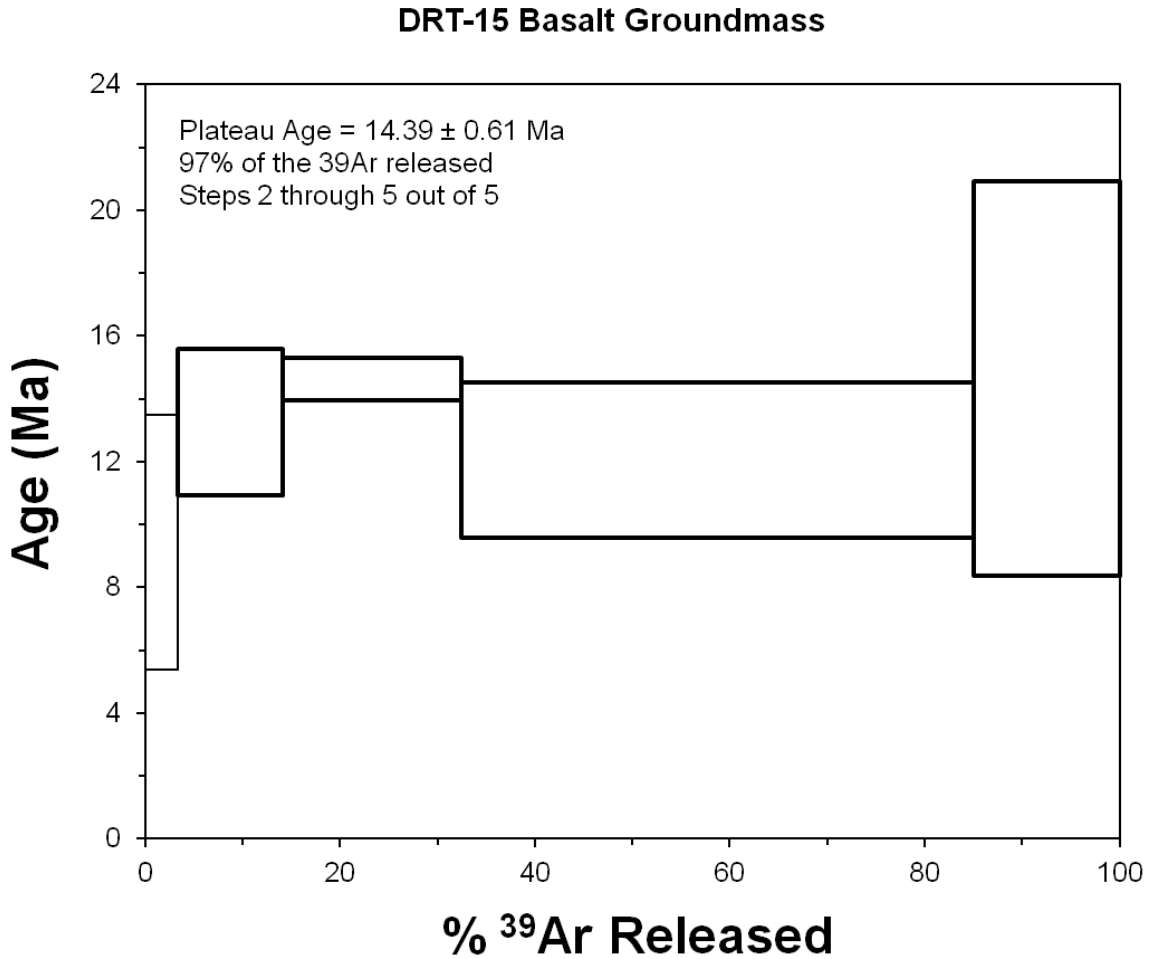


Figure 6: $^{40}\text{Ar}/^{39}\text{Ar}$ age spectrum for sample DRT-15; plateau steps have bold outlines.

Basalt groundmass, DRT-18 from below the main fossiliferous carbonate unit of section TOP 106, was analyzed by step heating. The first three steps yielded very little sample gas and did not produce reliable ages so they were omitted from the final data set and age calculations. The total gas age for the remaining steps is 15.64 ± 0.07 Ma (Table 2, Appendix A). There was no isochron defined for this sample and there was no plateau defined by the age spectrum (Figure 7). The total gas age of 15.64 ± 0.07 Ma is considered the most reliable age for sample DRT-18 (Table 1).

Figure 7

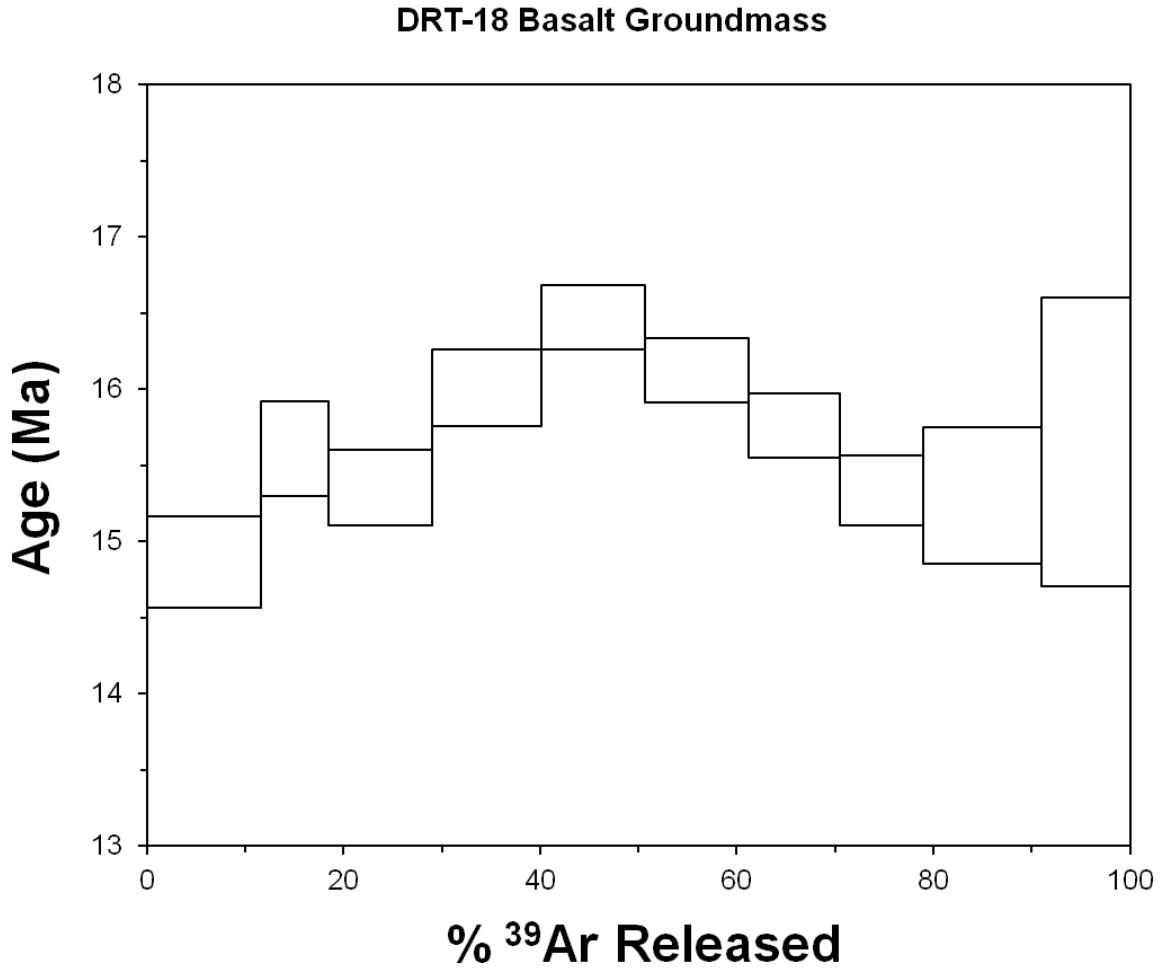


Figure 7: $^{40}\text{Ar}/^{39}\text{Ar}$ age spectrum for sample DRT-18.

Basalt groundmass sample DRT-06, which is from the top most basalt flow in the flow sequence that caps the TOP 8 section, was analyzed by step heating. The total gas age for DRT-06 is 16.03 ± 0.09 Ma (Table 3, Appendix A). The age spectrum for this sample yielded a plateau age of 16.32 ± 0.13 from steps 2-7 which accounted for 64% of the total ^{39}Ar released (Figure 8). There is no isochron defined by the data from this sample. The plateau age of 16.32 ± 0.13 Ma is considered the most reliable age for sample DRT-06 (Table 1).

Figure 8

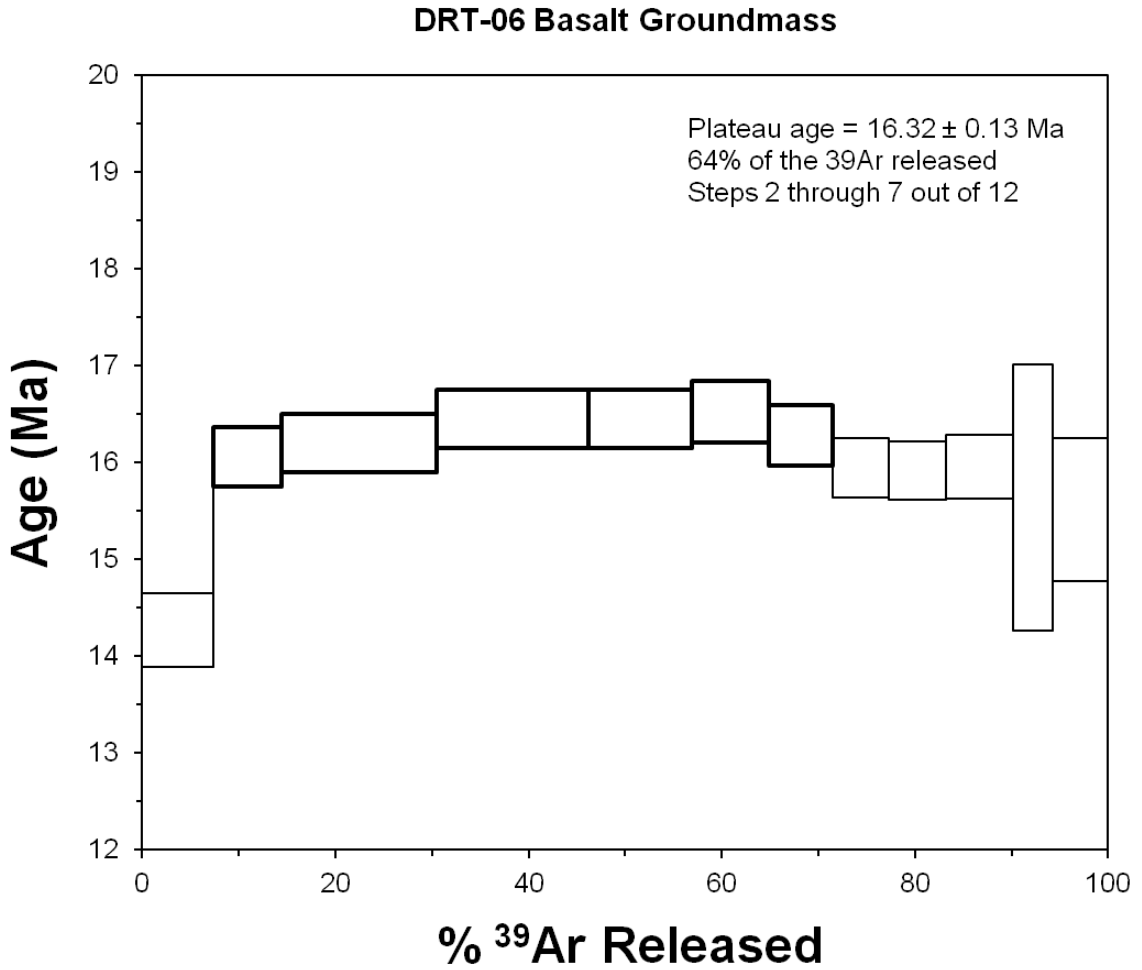


Figure 8: $^{40}\text{Ar}/^{39}\text{Ar}$ age spectrum for sample DRT-06; plateau steps have bold outlines.

For sample DRT-10 in section TOP 1, groundmass was analyzed by step heating from a basalt flow resting unconformably on top of the sedimentary sequence. The first four steps released only a very small amount of sample gas; due to the small amount of gas released calculated ages were not reliable and these steps were omitted from the final data set and age calculations. The total gas age for DRT-10 is 16.15 ± 0.07 Ma (Table 4, Appendix A). There was no isochron for this sample and there was no plateau segment defined by the age spectrum (Figure 9). The total gas age of 16.15 ± 0.07 Ma is considered the most reliable age for sample DRT-10 (Table 1).

Figure 9

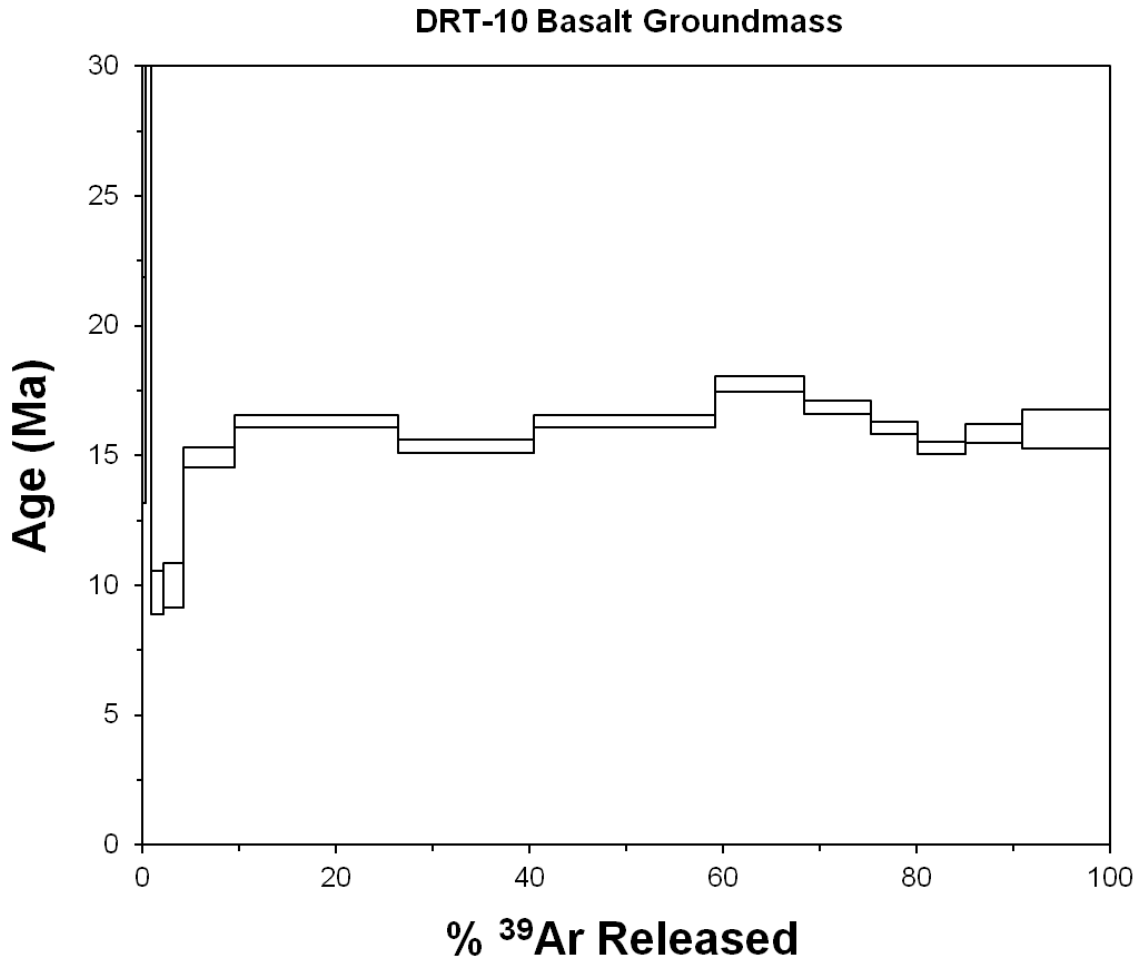


Figure 9: ⁴⁰Ar/³⁹Ar age spectrum for sample DRT-10.

For sample DRT-04, which is the basalt flow that is directly on top of DRT-08 in the flow succession that caps the TOP 8 section, groundmass was analyzed by step heating. The first step in the heating schedule released very little gas; therefore, reliable ages could not be calculated so this was omitted from the final data set. The total gas age for this sample is 16.78 ± 0.10 Ma (Table 5, Appendix A). This sample did not yield an isochron and there was no plateau defined by the age spectrum (Figure 10). The most reliable age for this sample is the total gas age of 16.78 ± 0.10 Ma (Table 1).

Figure 10

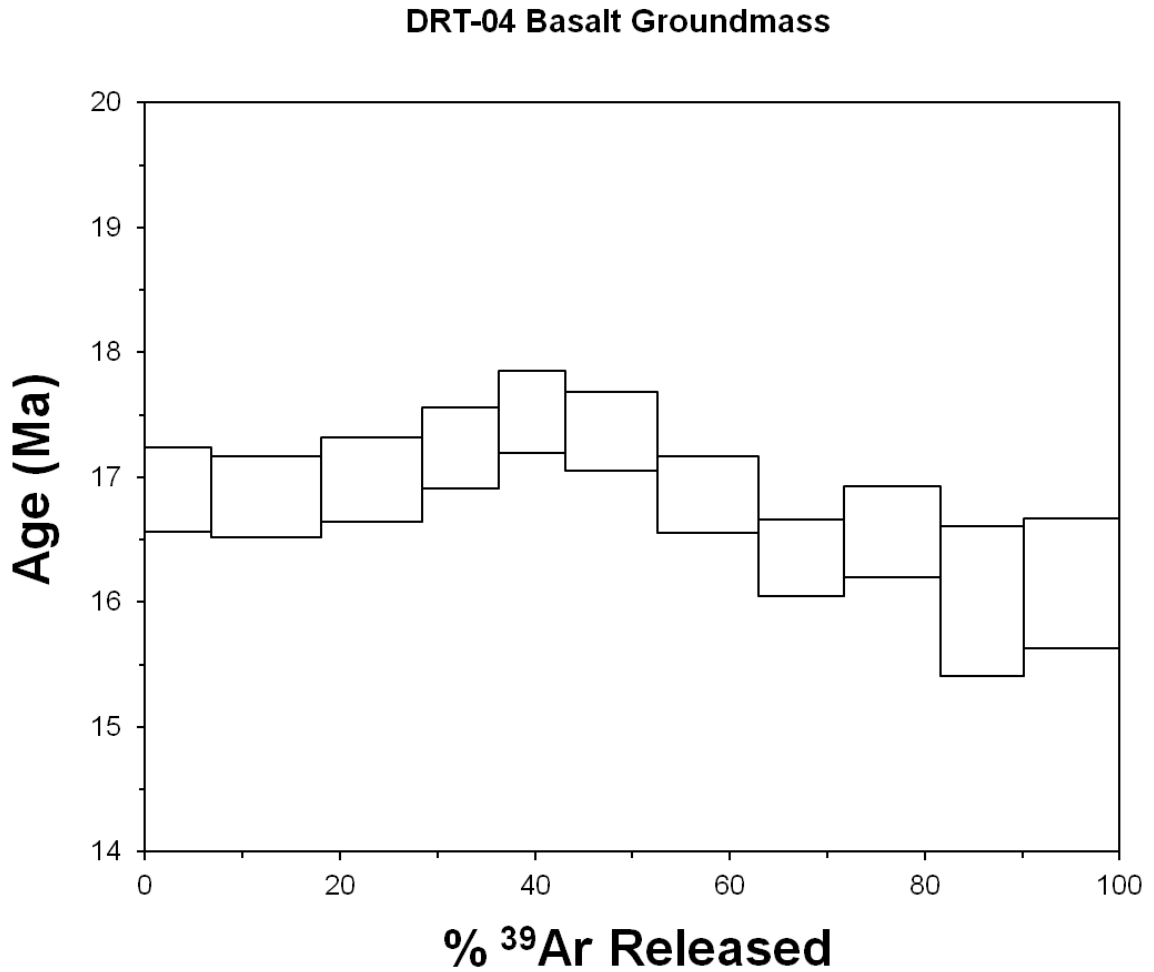


Figure 10: $^{40}\text{Ar}/^{39}\text{Ar}$ age spectrum for DRT-04 basalt groundmass.

For sample JK004 from the far north area of Nakwai, basalt groundmass was analyzed by step heating. The total gas age for JK004 is 16.61 ± 0.12 Ma (Table 6, Appendix A). The age spectrum for JK004 yielded a plateau age of 16.91 ± 0.32 from steps 2-8 which accounted for 55% of the total ^{39}Ar released (Figure 11). There is no isochron for this sample. The plateau age of 16.91 ± 0.32 Ma is considered the most reliable age for this sample (Table 1).

Figure 11

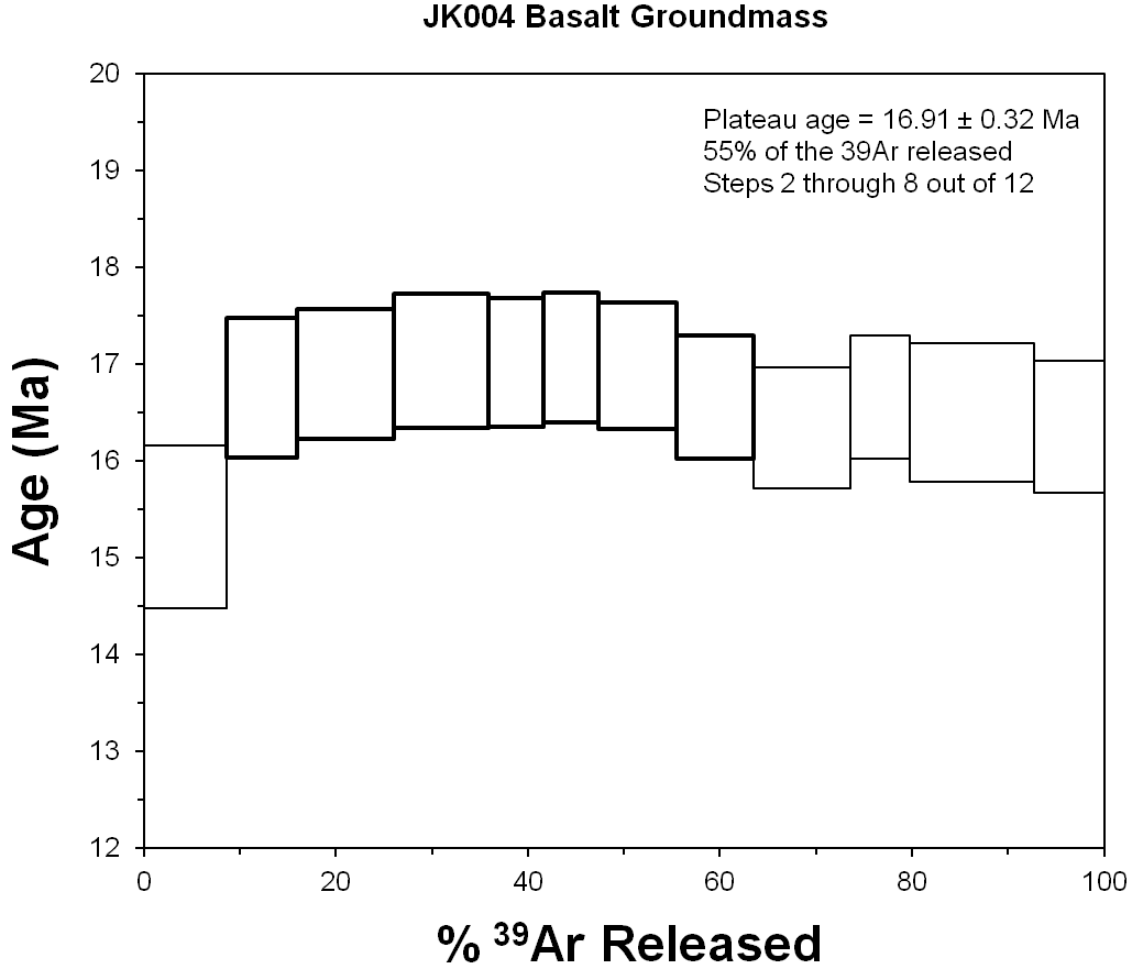


Figure 11: $^{40}\text{Ar}/^{39}\text{Ar}$ age spectrum of JK004 with plateau segment. Plateau segment is outlined in bold.

From the Top 80 section, basalt groundmass sample DRT-23, was analyzed by step heating. The total gas age for this sample is 17.08 ± 0.09 Ma (Table 7, Appendix A). Steps 3-8 of the age spectrum yielded a plateau age of 16.97 ± 0.14 Ma and account for 55% of the total ^{39}Ar released (Figure 12). There was no isochron for this sample. The most reliable age for sample DRT-23 is the plateau age of 16.97 ± 0.14 Ma (Table 1).

Figure 12

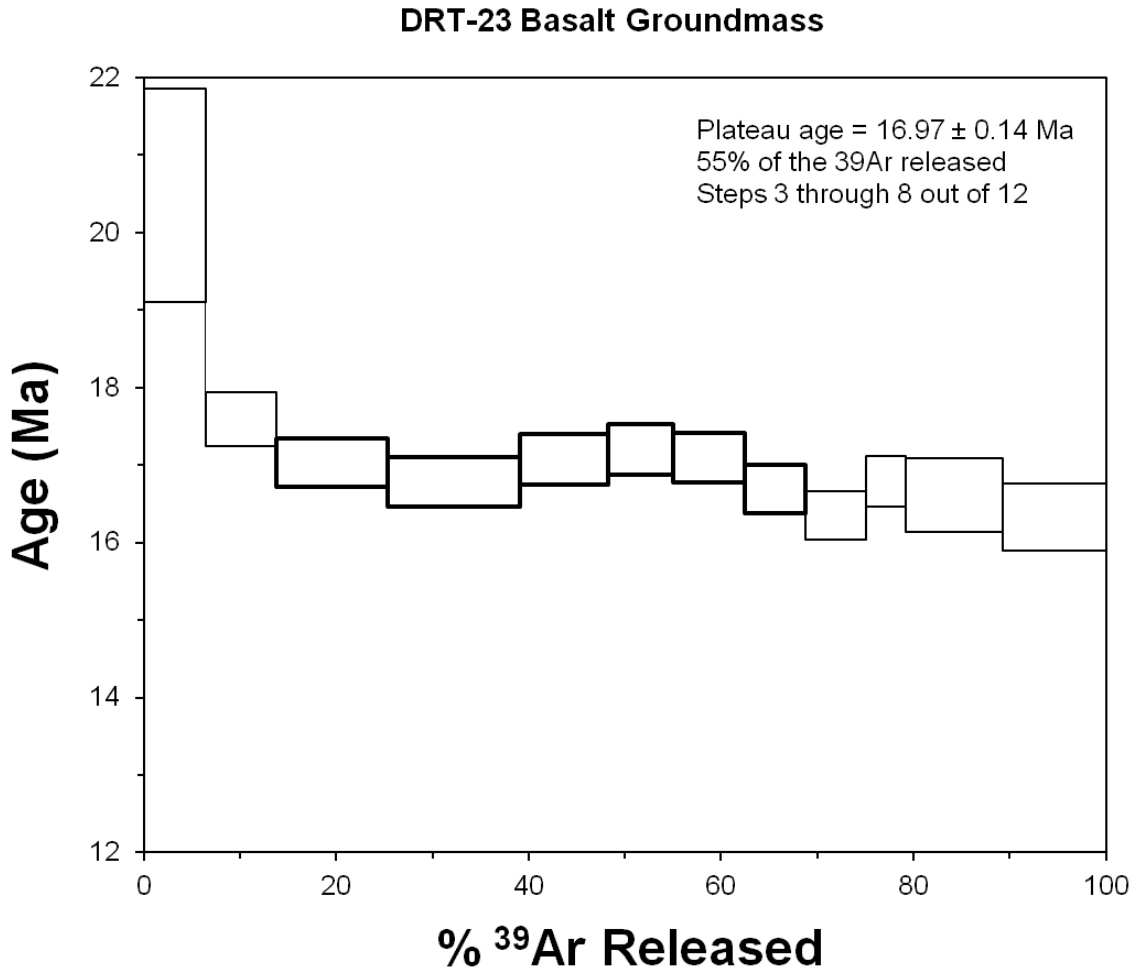


Figure 12: $^{40}\text{Ar}/^{39}\text{Ar}$ age spectrum for sample DRT-23. The steps in the plateau segment are outlined in bold.

Basalt sample DRT-08, from the base of the flow sequence capping the TOP 8 section, groundmass was analyzed by step heating. The total gas age for this sample is 16.53 ± 0.10 Ma (Table 8, Appendix A). The age spectrum for DRT-08 yielded a plateau age from steps 2-8 of 17.02 ± 0.14 Ma which accounted for 61% of the ^{39}Ar released (Figure 13). There is no isochron defined by the data from this sample. The most reliable age for sample DRT-08 is the plateau age of 17.02 ± 0.14 Ma (Table 1).

Figure 13

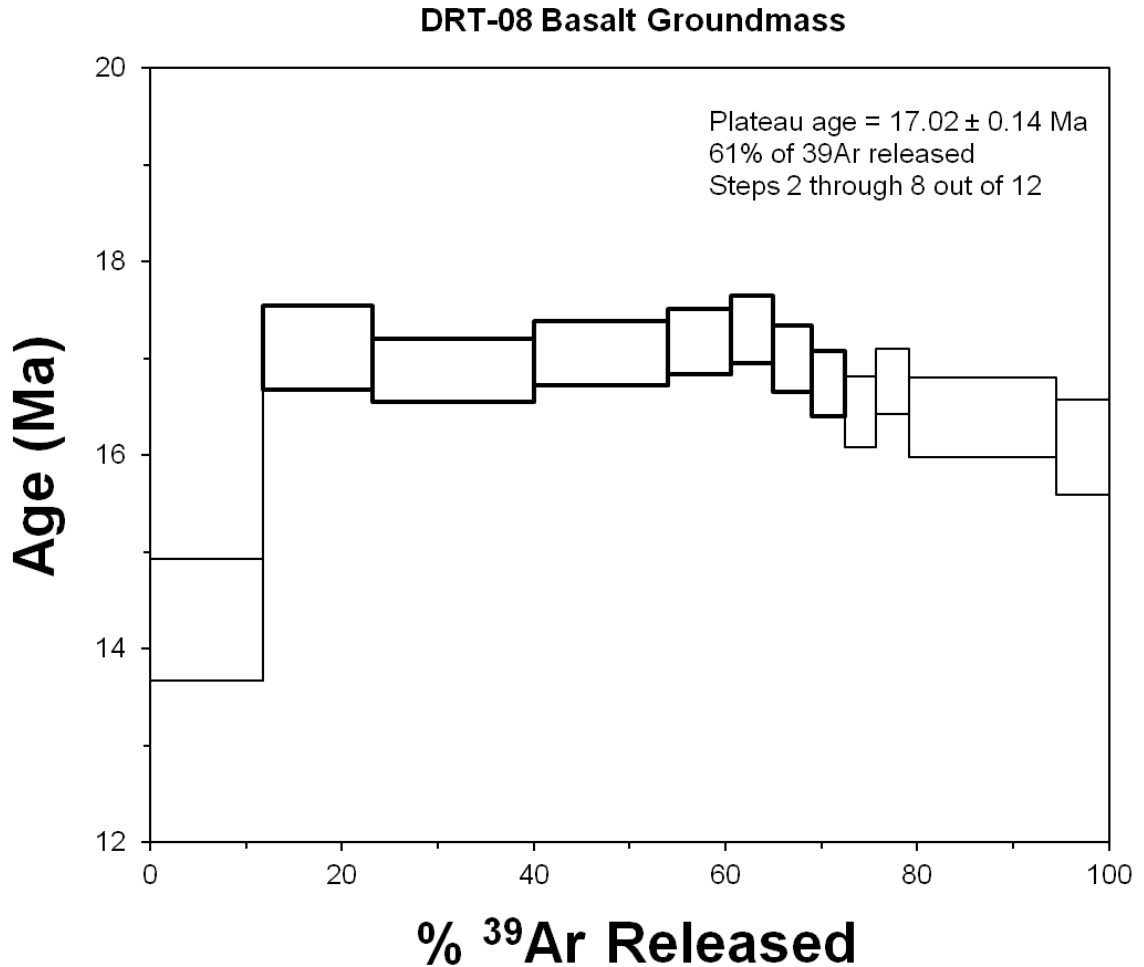


Figure 13: $^{40}\text{Ar}/^{39}\text{Ar}$ Ar age spectrum for DRT-08. Plateau segment is outlined in bold.

Pumice sample DRT-09 from the ash flow tuff in the upper portion of the sedimentary sequence in the TOP 8 section had 10 sanidine crystals out of the 27 individual crystals that were analyzed by single crystal laser fusion. The remaining 17 crystals were quartz. The apparent ages of the individual sanidines range in age from 20.22 – 21.74 Ma, with a mean age for this crystal population of 20.90 ± 0.40 Ma (10 fusions; Table 9, Appendix A). The weighted mean age for this crystal population is 20.89 ± 0.15 Ma and was based on all 10 analyses. The MSWD value for 10 out of 10 crystal fusions was 1.4 (Wendt and Carl, 1991). There is no isochron for this sample. The cumulative probability plot shows this sample population's age distribution

(Figure 14). The most reliable age for sample DRT-09 is the weighted mean age of 20.89 ± 0.15 Ma.

Figure 14

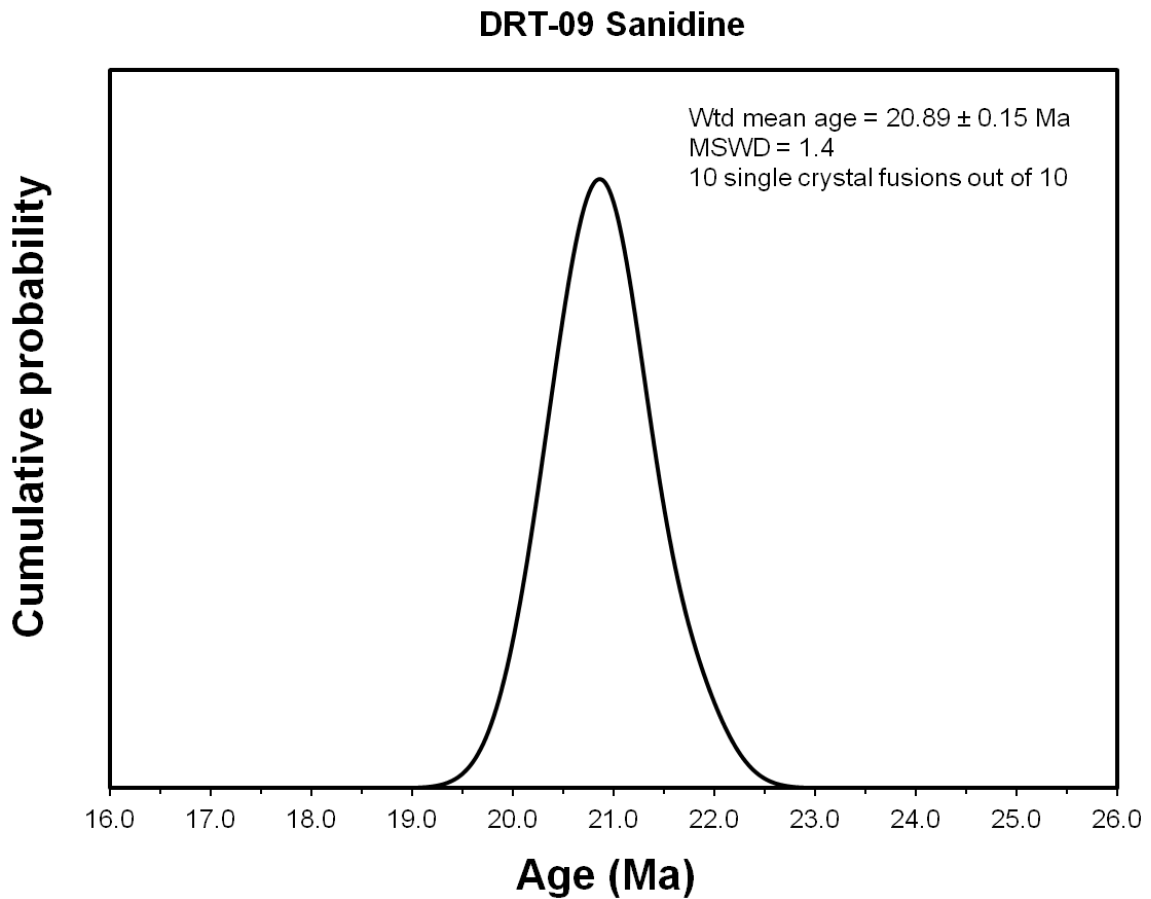


Figure 14: Cumulative probability plot of DRT-09 crystal population, 10 out of 10 fusions.

For sample DRT-22 from section TOP 46 there were 20 single crystals analyzed by single crystal laser fusion, with 2 out of 20 being sanidine and the remaining ones quartz. The analyses of the quartz crystals are not included in this data set. This sample is similar in stratigraphic level to sample DRT-13. Due to the small number of viable analyses the age of this sample is used as support of the age of DRT-13, which had a larger number of reproducible analyses and therefore a more reliable age. The mean age for this sample is 23.01 ± 0.48 Ma and the weighted mean age is 23.01 ± 0.14 Ma (Table 10, Appendix A). There is no isochron for this

sample. The weighted mean age of 23.01 ± 0.14 Ma is considered the most reliable age for sample DRT-22 (Table 1).

Sample DRT-20 from the TOP 46 section had 21 K-feldspars and 14 quartz crystals for a total of 35 single crystal fusions. This sample produced two distinct age populations (Figure 15; Table 11, Appendix A). The younger of the two age populations yielded very few analyses and will be used only as support of the age of sample DRT-13 since they are at similar stratigraphic levels. The mean age for the younger crystal population is 23.01 ± 0.07 Ma with a weighted mean age of 23.01 ± 0.25 Ma, based on the two single crystal fusions (Table 11, Appendix A). The mean age for the older population of crystals is 455.5 ± 100.3 Ma. The weighted mean age is 478.2 ± 2.6 Ma, which was based on 11 of 19 crystal fusions with an MSWD value of 1.3 (Table 11, Appendix A). There is no isochron for this sample. The weighted mean age for the younger crystal population of 23.01 ± 0.25 Ma is the preferred age for this sample because it is more likely the eruptive age of the unit; the older population is likely composed of xenocrysts from the basement which suggests that this unit was reworked (Table 1).

Figure 15

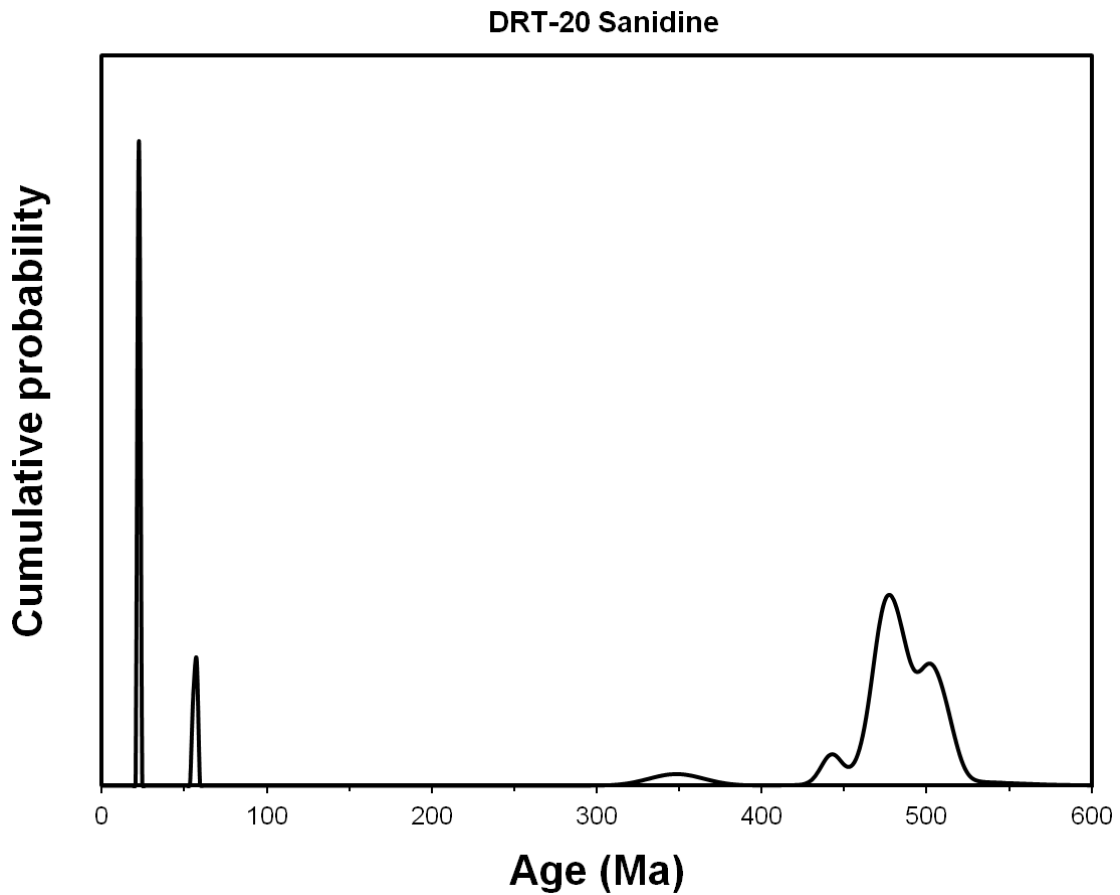


Figure 15: Cumulative probability plot showing the age distribution for all single crystal fusions in DRT-20. Due to the significant difference in age between the two populations of crystals a weighted mean age was not defined for the population as a whole, but was instead defined separately for each population.

There were 20 single crystal fusions for sample DRT-11, from the TOP 1 section. Five out of the 20 were K-feldspars and the remaining crystals were quartz. There were no young ages obtained in this analysis. The mean age for this sample is 503.7 ± 11.5 Ma, which is the most reliable age for this sample (Table 12, Appendix A). An isochron or age distribution plot was not shown for this sample because these data likely represent the age of the basement and not the age of the section.

Sample DRT-13, which is the second unit from the base of the TOP 1 section, had 55 crystal fusions; 31 were K-feldspars and the remaining crystals were quartz. This sample yielded

two distinct age populations (Table 13, Appendix A); the younger of the two populations defines the oldest securely dated age limit for Nakwai. The apparent ages for the 12 single crystal fusions from the younger crystal population range from 17.53-24.77 Ma, with a mean age of 22.32 ± 2.02 Ma (Table 13, Appendix A). The weighted mean age for the younger crystal population of 22.85 ± 0.22 Ma (MSWD=1.6) was based on 8 of 12 crystal fusions. The age distribution for the younger age population is shown on the cumulative probability diagram, with the initial population plotted against the refined population (Figure 16). The mean age of 448.26 ± 124.6 Ma for the older population of crystals is thought to reflect the age of the basement (19 total fusions, Table 13, Appendix A). There is no isochron for this sample; therefore the most reliable age is the weighted mean age of the younger crystal population, 22.85 ± 0.22 Ma (Table 1).

Figure 16

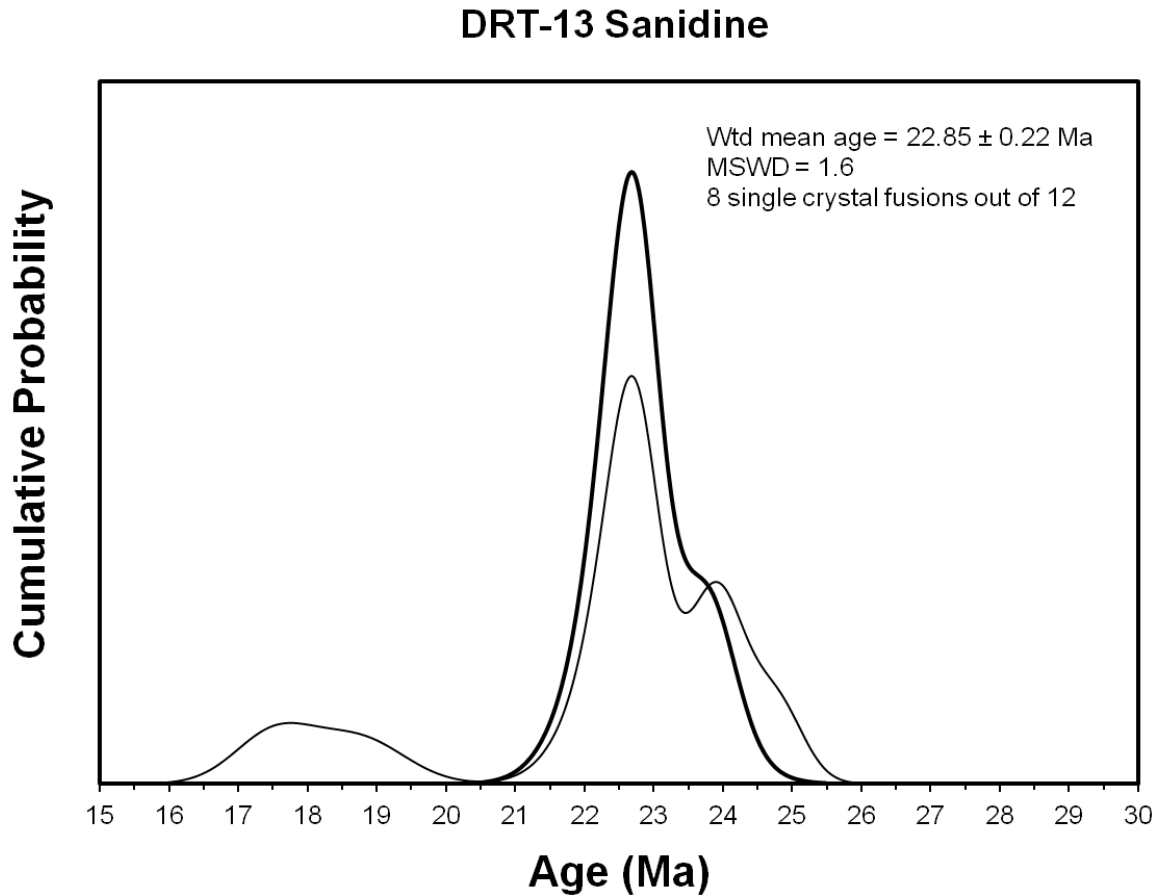


Figure 16: Cumulative probability plot for the distribution of the younger age population from DRT-13. The thin line represents the total population of younger crystals while the thick line represents the refined crystal population.

Sample DRT-19 from near the base of TOP 46 had 15 out of 22 single crystal fusions that were K-feldspars. The single crystals yielded a mean age of 469.1 ± 51.1 Ma for the sample (Table 14, Appendix A). These data do not define an isochron or a weighted mean age. The preferred age for this sample is the mean age of 469.1 ± 51.1 Ma (Table 1) and is again believed to reflect the age of the basement.

Sample DRT-24 was collected in the northern region of Nakwai, with 15 of the 20 single crystals fused being K-feldspars. The 15 single crystals from this sample yielded a mean age of 423.2 ± 73.3 Ma (Table 15, Appendix A). There is no isochron or weighted mean age for this

sample so the preferred age for DRT-24 is 423.2 ± 73.3 Ma (Table 1) and is again thought to reflect the age of the basement.

Paleontology

Measurements of six upper and 19 lower *Meroëhyrax kyongoi* molars from Nakwai were taken along with three lower molars from *M. bateae* and seven upper and 12 lower molars of *Paraplioxyrax ngororaensis* (Table 1, Appendix B). All species used for comparison in this study are members of the family Plioxyracidae (Rasmussen and Gutierrez, 2010).

Comparisons in tooth size were made to illustrate the difference in size among the three species. The mesiodistal length (MD) multiplied by the average (AvgW) of the mesial width (MW) and distal width (DW) yielded an approximate area for the base of each tooth and is reported as tooth size, recorded in mm^2 for each specimen.

For the upper molars there is a definite size difference between *M. kyongoi* and *P. ngororaensis* (Figure 17). The upper tooth size for *M. kyongoi* varies from $127.5\text{-}143.5$ mm^2 for the first molar (M1), 212.1 mm^2 for the second molar (M2), and $188.0\text{-}229.6$ mm^2 for the third molar (M3). The *P. ngororaensis* has upper tooth sizes that vary from $165.3\text{-}325.6$ mm^2 for M1, $225.4\text{-}307.1$ mm^2 for M2, and $278.4\text{-}483.0$ mm^2 for M3. The lower molars also show a larger size difference between *M. kyongoi* and *P. ngororaensis* than the upper molars, with the *M. bateae* specimens being similar in size to the *M. kyongoi* specimens (Figure 18). The lower molars of *M. kyongoi* range in size from $49.6\text{-}85.9$ mm^2 for m1, $66.8\text{-}112.6$ mm^2 for m2, and $110.6\text{-}144.3$ mm^2 for m3. The *M. bateae* specimens range in size from 71.5 mm^2 for m1, 68.4 mm^2 for m2 and 110.8 mm^2 for m3. The lower tooth size for *P. ngororaensis* range from $116.4\text{-}162.5$ mm^2 for m1, $168.3\text{-}233.0$ mm^2 for m2, and $212.9\text{-}286.6$ mm^2 for m3.

Figure 17

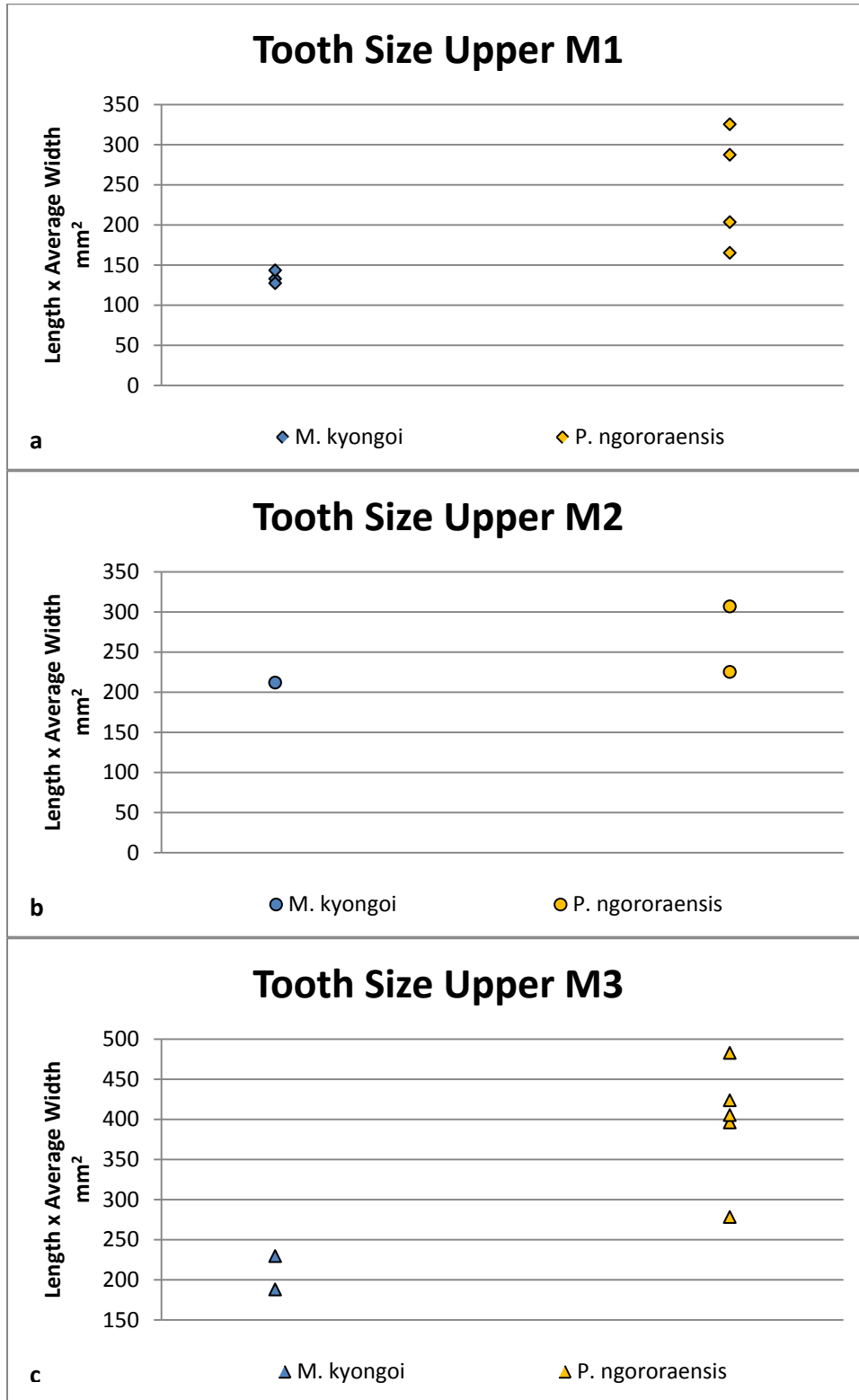


Figure 17: Upper molar size with *M. kyongoi* (blue marker) compared to *P. ngororaensis* (yellow marker): (a) first molar (M1), (b) second molar (M2), and (c) third molar (M3).

Figure 18

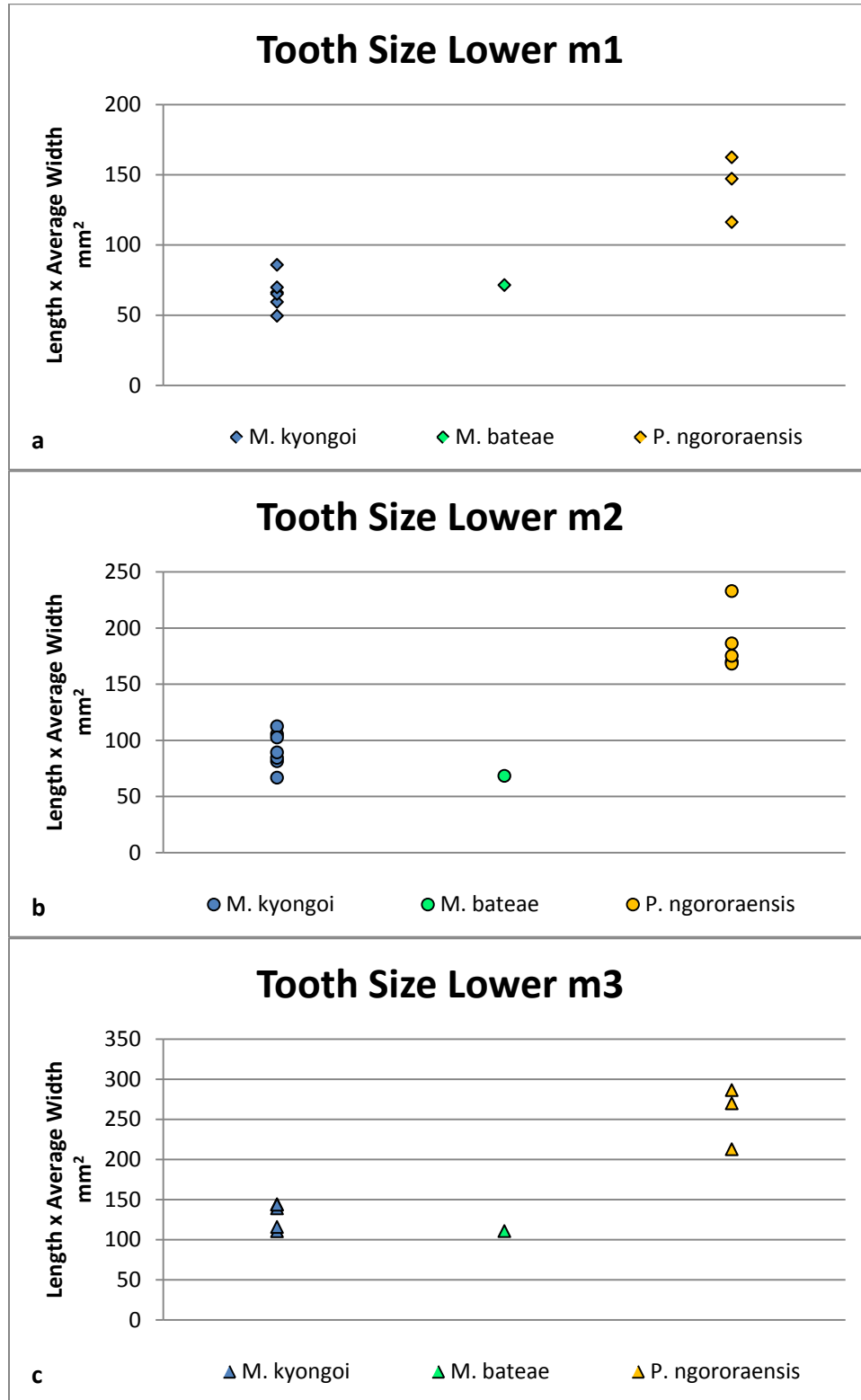


Figure 18: Lower molar size with *M. kyongoi* (blue marker) compared against *M. bateae* (green marker) and *P. ngororaensis* (yellow marker): (a) first molar (m1), (b) second molar (m2), and (c) third molar (m3).

Mesiodistal length was compared to MW, DW, and the AvgW using bivariate plots to discern whether there is any correlation between the measurements (Table 2). When comparing all of the measurements of the three upper molars of the *M. kyongoi* and *P. ngororaensis* the correlation is significant with the MD vs MW being $r=0.63$, $p=0.007$, MD vs DW of $r=0.51$, $p=0.046$, and the MD vs AvgW being $r=0.78$, $p=0.0002$ (Figure 19). When the data are examined by the tooth number (i.e. M1, M2, or M3), the majority of the correlations are not statistically significant (Figure 1, Appendix B). When conducting the same comparisons on the lower molars from all three species of hyrax all length to width correlations are statistically significant (Table 3; Figure 2, Appendix B).

Figure 19

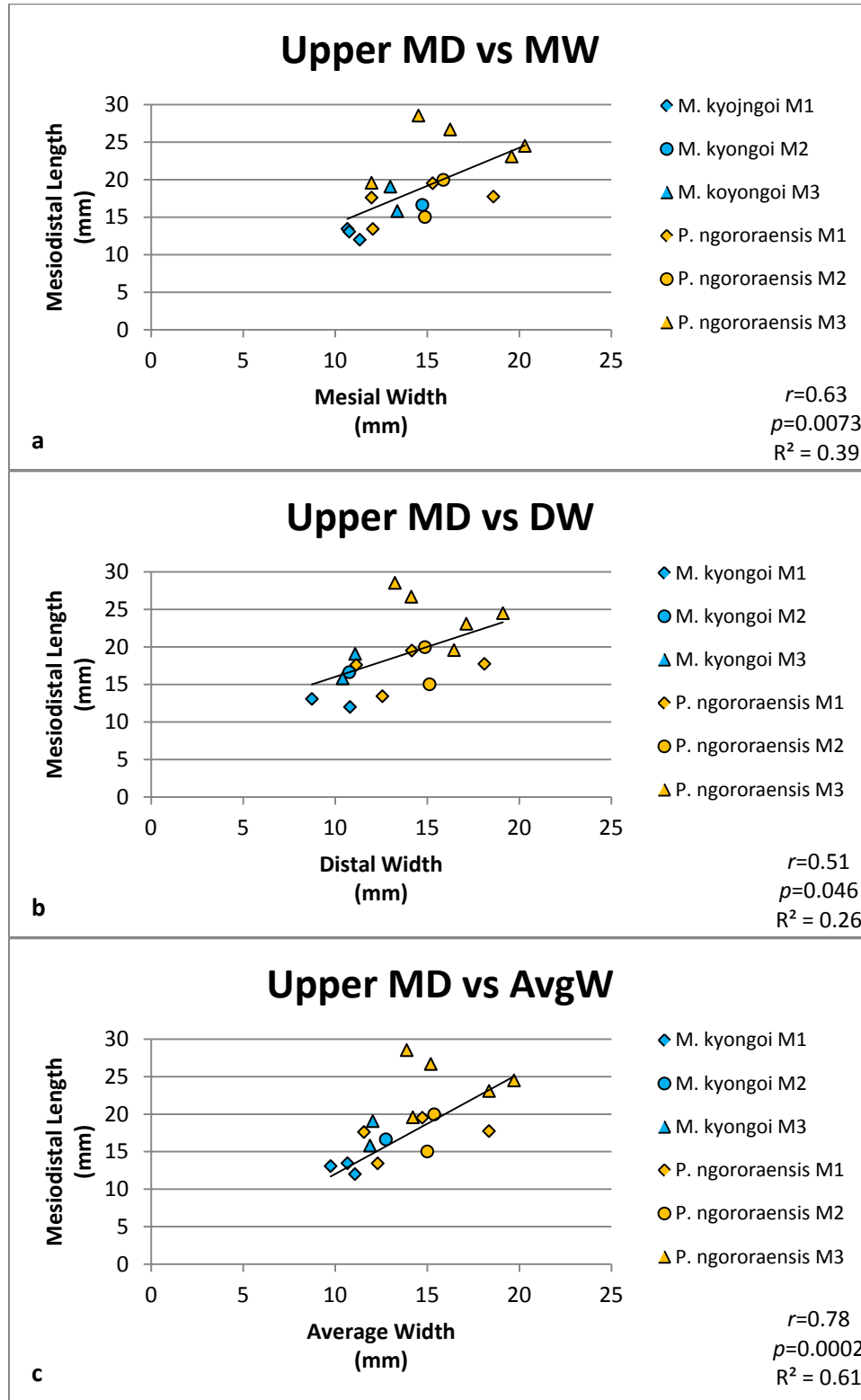


Figure 19: Upper mesiodistal length (MD) with (a) mesial width (MW), (b) distal width (DW), and (c) average width (AvgW) of *M. kyongoi* (blue marker) and *P. ngororaensis* (yellow marker). The line represents the linear regression of the measurements within the graph.

Table 2

	<i>r</i>	<i>p</i>
Lower MD vs MW	0.79	<0.0001
Lower MD vs DW	0.69	<0.0001
Lower MD vs AvgW	0.68	<0.0001
Lower MD vs MW m1	0.85	0.002
Lower MD vs MW m2	0.88	<0.0001
Lower MD vs DW m3	0.86	0.02
Lower MD vs DW m1	0.79	0.006
Lower MD vs DW m2	0.84	0.0003
Lower MD vs DW m3	0.91	0.0007
Lower MD vs AvgW m1	0.83	0.003
Lower MD vs AvgW m2	0.87	0.0001
Lower MD vs AvgW m3	0.90	0.001

Table 2: Correlation coefficients (*r*) and significance (*p*) for mesiodistal length (MD) to mesial width (MW), distal width (DW), and average width (AvgW) of the lower molars from *M. kyongoi*, *M. bateae*, and *P. ngororaensis*.

Comparisons were also made between MD and the three crown height measurements: protocone height (PH), paracone height (PaH), and height to the base of the valley between the protocone and the hypocone (PHV) on the upper molars; and protoconid height (PH), metaconid height (MH), and talonid basin (TB) for the lower molars (Table 2). The correlation between the MD and the crown height measurements (PH, PaH, and PHV) for the upper molars is very weak so these comparisons were not separated by tooth number (Figure 20). In the case of the lower molars, MD vs PH and MD vs MH are weakly correlated ($r=0.51$, $p=0.11$ and $r=0.47$, $p=0.15$ respectively) but approach statistical significance, while the MD vs TB is very weakly correlated (Figure 21). These comparisons were separated by tooth number but did not yield greater correlation strength or statistical significance (Figure 3, Appendix B).

Figure 20

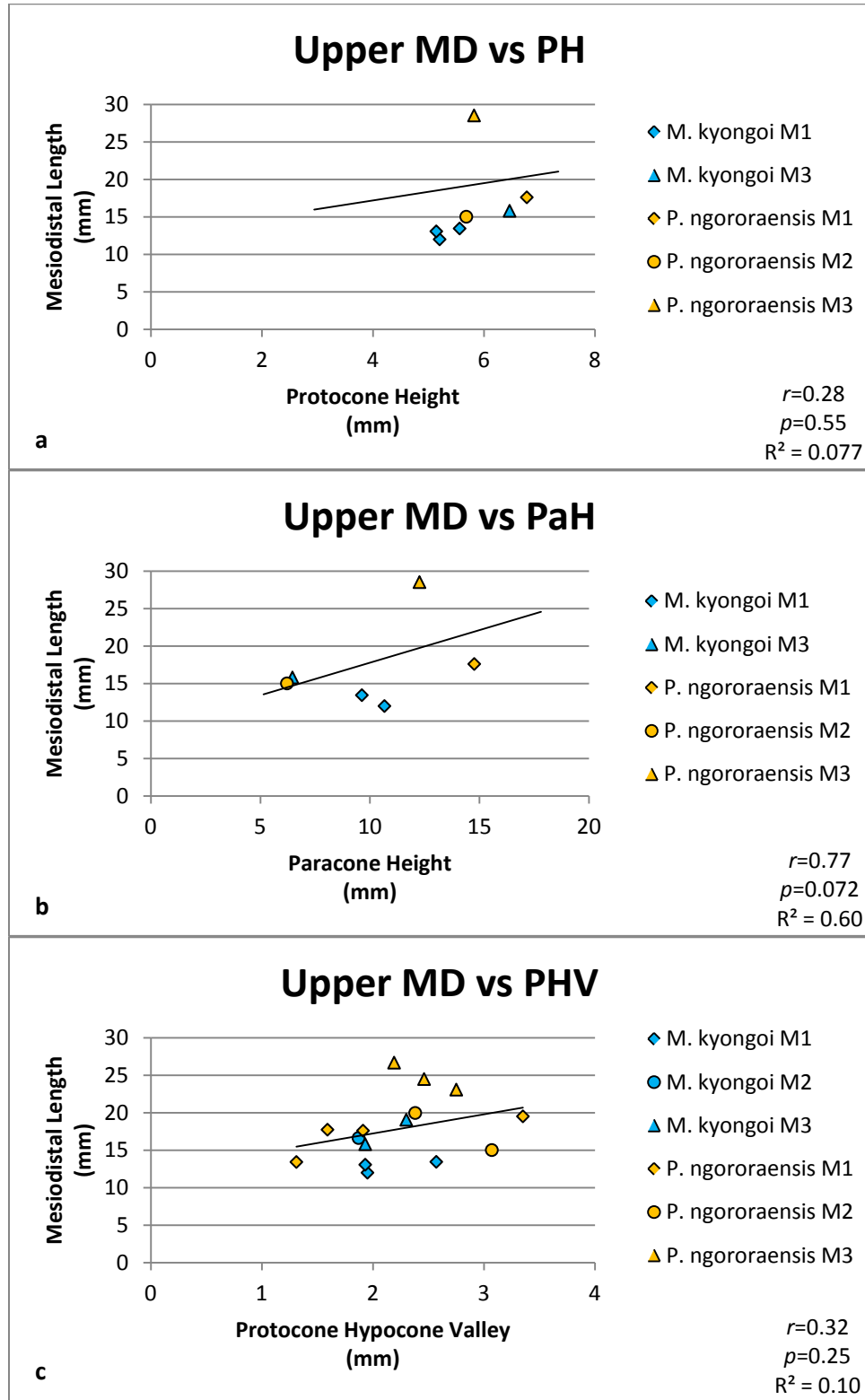


Figure 20: Upper molar mesiodistal length (MD) compared to the three crown height measurements. The crown height measurements are: (a) protocone height (PH), (b) paracone height (PaH), and (c) the height of the valley between the protocone and hypocone (PHV). Comparisons were made between *M. kyongoi* (blue marker), and *P. ngororaensis* (yellow marker). The line represents the linear regression of the measurements within the graph.

Figure 21

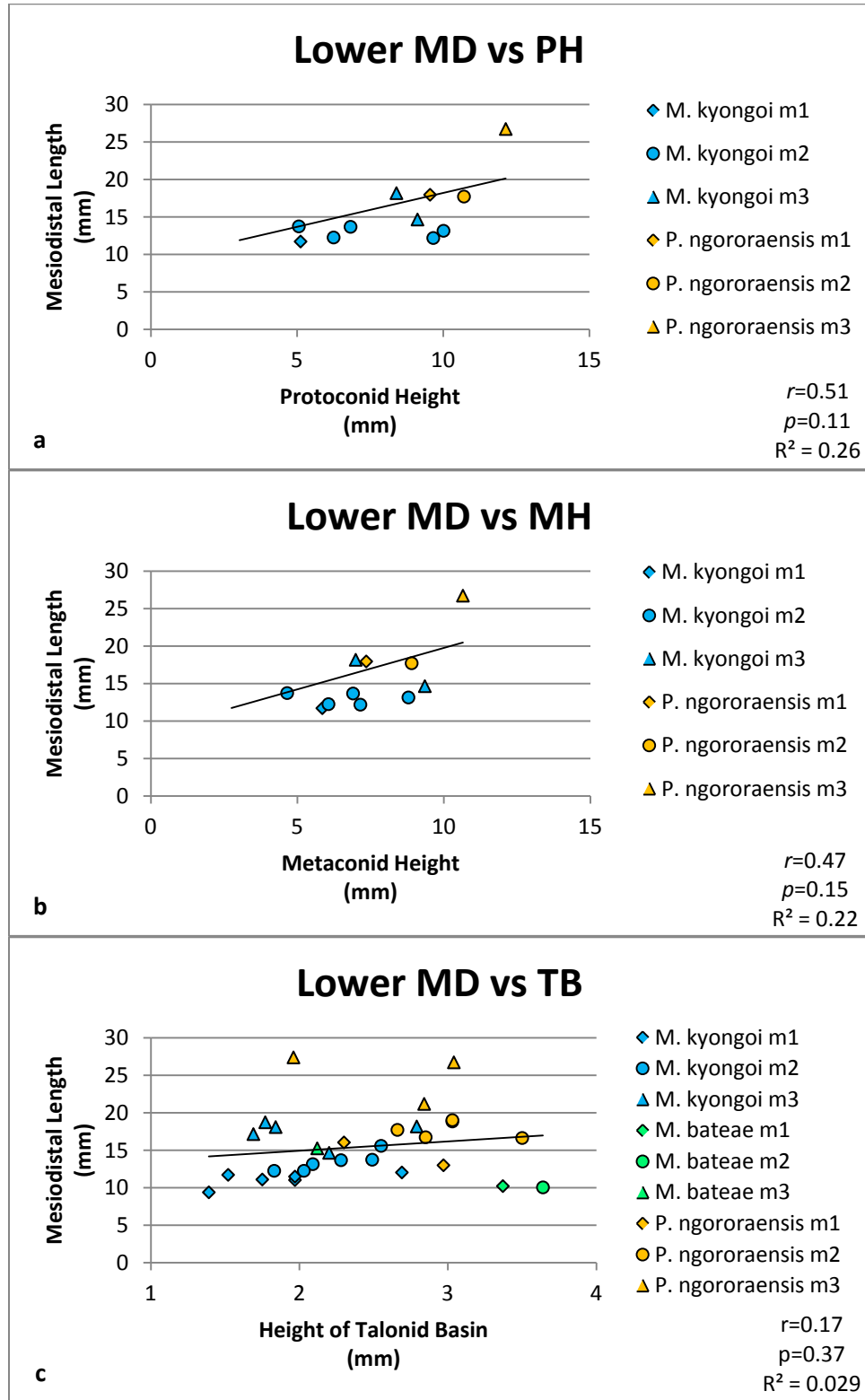


Figure 21: Lower molar mesiodistal length (MD) compared to the three crown height measurements. The crown height measurements are: (a) protoconid height (PH), (b) metaconid height (MH), and (c) the height of the talonid basin (TB). Comparisons were made between *M. kyongoi* (blue marker), *M. bateae* (green marker), and *P. ngororaensis* (yellow marker). The line is the linear regression of the measurements within the graph.

The morphology of the molars of members of Pliohyracidae are described as being hypsodont with this morphology used as a way to distinguish pliohyracids from other hyrax families (Ducrocq et al., 2010; Rasmussen and Gutierrez, 2010). In order to establish the degree of hypsodonty, a Hypsodonty Index (HI) was determined for the lower molars of the three species of hyrax in this study, following the guidelines of Janis (1988). The lower molars were chosen because they have a stronger correlation between the MD and crown height measurements than the upper molars. Following Janis (1988), qualifying degrees of hypsodonty is as follows: HI values greater than 1.5 are considered hypsodont while HI values of less than 1.5 are considered brachydont. However, teeth with HI values greater than 1.5 can be further divided, with HI values from 1.5 to 3 considered mesodont. Other researchers use slightly different definitions, considering HI values greater than 1.2 classified as hypsodont, HI values from 0.8 to 1.2 as mesodont, and HI values below 0.8 as brachydont (Fortelius et al., 2006; Koenigswald, 2011).

Unworn teeth are preferred for taking crown height measurements, but few unworn teeth were available for this study. Teeth that were moderately to heavily worn were excluded because full crown height is required to define HI as accurately as possible. Crown height measurements from the protoconid (PH; Figure 22) and the metaconid (MH; Figure 23) were used to determine two separate HI values for each molar. *M. kyongoi* has a PH HI value of 0.44 for the first molar (m1), 0.37 to 0.76 for the second molar (m2), and 0.46 for the third molar (m3), a MH HI value of 0.5 for m1, 0.5 to 0.67 for m2, and 0.38 for m3. Thus, the lower molars are considered brachydont in comparison to other herbivorous mammals. *M. bateae* has a PH HI value of 0.59 for m1, 0.68 for m2, and 0.41 for m3, a MH HI value of 0.53 for m1, no MH HI values for m2, and 0.38 for m3. These results indicate that it is also brachydont. *Parapliohyrax ngororaensis* has a PH HI value of 0.5 for m2, 0.45 for m3, and no PH HI values for m1, a MH HI

value of 0.47 for m2, 0.4 for m3, and no MH HI values for m1. These measurements also indicate brachydonty.

Figure 22

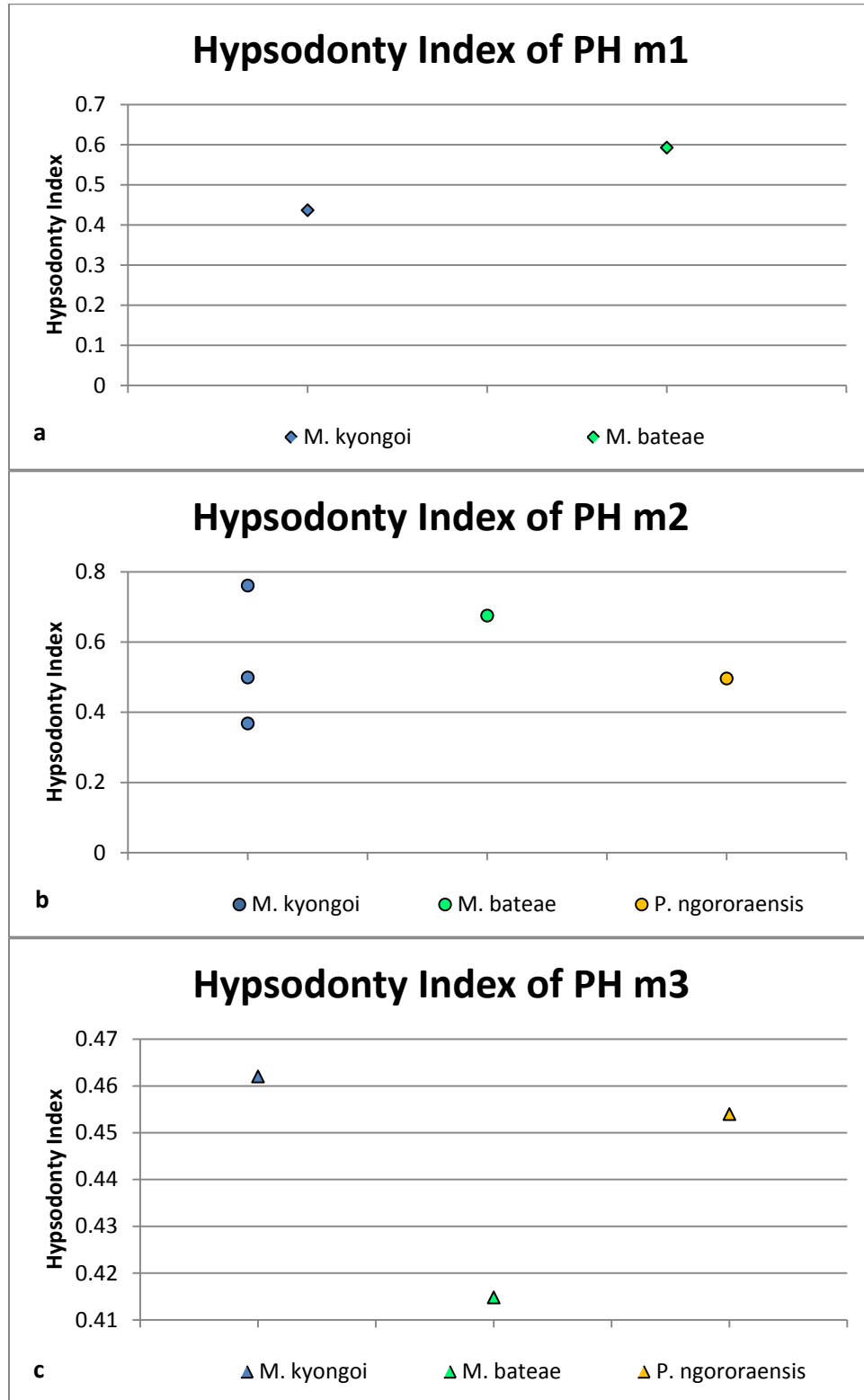


Figure 22: Hypsodonty Index of the lower molars using the protoconid height (PH) as the measurement for height of the crown. All teeth that were considered moderately to heavily worn were excluded from these comparisons. Comparisons are between *M. kyongoi* (blue marker), *M. bateae* (green marker), and *P. ngororaensis* (yellow marker) and are separated by tooth number.

Figure 23

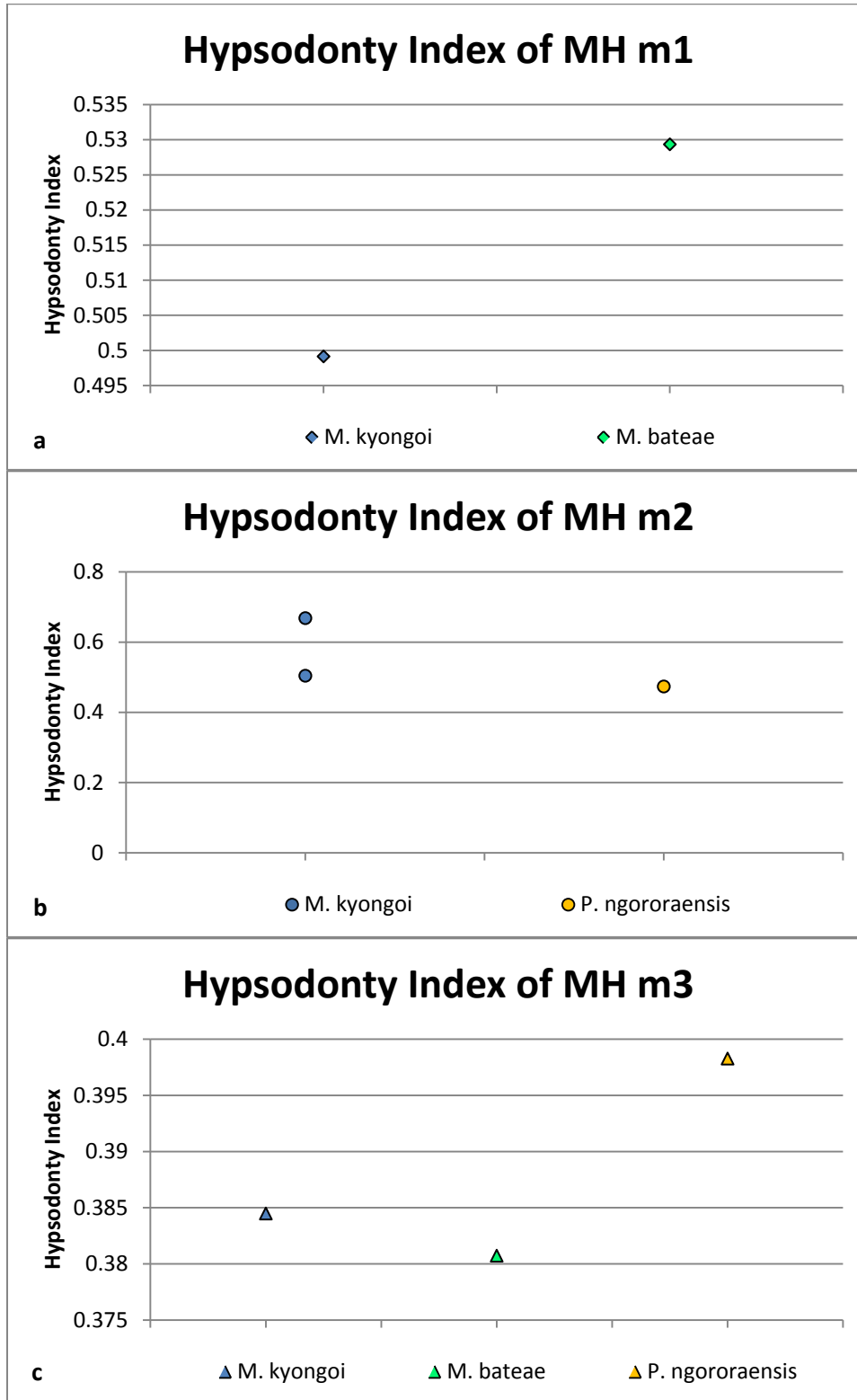


Figure 23: Hypsodonty Index of the lower molars, separated by tooth number, using the metaconid height (MH) as the measurement for height of the crown. All teeth that were considered moderately to heavily worn were excluded from these comparisons. Comparisons are between *M. kyongoi* (blue marker), *M. bateae* (green marker), and *P. ngororaensis* (yellow marker).

CHAPTER 5

DISCUSSION

The paleontological record of the Turkana Basin is especially important for understanding the African Mid-Tertiary Event (AMTE). Several fossil-bearing sites from the Turkana Basin have been dated, ranging from the late Oligocene through the early Miocene. However, the fossil record through the AMTE is not continuous (Gutierrez, 2011; Leakey et al., 2011). The timing of the AMTE is thought to be at, or near, the Oligocene – Miocene boundary (~23 Ma); studying fossil localities that date to the late Oligocene and early Miocene is thus crucial to understanding the early stages of this faunal transition. A large temporal gap in the East African fossil record occurs just prior to the Oligocene – Miocene boundary at ~24 Ma and continues until the previously recorded early Miocene sites which have been dated starting at ~20 Ma (Boschetto et al., 1992; Gutierrez, 2011; Kappelman et al., 2003; Leakey et al., 2011; Werdelin, 2010).

Prior to the $^{40}\text{Ar}/^{39}\text{Ar}$ dating of the basalts, volcanoclastic mudstones/siltstones, and air fall tuffs in this study, the Nakwai region was thought to be one of the Turkana Basin's late Oligocene fossil localities. This age was based on biostratigraphic evidence that suggested that the fossils from Nakwai were contemporaneous with those from the Eragaleit beds, a fossiliferous section of Losodok (Rasmussen and Gutierrez, 2009). Whole rock K-Ar analyses of the Eragaleit basalts directly above and below the fossiliferous units provide age constraints of 24 Ma to 27 Ma (Boschetto et al., 1992). The new earliest Miocene age of 23 Ma refutes the hypothesis that the uppermost sediments of Nakwai are exactly contemporaneous with those at Losodok and serve to underscore the importance of Nakwai to understanding the AMTE. This conclusion has important implications for the assessment of the fauna because the mammalian faunas of the late Oligocene are fundamentally different from those of the early Miocene

(Gutierrez, 2011; Rasmussen and Gutierrez, 2009). With the uppermost portion of Nakwai now dated to the earliest Miocene, it helps to fill in this temporal gap in the fossil record. This result gives researchers the opportunity to study a more continuous fossil record through the AMTE, and will offer further insights into the dynamics of the event.

It was not until recently that there were any publications describing the fauna from Nakwai and from Losodok. Although the faunas at these two sites are very similar, there are more larger bodied individuals preserved at Losodok; this difference between the sites suggests the presence of a taphonomic bias (Gutierrez, 2011). The faunas from these two localities were described as a new late Oligocene fauna by Rasmussen and Gutierrez (2009), but this conclusion should be considered provisional until more work has been completed. Rasmussen and Gutierrez (2009) were the first to describe the Nakwai fauna; after this publication researchers did not differentiate between the faunas of Nakwai and Losodok and instead have referred to them as one group (Gutierrez, 2011; Leakey et al., 2011). Due to the grouping of the Nakwai and Losodok fauna, the faunal list from the Rasmussen and Gutierrez (2009) publication will have to be re-examined in order to discuss how these dates affect previous ideas and the potential implications to the AMTE.

Rasmussen and Gutierrez (2009) discuss several mammal species found at both Losodok and Nakwai which represent the latest occurrences of these mammals in the region. For example, the pachyhyracine hyracoids, *Thyrohyrax*, and *Arsinoitherium* (order Embrithopoda), had not been identified from any of the previously known early Miocene sites and were thought to have been extinct by the Miocene. With Nakwai now established as a unique early Miocene site, it extends the most recent record of the pachyhyracine hyracoids and *Thyrohyrax* beyond the Oligocene – Miocene boundary. There were no *Arsinoitherium* specimens recovered from Nakwai, which supports the idea that they were extinct by the end of the Oligocene (Rasmussen

and Gutierrez, 2009). The absence of *Arsinoitherium* also supports the idea of taphonomic bias between the Nakwai and Losodok localities (Gutierrez, 2011). There were also several other species of mammals recovered from Losodok/Nakwai, including *Brachyhyrax*, *Afrohyrax*, *Meroëhyrax*, *Prodeinotherium* (order Proboscidea), and *Diamantomys* (order Rodentia) (Rasmussen and Gutierrez, 2009). The new dates for Nakwai do not affect the current position that these are the oldest occurrences for these species since they were found in both localities. The only exception is *Prodeinotherium* (only recovered from Losodok), and this discovery further supports the idea of taphonomic bias.

One of the most important specimens described is *Miopriodon hodopeus*, a true carnivoran and potentially one of the very first immigrants from Eurasia during the AMTE (Rasmussen and Gutierrez, 2009). *Miopriodon hodopeus* has not been recorded from Losodok, and the presences of this species at Nakwai suggests that the first Eurasian immigrants may not have arrived in Africa until after the Oligocene – Miocene boundary. If ongoing research at Nakwai continues to record the presence of the first Eurasian immigrants, then it will help further constrain the timing of the AMTE and potentially establish it as an early Miocene event.

The upper portion of the sedimentary succession at Nakwai has now been dated at 22.85 Ma with the oldest capping basalt yielding an age of 17.02 Ma (Appendix A, Table 8). The basalts that cap most of the sediments appear to have erupted in quick succession with many of the uncertainties overlapping at 1σ and little evidence of soil formation between flows. In the far north region of Nakwai, the capping basalts were dated to 16.91 Ma, making them statistically indistinguishable from the other capping basalts throughout Nakwai. The basalts from TOP 106 are unlike the basalts found in other areas of Nakwai in that they are much younger in age, with sample DRT-18 dating to 15.64 Ma and sample DRT-15 to 14.39 Ma, with

fossiliferous limestones in between. This limestone unit indicates that there was a body of water, possibly a lake, present for a period of time between these flows. Sample DRT-17 (which was determined to be unsuitable for dating) was collected from a basalt outcrop found stratigraphically between DRT-18 and the limestone unit. This basalt outcrop has jointing and weathering patterns that suggest that it is a pillow basalt, indicating that this flow had erupted at least partly in water, thus offering additional support of the presence of a lake. (See Figure 24 for a general stratigraphic relationship based on the $^{40}\text{Ar}/^{39}\text{Ar}$ ages.)

Figure 24

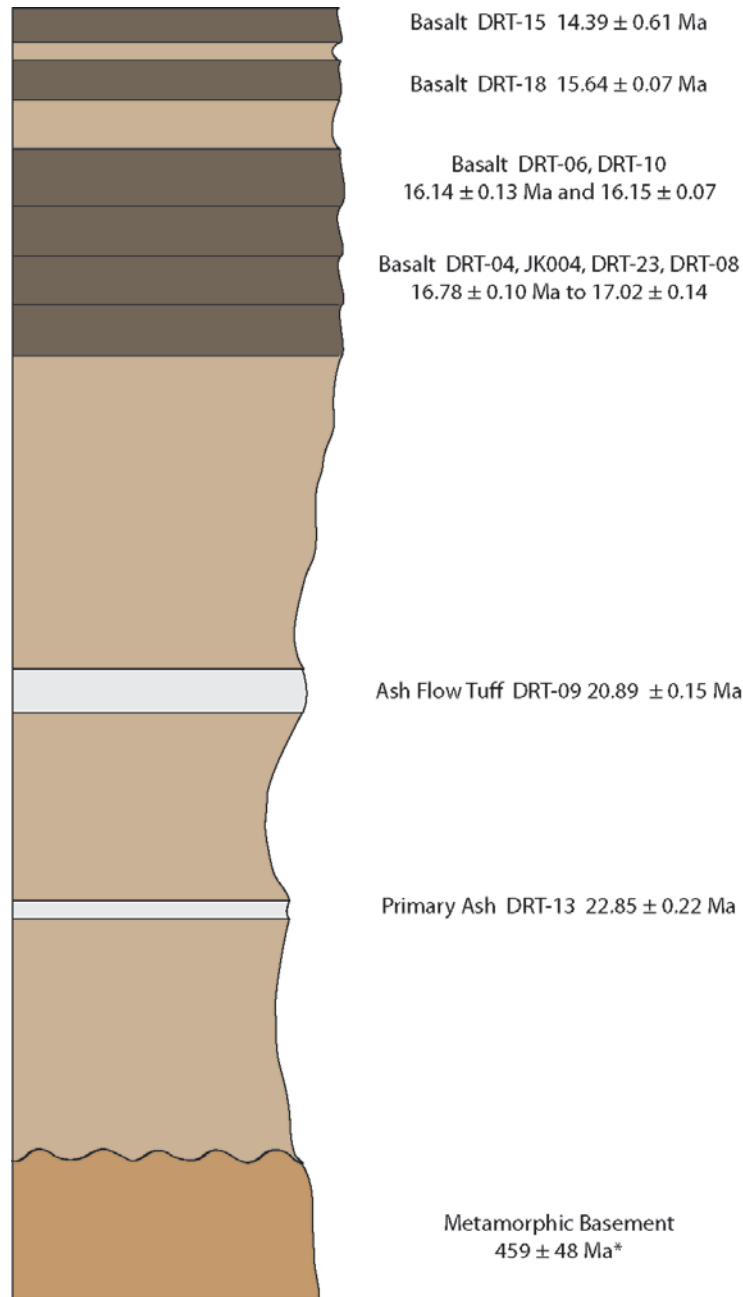


Figure 24: Generalized stratigraphic column of Nakwai. Stratigraphy is based on the $^{40}\text{Ar}/^{39}\text{Ar}$ dates presented in this study. This column is not scaled to represent the actual thickness of units within Nakwai.

* The older populations of single crystals that were found while dating the ash units near the base of the section are inferred to be xenocrysts from the metamorphic basement. The age for the metamorphic basement in this figure is the average of all the older crystal populations. These ages are very similar to the previously recorded K-Ar ages of 433 to 522 Ma for the Turkana Basin; these are regarded as cooling ages of the Pan African Orogeny (Brown and McDougall, 2011).

The original hypothesis of this study regarding dentition was that by comparing the dental measurements a trend of a difference in hypsodonty would emerge by following the Pliohyracidae family. The comparison of dental measurements among *Meroëhyrax kyongoi*, *Meroëhyrax bateae*, and *Parapliohyrax ngororaensis* yielded some surprising results. The data indicates that although the size of tooth size differed by species and increased through time, the degree of hypsodonty remained constant. The sample size in this study was not large enough to be representative of the Pliohyracidae family and it did not include specimens of the genus *Prohyrax*. In order to obtain a more representative view on the degree of hypsodonty in this hyrax family, a more comprehensive study including numerous specimens from all three genera of pliohyracines is necessary.

Hypsodonty has been used as a way to describe the difference in morphology between different genera of fossil hyracoids (Rasmussen and Gutierrez, 2010). In the descriptive sense for hyraxes, hypsodonty is an extremely useful term; however, the crown height measurements from the pliohyracines in this study do not represent hypsodonty and are considered instead to be brachydont. The Hypsodonty Index (HI) was created as a way to standardize crown height measurements so that comparisons could be made across a wide variety of herbivores. The HI values for the hyracoids determined in this study indicate that all three species are brachydont when compared to other hypsodont herbivores (Results, Figure 20). Only one crown height measurement from *Meroëhyrax kyongoi* approached a mesodont value, following the HI criteria of Fortelius et al., (2006) and Koenigswald, (2011). The absence of evolutionary trends in hypsodonty could indicate that there were not any changes in environmental factors that would affect a change in hypsodonty or that there simply was not enough time for a trend to emerge.

Selenodonty has also been a very useful term for describing the dental morphology of fossil hyracoids and offers some insight into what types of vegetation they ate. There is,

unfortunately, no quantitative measure for the degree of selenodonty. Selenodonty in artiodactyls is defined by the mesial and distal extension of the main cusps in the form of cristids that form continuous crescent shaped enamel ridges (Sánchez et al., 2010). Following this definition of selenodonty some hyracoids, including those in this study, do possess selenodont lower cheek teeth. Selenodonty in hyracoids differs from selenodonty in modern artiodactyls; hyraxes have only a single row of crescents as opposed to the lingual and buccal crescents of modern artiodactyls. This difference illustrates the variability in this dental characteristic between these two groups. Prior to the geographic contact between Afro-Arabia and Eurasia, hyracoids were a very diverse group of mammals that filled a variety of niches (Leakey et al., 2011). The presence of selenodonty in some hyraxes could be a characteristic that they evolved to lessen competition for resources, thus creating the niches that were eventually taken over by the artiodactyl immigrants from Eurasia.

CHAPTER 6

CONCLUSIONS

The new $^{40}\text{Ar}/^{39}\text{Ar}$ dates from the Nakwai region constrain the upper age of the Nakwai sedimentary sequence from 22.85 Ma to 17.02 Ma in the main section. Ages of 15.64 Ma – 14.39 Ma were obtained in the TOP 106 section which is to the north of the main sequence. These dates place the upper portion of the Nakwai fossiliferous sections in the earliest Miocene, thus filling in a temporal gap between the nearby late Oligocene fossiliferous locality of Losodok, and other early Miocene localities (of ~20 Ma) in the region. The fauna from Nakwai bridges the gap between the distinctly different late Oligocene and early Miocene faunas. The Nakwai fauna includes specimens of *Thyrohyrax* and pachyhyracine hyracoids which are holdovers from the Oligocene that were previously thought to have gone extinct by the end of the Oligocene. A true carnivoran, *Miopriodon hodopeus*, has also been recovered from Nakwai. This carnivoran is potentially one of the first immigrants from Eurasia, and its presence may offer some of the earliest evidence of the faunal transition of the AMTE. The early Miocene arrival of these Eurasian immigrants suggests that the timing of the AMTE is at the Oligocene – Miocene boundary or during the very early Miocene.

The dental comparisons among *Meroëhyrax kyongoi*, *Meroëhyrax bateae*, and *Paraplioxyrax ngororaensis* show an increase in tooth size between the early Miocene species (*Meroëhyrax spp.*) and the mid Miocene species (*Paraplioxyrax ngororaensis*). The crown height measurements from the three species were used to determine the degree of hypsodonty using the Hypsodonty Index (HI). When comparing the HI from all three species, there was no discernible increase in hypsodonty through time. When compared to other hyracoid specimens from Nakwai (e.g. *Brachyhyrax*), *Meroëhyrax spp.* and *Paraplioxyrax ngororaensis* appear to be hypsodont; however, the HI indicates that they are brachydont when compared to other

herbivores. Although these hyracoids are not technically hypsodont, the use of this term in a strictly descriptive sense is very helpful when describing the overall tooth morphology. Similarly the term selenodonty has been very useful in a qualitative description of the dental morphology of certain hyracoids. Although there is as yet no way to quantify the degree of selenodonty, the lower molars of *Meroëhyrax* and *Paraplioxyrax* are selenodont in that the enamel ridges of the occlusal surface form continuous crescent shaped ridges.

The $^{40}\text{Ar}/^{39}\text{Ar}$ ages of Nakwai and ongoing research in the region will give further insight into the timing of the AMTE. Studying the faunal assemblages from Nakwai and other fossil localities through this period of the faunal transition will help to further our understanding of the dynamics of the AMTE. Although *Meroëhyrax kyongoi*, *Meroëhyrax bateae*, and *Paraplioxyrax ngororaensis* are not considered hypsodont, more research is needed to determine if there are evolutionary trends in crown height in the Plioxyracidae family.

APPENDIX A: $^{40}\text{Ar}/^{39}\text{Ar}$ DATA TABLES

Table 1

Reynoso-UNLV, DRT-15, Basalt Groundmass, 33.78 mg, J = 0.001745 ± 0.52%														
4 amu discrimination = 1.0522 ± 0.07%, 40/39K = 0.0243 ± 80.90%, 36/37Ca = 0.000239 ± 8.17%, 39/37Ca = 0.000655 ± 3.50%														
step	T (C)	t (min.)	36Ar	37Ar	38Ar	39Ar	40Ar	% 40Ar*	% 39Ar rlsd	Ca/K	40Ar*/39ArK	Age (Ma)	1s.d.	
1	960	12	0.284	0.151	0.077	0.815	74.790	6.3	3.4	10.5387248	3.005840	9.44	2.03	
2	1040	12	0.313	0.362	0.119	2.590	91.050	19.9	10.7	7.9443341	4.227242	13.26	1.16	
3	1130	12	0.227	1.807	0.145	4.434	75.399	60.1	18.3	23.2647074	4.668682	14.64	0.34	
4	1210	12	0.571	33.210	0.440	12.718	144.101	45.3	52.6	154.607326	3.841139	12.05	1.24	
5	1400	12	0.399	22.462	0.162	3.619	80.045	38.1	15.0	391.201358	4.671244	14.65	3.14	
Cumulative %39Ar rlsd =									100.0	Total gas age =		12.96	0.60	
note: isotope beams in mV, rlsd = released, error in age includes J error, all errors 1 sigma											Plateau age =		14.39	0.61
(36Ar through 40Ar are measured beam intensities, corrected for decay for the age calculations)											(steps 2-5)			
											Isochron age =		10.60	1.50
											(steps 1-4)			

Table 1: Sample DRT-15 Basalt Groundmass Step Heating Data

Table 2

Reynoso-UNLV, DRT-18, Basalt Groundmass, 68.50 mg, J = 0.001749 ± 0.47%														
4 amu discrimination = 1.0522 ± 0.07%, 40/39K = 0.0243 ± 80.90%, 36/37Ca = 0.000239 ± 8.17%, 39/37Ca = 0.000655 ± 3.50%														
step	T (C)	t (min.)	36Ar	37Ar	38Ar	39Ar	40Ar	% 40Ar*	% 39Ar rlsd	Ca/K	40Ar*/39ArK	Age (Ma)	1s.d.	
1	720	12	1.176	2.553	3.811	77.319	687.856	55.2	11.7	1.88384096	4.729898	14.86	0.15	
2	780	12	0.330	1.308	2.469	45.192	312.143	79.6	6.8	1.65119009	4.969607	15.61	0.16	
3	830	12	0.426	3.043	3.230	69.828	451.934	80.5	10.5	2.48671787	4.887455	15.36	0.13	
4	880	12	0.544	2.714	2.705	74.036	521.363	76.4	11.2	2.09156913	5.095894	16.01	0.13	
5	940	12	0.420	1.474	1.716	69.770	471.629	83.1	10.5	1.20510393	5.244916	16.47	0.11	
6	1000	12	0.352	1.308	1.293	69.930	445.958	86.7	10.5	1.06689792	5.133306	16.13	0.10	
7	1060	12	0.279	1.872	1.060	61.964	376.644	90.3	9.3	1.72355932	5.016602	15.76	0.11	
8	1130	12	0.212	4.405	0.945	55.900	316.851	97.8	8.4	4.49921689	4.880423	15.33	0.12	
9	1210	12	0.610	34.691	1.476	79.458	487.104	85.2	12.0	25.0735586	4.870195	15.30	0.22	
10	1400	12	0.847	59.899	1.176	60.100	418.454	77.1	9.1	57.766793	4.982714	15.65	0.47	
Cumulative %39Ar rlsd =									100.0	Total gas age =		15.64	0.07	
note: isotope beams in mV, rlsd = released, error in age includes J error, all errors 1 sigma											No Plateau			
(36Ar through 40Ar are measured beam intensities, corrected for decay for the age calculations)											No Isochron			

Table 2: Sample DRT-18 Basalt Groundmass Step Heating Data

Table 3

Reynoso-UNLV, DRT-06, Basalt Groundmass, 65.33 mg, J = 0.001712 ± 0.39%														
4 amu discrimination = 1.0614 ± 0.56%, 40/39K = 0.0243 ± 80.90%, 36/37Ca = 0.000239 ± 8.17%, 39/37Ca = 0.000655 ± 3.50%														
step	T (C)	t (min.)	36Ar	37Ar	38Ar	39Ar	40Ar	% 40Ar*	% 39Ar rlsd	Ca/K	40Ar*/39ArK	Age (Ma)	1s.d.	
1	600	12	0.787	2.018	5.741	46.232	423.235	50.7	7.3	3.66477566	4.638567	14.27	0.19	
2	650	12	0.136	1.482	3.821	44.941	263.274	90.1	7.1	2.76798398	5.222360	16.06	0.15	
3	720	12	0.182	3.110	4.684	100.426	563.722	93.6	16.0	2.59927047	5.269402	16.20	0.15	
4	780	12	0.168	3.205	2.949	98.993	560.042	94.3	15.7	2.71753667	5.351081	16.45	0.15	
5	830	12	0.165	2.555	1.778	67.731	395.025	91.9	10.8	3.16672822	5.350101	16.45	0.15	
6	880	12	0.138	2.238	1.153	50.096	295.964	91.6	8.0	3.75090951	5.373300	16.52	0.16	
7	940	12	0.130	1.933	0.914	41.744	247.779	90.8	6.6	3.88807195	5.294232	16.28	0.16	
8	1000	12	0.123	1.379	0.774	36.455	215.633	89.7	5.8	3.17552565	5.185448	15.95	0.15	
9	1060	12	0.108	1.467	0.711	36.849	212.893	91.7	5.9	3.34220793	5.176302	15.92	0.15	
10	1130	12	0.166	4.987	0.884	44.408	254.798	92.4	7.1	9.44409875	5.188388	15.95	0.16	
11	1210	12	0.373	25.197	0.813	25.254	156.128	83.4	4.0	85.7254316	5.086155	15.64	0.69	
12	1400	12	0.326	18.406	1.120	36.323	221.130	85.6	5.8	43.0211588	5.044680	15.51	0.37	
Cumulative %39Ar rlsd =									100.0	Total gas age =		16.03	0.09	
note: isotope beams in mV, rlsd = released, error in age includes J error, all errors 1 sigma											Plateau age =		16.32	0.13
(36Ar through 40Ar are measured beam intensities, corrected for decay for the age calculations)											No Isochron			

Table 3: Sample DRT-06 basalt Basalt Groundmass Step Heating Data

Table 4

Reynoso-UNLV, DRT-10, Basalt Groundmass, 63.06 mg, J = 0.001734 ± 0.52%														
4 amu discrimination = 1.0522 ± 0.07%, 40/39K = 0.0243 ± 80.90%, 36/37Ca = 0.000239 ± 8.17%, 39/37Ca = 0.000655 ± 3.50%														
step	T (C)	t (min.)	36Ar	37Ar	38Ar	39Ar	40Ar	% 40Ar*	% 39Ar rlsd	Ca/K	40Ar*/39ArK	Age (Ma)	1s.d.	
1	550	12	1.010	0.220	0.390	2.110	287.395	4.6	0.4	5.71650349	5.625886	17.51	2.19	
2	600	12	1.060	0.320	0.537	3.261	370.389	23.8	0.6	5.3795732	25.138740	76.98	2.88	
3	650	12	1.741	0.574	0.872	7.246	502.820	4.7	1.2	4.34144183	3.111999	9.71	0.41	
4	700	12	0.967	0.685	0.906	12.035	301.147	14.1	2.1	3.11827046	3.202960	9.99	0.42	
5	750	12	0.518	1.520	1.833	30.874	288.524	57.3	5.3	2.69691912	4.792731	14.93	0.20	
6	800	12	0.431	4.554	4.613	98.469	624.312	86.3	16.9	2.5333227	5.241254	16.32	0.12	
7	830	12	0.304	3.364	3.467	81.571	477.506	89.4	14.0	2.25882866	4.927800	15.35	0.13	
8	870	12	0.383	4.062	4.155	109.783	669.716	89.2	18.8	2.0264654	5.232868	16.30	0.12	
9	910	12	0.226	2.155	1.954	53.165	359.063	91.8	9.1	2.22013694	5.697225	17.74	0.15	
10	980	12	0.330	2.103	1.144	40.172	297.860	82.3	6.9	2.86783509	5.415791	16.86	0.13	
11	1050	12	0.262	1.780	0.647	28.738	210.451	84.2	4.9	3.39364798	5.156102	16.06	0.12	
12	1120	12	0.288	2.602	0.593	28.852	211.206	82.3	4.9	4.94340446	4.909101	15.29	0.12	
13	1200	12	0.401	9.070	0.745	34.149	263.310	77.1	5.9	14.5987249	5.088698	15.85	0.18	
14	1400	12	0.871	40.452	1.592	52.907	434.937	67.4	9.1	42.3562919	5.146104	16.03	0.38	
Cumulative %39Ar rlsd =									100.0	Total gas age =		16.29	0.07	
note: isotope beams in mV, rlsd = released, error in age includes J error, all errors 1 sigma											No Plateau			
(36Ar through 40Ar are measured beam intensities, corrected for decay for the age calculations)											No Isochron			

Table 4: Sample DRT-10 Basalt Groundmass Step Heating Data

Table 5

Reynoso-UNLV, DRT-04, Basalt Groundmass, 64.99 mg, J = 0.001702 ± 0.35%														
4 amu discrimination = 1.0614 ± 0.56%, 40/39K = 0.0243 ± 80.90%, 36/37Ca = 0.000239 ± 8.17%, 39/37Ca = 0.000655 ± 3.50%														
step	T (C)	t (min.)	36Ar	37Ar	38Ar	39Ar	40Ar	% 40Ar*	% 39Ar rlsd	Ca/K	40Ar*/39ArK	Age (Ma)	1s.d.	
1	650	12	0.244	1.372	0.769	34.990	252.755	77.4	6.9	3.24274951	5.529122	16.90	0.17	
2	720	12	0.291	2.893	0.978	57.184	382.474	82.6	11.2	4.18498155	5.511370	16.84	0.16	
3	780	12	0.365	2.901	0.812	53.143	383.392	77.2	10.4	4.51608603	5.557065	16.98	0.17	
4	830	12	0.166	1.999	0.573	39.903	260.697	87.2	7.8	4.14401989	5.640904	17.24	0.16	
5	880	12	0.119	1.588	0.502	34.870	223.779	90.7	6.8	3.76674766	5.734949	17.52	0.16	
6	940	12	0.138	1.908	0.667	48.341	303.352	91.7	9.5	3.26413879	5.683979	17.37	0.16	
7	1000	12	0.133	1.955	0.757	52.362	315.893	92.5	10.3	3.08755421	5.517616	16.86	0.15	
8	1060	12	0.143	2.262	0.711	45.064	270.494	90.5	8.8	4.15220185	5.349656	16.35	0.15	
9	1130	12	0.241	7.929	0.854	50.747	312.085	89.3	9.9	12.957165	5.418018	16.56	0.18	
10	1210	12	0.320	17.550	0.773	43.392	261.630	88.0	8.5	33.7382555	5.236615	16.01	0.30	
11	1400	12	0.353	16.254	0.900	50.059	315.399	85.5	9.8	27.0340552	5.282289	16.15	0.26	
									Cumulative %39Ar rlsd =	100.0	Total gas age =		16.78	0.10
note: isotope beams in mV, rlsd = released, error in age includes J error, all errors 1 sigma											No plateau			
(36Ar through 40Ar are measured beam intensities, corrected for decay for the age calculations)											No isochron			

Table 5: Sample DRT-04 Basalt Groundmass Step Heating Data

Table 6

Reynoso-UNLV, JK004, Basalt Groundmass, 66.2 mg, J = 0.001645 ± 1.72%														
4 amu discrimination = 1.0614 ± 0.56%, 40/39K = 0.0243 ± 80.90%, 36/37Ca = 0.000239 ± 8.17%, 39/37Ca = 0.000655 ± 3.50%														
step	T (C)	t (min.)	36Ar	37Ar	38Ar	39Ar	40Ar	% 40Ar*	% 39Ar rlsd	Ca/K	40Ar*/39ArK	Age (Ma)	1s.d.	
1	600	12	2.514	1.764	3.140	62.116	1011.320	31.6	8.7	2.44386014	5.184555	15.32	0.42	
2	660	12	0.565	1.476	1.849	52.288	443.934	66.9	7.3	2.42920275	5.672411	16.76	0.36	
3	720	12	0.664	2.238	1.691	71.647	581.632	70.3	10.0	2.68827397	5.720368	16.90	0.33	
4	780	12	0.933	2.288	1.329	70.808	654.898	62.1	9.9	2.78097192	5.766628	17.03	0.34	
5	830	12	0.277	1.345	0.620	40.354	300.469	77.9	5.6	2.8685963	5.760165	17.01	0.33	
6	880	12	0.249	1.220	0.604	41.288	299.080	80.4	5.8	2.54290112	5.778193	17.07	0.33	
7	940	12	0.282	1.598	0.838	58.403	404.576	83.5	8.2	2.35457122	5.749620	16.98	0.33	
8	1000	12	0.177	1.541	0.843	57.398	363.270	89.8	8.0	2.31031193	5.639762	16.66	0.32	
9	1060	12	0.172	2.073	1.044	71.425	431.383	92.0	10.0	2.4976809	5.530264	16.34	0.31	
10	1130	12	0.133	2.009	0.702	44.524	273.823	93.6	6.2	3.88458867	5.639422	16.66	0.32	
11	1210	12	0.597	23.941	2.012	92.823	607.669	94.9	13.0	22.3212095	5.583991	16.50	0.36	
12	1400	12	0.318	9.924	1.132	51.844	343.522	85.2	7.3	16.5389555	5.535364	16.35	0.34	
									Cumulative %39Ar rlsd =	100.0	Total gas age =		16.61	0.12
note: isotope beams in mV, rlsd = released, error in age includes J error, all errors 1 sigma											Plateau age =		16.91	0.32
(36Ar through 40Ar are measured beam intensities, corrected for decay for the age calculations)											(steps 2-8)			
											No Isochron			

Table 6: Sample JK004 Basalt Groundmass Step Heating Data

Table 7

Reynoso-UNLV, DRT-23, Basalt Groundmass, 65.53 mg, J = 0.001752 ± 0.37%														
4 amu discrimination = 1.0614 ± 0.56%, 40/39K = 0.0243 ± 80.90%, 36/37Ca = 0.000239 ± 8.17%, 39/37Ca = 0.000655 ± 3.50%														
step	T (C)	t (min.)	36Ar	37Ar	38Ar	39Ar	40Ar	% 40Ar*	% 39Ar rlsd	Ca/K	40Ar*/39ArK	Age (Ma)	1s.d.	
1	600	12	1.560	1.655	1.285	45.783	722.063	41.1	6.4	3.06438173	6.515446	20.48	0.69	
2	660	12	0.303	1.114	0.901	52.370	368.305	79.8	7.3	1.80258511	5.592685	17.59	0.17	
3	720	12	0.249	1.648	1.196	82.767	505.629	88.5	11.6	1.68724791	5.412845	17.03	0.16	
4	780	12	0.342	2.395	1.379	98.358	605.502	86.4	13.8	2.06357973	5.333644	16.78	0.16	
5	830	12	0.274	2.014	0.929	65.494	419.818	84.8	9.2	2.60645645	5.426898	17.07	0.16	
6	880	12	0.205	1.604	0.692	48.189	310.481	85.4	6.8	2.8214707	5.466184	17.20	0.16	
7	940	12	0.196	1.666	0.773	52.854	332.370	87.3	7.4	2.67176176	5.433605	17.09	0.16	
8	1000	12	0.150	1.578	0.683	45.399	273.818	89.3	6.4	2.94642403	5.303627	16.69	0.16	
9	1060	12	0.140	1.890	0.698	44.777	262.160	90.2	6.3	3.578652	5.196026	16.35	0.15	
10	1130	12	0.103	1.858	0.504	28.939	170.149	94.6	4.1	5.44635	5.336199	16.79	0.16	
11	1210	12	0.385	19.160	1.588	72.180	426.291	89.6	10.1	22.6276002	5.280317	16.61	0.24	
12	1400	12	0.416	17.444	1.771	76.769	461.248	87.1	10.8	19.3516188	5.188044	16.32	0.22	
Cumulative %39Ar rlsd =									100.0	Total gas age =		17.08	0.09	
note: isotope beams in mV, rlsd = released, error in age includes J error, all errors 1 sigma											Plateau age =		16.97	0.14
(36Ar through 40Ar are measured beam intensities, corrected for decay for the age calculations)											(steps 3-8)			
											No Isochron			

Table 7: Sample DRT-23 Basalt Groundmass Step Heating Data

Table 8

Reynoso-UNLV, DRT-08, Basalt Groundmass, 64.51 mg, J = 0.001726 ± 0.48%														
4 amu discrimination = 1.0614 ± 0.56%, 40/39K = 0.0243 ± 80.90%, 36/37Ca = 0.000239 ± 8.17%, 39/37Ca = 0.000655 ± 3.50%														
step	T (C)	t (min.)	36Ar	37Ar	38Ar	39Ar	40Ar	% 40Ar*	% 39Ar rlsd	Ca/K	40Ar*/39ArK	Age (Ma)	1s.d.	
1	600	12	3.518	3.880	2.171	85.756	1358.430	28.8	11.7	3.81944535	4.610977	14.30	0.31	
2	660	12	0.254	2.579	1.189	83.625	518.138	89.0	11.5	2.60254311	5.521291	17.11	0.22	
3	720	12	0.254	3.601	1.717	122.698	719.949	92.3	16.8	2.47658245	5.444459	16.87	0.16	
4	780	12	0.269	2.530	1.381	102.036	621.388	90.1	14.0	2.09212067	5.503136	17.06	0.17	
5	830	12	0.173	1.228	0.672	47.837	304.266	87.8	6.6	2.16602368	5.541068	17.17	0.17	
6	880	12	0.169	0.911	0.453	32.308	220.059	83.3	4.4	2.37937801	5.583543	17.30	0.18	
7	940	12	0.166	0.862	0.422	29.005	199.239	82.0	4.0	2.50787229	5.484981	17.00	0.17	
8	1000	12	0.121	0.994	0.379	25.457	164.947	86.3	3.5	3.295699	5.401023	16.74	0.17	
9	1060	12	0.123	1.297	0.362	23.374	151.420	85.2	3.2	4.6854035	5.307029	16.45	0.18	
10	1130	12	0.129	1.949	0.402	25.327	159.906	89.6	3.5	6.50118265	5.408478	16.76	0.17	
11	1210	12	0.589	21.322	1.866	112.053	687.644	85.8	15.4	16.1196094	5.288557	16.39	0.21	
12	1400	12	0.343	10.605	0.719	40.397	272.602	79.0	5.5	22.2776359	5.188101	16.08	0.25	
Cumulative %39Ar rlsd =									100.0	Total gas age =		16.53	0.10	
note: isotope beams in mV, rlsd = released, error in age includes J error, all errors 1 sigma											Plateau age =		17.02	0.14
(36Ar through 40Ar are measured beam intensities, corrected for decay for the age calculations)											(steps 2-8)			
											No Isochron			

Table 8: Sample DRT-08 Basalt Groundmass Step Heating Data

Table 9

Reynoso-UNLV, DRT-09, Single Crystal Sanidine, J = 0.001702 ± 1.36%													
4 amu discrimination = 1.0614 ± 0.56%, 40/39K = 0.0243 ± 80.90%, 36/37Ca = 0.000239 ± 8.17%, 39/37Ca = 0.000655 ± 3.50%													
4 amu discrimination = 1.0317 ± 0.92% (10)													
Crystal	T (C)	t (min.)	36Ar	37Ar	38Ar	39Ar	40Ar	%40Ar*	Ca/K	40Ar*/39ArK	Age (Ma)	1s.d.	
1	1600	2	0.044	0.026	0.084	5.299	41.736	88.3	0.5783847	6.6206	20.22	0.36	
2	1600	2	0.059	0.032	0.126	8.523	67.743	86.5	0.4425686	6.7042	20.47	0.34	
3	1600	2	0.086	0.031	0.192	13.228	107.164	84.3	0.2762314	6.7543	20.62	0.34	
4	1600	2	0.059	0.023	0.167	11.685	89.904	89.8	0.2320064	6.8030	20.77	0.35	
5	1600	2	0.055	0.026	0.141	9.755	76.212	89.5	0.3141634	6.8482	20.91	0.34	
6	1600	2	0.073	0.028	0.127	7.941	69.013	80.8	0.4156263	6.8607	20.94	0.36	
7	1600	2	0.025	0.027	0.031	1.657	14.751	88.5	1.9494152	6.8782	21.00	0.43	
8	1600	2	0.038	0.017	0.105	7.646	59.305	91.8	0.2620708	6.9095	21.09	0.36	
9	1600	2	0.065	0.019	0.122	8.335	70.172	84.4	0.2686908	6.9441	21.20	0.35	
10	1600	2	0.038	0.019	0.124	9.099	69.492	95.5	0.2461287	7.1230	21.74	0.36	
note: isotope beams in mV rlsd = released, error in age includes J error, all errors 1 sigma										Mean ± s.d. =		20.90	0.40
(36Ar through 40Ar are measured beam intensities, corrected for decay in age calculations)										Wtd mean age =		20.89	0.15
										(10 fusions)			
										No isochron			

Table 9: Sample DRT-09 Single Crystal Sanidine Data

Table 10

Reynoso-UNLV, DRT-22, Single Crystal Sanidine, J = 0.001734 ± 1.52%													
4 amu discrimination = 1.0522 ± 0.07%, 40/39K = 0.0243 ± 80.90%, 36/37Ca = 0.000239 ± 8.17%, 39/37Ca = 0.000655 ± 3.50%													
Crystal	T (C)	t (min.)	36Ar	37Ar	38Ar	39Ar	40Ar	%40Ar*	Ca/K	40Ar*/39ArK	Age (Ma)	1s.d.	
1	1600	2	0.058	0.027	0.817	61.356	448.38	98.8	0.0479294	7.2479	22.53	0.40	
2	1600	2	0.052	0.036	0.358	25.884	199.936	98.5	0.1514877	7.5558	23.48	0.40	
note: isotope beams in mV rlsd = released, error in age includes J error, all errors 1 sigma										Mean ± s.d. =		23.01	0.48
(36Ar through 40Ar are measured beam intensities, corrected for decay in age calculations)										Wtd mean age =		23.01	0.14
										(2 fusions)			
										No isochron			

Table 10: Sample DRT-22 Single Crystal Sanidine Data

Table 11

Reynoso-UNLV, DRT-20, Single Crystal Sanidine, J = 0.00173 ± 1.33%													
4 amu discrimination = 1.0614 ± 0.56%, 40/39K = 0.0243 ± 80.90%, 36/37Ca = 0.000239 ± 8.17%, 39/37Ca = 0.000655 ± 3.50%													
4 amu discrimination = 1.0527 ± 0.41% (12-21)													
Crystal	T (C)	t (min.)	36Ar	37Ar	38Ar	39Ar	40Ar	%40Ar*	Ca/K	40Ar*/39ArK	Age (Ma)	1s.d.	
1	1600	2	0.041	0.030	0.190	13.294	103.47	97.4	0.2370959	7.3983	22.94	0.35	
2	1600	2	0.050	0.024	0.256	18.778	147.663	95.1	0.1337192	7.4415	23.08	0.36	
3	1600	2	0.072	0.028	0.362	26.283	494.898	97.3	0.1114584	18.4644	56.73	0.85	
4	1600	2	0.103	0.070	0.281	17.280	2124.68	99.1	0.4256303	123.0914	348.28	16.49	
5	1600	2	0.062	0.250	0.047	1.725	325.290	90.0	15.218404	160.6381	442.40	6.43	
6	1600	2	0.070	0.050	0.229	15.334	2584.26	99.5	0.341168	169.8698	464.81	7.24	
7	1600	2	0.077	0.020	0.556	43.088	7375.26	99.8	0.0487654	172.7720	471.79	5.94	
8	1600	2	0.100	0.014	0.432	31.414	5386.16	99.6	0.0466259	173.0017	472.34	6.26	
9	1600	2	0.087	0.060	0.440	29.379	5053.86	99.7	0.2145706	173.4061	473.32	8.72	
10	1600	2	0.118	0.027	0.782	34.894	6030.89	99.6	0.0812933	174.0736	474.92	5.97	
11	1600	2	0.128	0.030	0.745	54.928	9622.96	99.5	0.0571415	176.1301	479.84	6.39	
12	1600	2	0.099	0.029	0.816	59.998	10519.20	99.6	0.050569	176.5152	480.76	6.36	
13	1600	2	0.082	0.033	0.338	23.702	4170.86	99.6	0.1456673	177.5691	483.28	6.79	
14	1600	2	0.147	0.021	0.365	25.715	4572.89	99.3	0.0857976	178.5309	485.58	6.09	
15	1600	2	0.091	0.029	0.630	46.842	8390.05	99.8	0.064772	181.0462	491.57	6.51	
16	1600	2	0.215	0.046	0.910	66.016	12091.40	99.4	0.0729011	184.0446	498.68	6.58	
17	1600	2	0.090	0.061	0.199	13.243	2442.66	99.3	0.4839805	185.2638	501.56	6.41	
18	1600	2	0.115	0.019	0.846	63.574	11687.70	99.8	0.0313986	185.5384	502.21	6.78	
19	1600	2	0.087	0.034	0.447	32.453	5994.22	99.7	0.1096108	186.5668	504.64	39.67	
20	1600	2	0.068	0.018	0.278	20.264	3782.37	99.7	0.0933234	188.2219	508.54	6.34	
21	1600	2	0.096	0.034	0.215	14.326	2715.12	99.3	0.2493525	190.3630	513.57	6.43	
note: isotope beams in mV rlsd = released, error in age includes J error, all errors 1 sigma										Mean ± s.d. =		414.33	158.79
(36Ar through 40Ar are measured beam intensities, corrected for decay in age calculations)										Mean ± s.d., younger pop =		23.01	0.07
										Mean ± s.d., older pop =		455.52	100.26
										Wtd mean age, younger pop (2 fusions)=		23.01	0.25
										Wtd mean age, older pop (11 fusions)=		478.20	2.60
										No isochron			

Table 11: Sample DRT-20 Single Crystal Sanidine Data

Table 12

Reynoso-UNLV, DRT-11, Single Crystal Sanidine, J = 0.001709 ± 1.32%													
4 amu discrimination = 1.0614 ± 0.56%, 40/39K = 0.0243 ± 80.90%, 36/37Ca = 0.000239 ± 8.17%, 39/37Ca = 0.000655 ± 3.50%													
Crystal	T (C)	t (min.)	36Ar	37Ar	38Ar	39Ar	40Ar	%40Ar*	Ca/K	40Ar*/39ArK	Age (Ma)	1s.d.	
1	1600	2	0.057	0.029	0.157	10.220	1868.52	99.7	0.3021056	184.5071	494.47	7.57	
2	1600	2	0.055	0.025	0.123	7.733	1426.36	99.7	0.3441978	186.0645	498.11	6.61	
3	1600	2	0.074	0.036	0.321	21.445	3965.620	99.7	0.1787208	186.8027	499.84	24.08	
4	1600	2	0.115	0.033	0.176	11.125	2074.19	99.0	0.3158108	186.8108	499.86	6.59	
5	1600	2	0.049	0.026	0.180	12.341	2419.04	99.9	0.2242986	198.2301	526.35	6.84	
note: isotope beams in mV rlsd = released, error in age includes J error, all errors 1 sigma										Mean ± s.d. =		503.72	11.48
(36Ar through 40Ar are measured beam intensities, corrected for decay in age calculations)										No Wtd mean age			
										No isochron			

Table 12: Sample DRT-11 Single Crystal Sanidine Data

Table 13

Reynoso-UNLV, DRT-13, Single Crystal Sanidine, J = 0.001715 ± 1.27%												
4 amu discrimination = 1.0522 ± 0.07%, 40/39K = 0.0243 ± 80.90%, 36/37Ca = 0.000239 ± 8.17%, 39/37Ca = 0.000655 ± 3.50%												
4 amu discrimination = 1.0317 ± 0.92% (13-15)												
4 amu discrimination = 1.0359 ± 0.56% (16-24)												
4 amu discrimination = 1.0176 ± 1.79% (25-32)												
Crystal	T (C)	t (min.)	36Ar	37Ar	38Ar	39Ar	40Ar	%40Ar*	Ca/K	40Ar*/39ArK	Age (Ma)	1s.d.
1	1600	2	0.026	0.022	0.028	1.718	14.991	73.4	1.6044689	5.6918	17.53	0.58
2	1600	2	0.022	0.025	0.020	1.291	11.892	76.9	2.4267898	6.0921	18.75	0.65
3	1600	2	0.023	0.017	0.081	5.795	46.309	93.8	0.3674489	7.2398	22.26	0.59
4	1600	2	0.063	0.071	0.128	8.118	65.906	92.7	1.0756386	7.2918	22.42	0.36
5	1600	2	0.017	0.022	0.038	2.289	19.273	94.8	1.204111	7.2945	22.43	0.61
6	1600	2	0.021	0.023	0.053	3.084	25.619	94.8	0.9258296	7.3894	22.72	0.43
7	1600	2	0.058	0.064	0.165	11.019	86.585	96.1	0.7142608	7.3913	22.73	0.31
8	1600	2	0.063	0.056	0.126	7.901	65.309	92.6	0.8716488	7.4126	22.79	0.33
9	1600	2	0.015	0.018	0.041	2.531	21.408	98.2	0.8828633	7.6644	23.56	0.63
10	1600	2	0.027	0.025	0.092	6.397	54.841	92.8	0.485104	7.7430	23.80	0.37
11	1600	2	0.025	0.024	0.085	5.771	49.898	93.2	0.5162198	7.8216	24.04	0.36
12	1600	2	0.030	0.025	0.087	5.999	54.523	91.1	0.517292	8.0617	24.77	0.38
13	1600	2	0.066	0.104	0.091	5.010	101.566	94.6	2.5539263	18.8904	57.52	0.80
14	1600	2	0.032	0.059	0.010	0.106	10.503	52.1	70.259681	48.4143	143.90	6.21
15	1600	2	0.065	0.090	0.024	0.454	74.970	93.1	24.519185	152.3575	418.79	5.73
16	1600	2	0.076	0.090	0.024	0.222	46.882	81.7	50.45648	170.2198	462.09	6.39
17	1600	2	0.099	0.094	0.150	9.895	1700.77	99.1	1.168366	172.1664	466.74	5.29
18	1600	2	0.124	0.022	0.179	11.440	1993.420	98.5	0.2386942	172.8018	468.26	6.05
19	1600	2	0.041	0.055	0.016	0.187	39.783	82.2	36.907028	174.6896	472.76	8.29
20	1600	2	0.037	0.061	0.018	0.326	63.094	90.9	23.403883	175.8839	475.60	8.86
21	1600	2	0.028	0.021	0.084	5.358	944.441	99.6	0.490943	176.0202	475.93	10.76
22	1600	2	0.037	0.027	0.148	10.302	1829.720	99.7	0.3253094	178.3249	481.39	6.15
23	1600	2	0.131	0.150	0.200	12.743	2294.71	99.0	1.4478243	180.1305	485.67	5.44
24	1600	2	0.130	0.047	0.317	21.655	3915.96	99.4	0.2668772	181.6902	489.35	5.48
25	1600	2	0.037	0.027	0.152	11.058	2002.460	99.7	0.3030674	181.8699	489.77	6.26
26	1600	2	0.030	0.022	0.111	7.939	1449.810	99.7	0.3471013	182.5648	491.41	11.05
27	1600	2	0.066	0.203	0.033	0.838	158.929	96.8	30.001655	184.4897	495.94	5.68
28	1600	2	0.064	0.081	0.022	0.437	87.176	94.4	22.916859	187.7216	503.52	9.10
29	1600	2	0.023	0.015	0.045	2.919	549.509	99.5	0.6437063	187.9455	504.05	11.31
30	1600	2	0.104	0.112	0.166	9.791	1989.91	99.2	1.4069639	203.7502	540.65	6.30
31	1600	2	0.041	0.059	0.017	0.166	44.381	84.2	44.683085	227.1832	593.60	11.67
note: isotope beams in mV rlsd = released, error in age includes J error, all errors 1 sigma										Mean ± s.d. =	283.38	229.27
(36Ar through 40Ar are measured beam intensities, corrected for decay in age calculations)										Mean ± s.d., younger pop =	22.32	2.02
										Mean ± s.d., older pop =	448.26	7.20
										Wtd mean age, younger pop (8 fusions) =	22.85	0.22
										No Wtd mean age, older pop		
										No isochron		

Table 13: Sample DRT-13 Single Crystal Sanidine Data

Table 14

Reynoso-UNLV, DRT-19, Single Crystal Sanidine, J = 0.001725 ± 1.24%												
4 amu discrimination = 1.0522 ± 0.07%, 40/39K = 0.0243 ± 80.90%, 36/37Ca = 0.000239 ± 8.17%, 39/37Ca = 0.000655 ± 3.50%												
4 amu discrimination = 1.0527 ± 0.41% (12-18)												
Crystal	T (C)	t (min.)	36Ar	37Ar	38Ar	39Ar	40Ar	%40Ar*	Ca/K	40Ar*/39ArK	Age (Ma)	1s.d.
1	1600	2	0.062	0.037	0.020	0.072	13.391	75.0	47.223238	126.0386	354.92	15.65
2	1600	2	0.052	0.082	0.022	0.531	81.426	93.0	14.09447	141.9920	395.25	8.26
3	1600	2	0.082	0.188	0.031	0.588	97.690	91.6	29.254409	152.3665	420.99	5.40
4	1600	2	0.076	0.141	0.030	0.372	63.831	89.6	34.726342	152.8422	422.17	6.13
5	1600	2	0.084	0.146	0.046	1.014	179.247	95.1	13.123052	169.1487	461.88	5.25
6	1600	2	0.200	0.051	0.426	28.124	4857.89	99.0	0.164952	172.9339	470.98	6.69
7	1600	2	0.069	0.123	0.025	0.391	72.871	93.7	28.779915	174.3562	474.39	8.24
8	1600	2	0.075	0.035	0.266	19.224	3385.63	99.6	0.1656108	177.3969	481.65	5.71
9	1600	2	0.092	0.040	0.253	17.116	3044.51	99.6	0.212334	179.1316	485.78	5.32
10	1600	2	0.080	0.353	0.049	1.851	336.376	97.9	17.399514	179.7338	487.21	5.62
11	1600	2	0.063	0.156	0.028	0.678	126.855	97.9	21.010793	183.9919	497.29	6.22
12	1600	2	0.218	0.059	0.890	64.970	11973.20	99.6	0.0825064	185.6022	501.09	5.47
13	1600	2	0.115	0.045	0.296	20.784	3912.18	99.5	0.1967178	189.4237	510.08	5.62
14	1600	2	0.067	0.054	0.166	9.946	1965.19	99.5	0.493906	198.7422	531.81	13.10
15	1600	2	0.099	0.053	0.454	32.328	6498.85	99.8	0.148954	202.8353	541.27	5.92
note: isotope beams in mV rlsd = released, error in age includes J error, all errors 1 sigma										Mean ± s.d. =	469.12	51.06
(36Ar through 40Ar are measured beam intensities, corrected for decay in age calculations)										No Wtd mean age		
										No isochron		

Table 14: Sample DRT-19 Single Crystal Sanidine Data

Table 15

Reynoso-UNLV, DRT-24, Single Crystal Sanidine, J = 0.001738 ± 1.76%												
4 amu discrimination = 1.0522 ± 0.07%, 40/39K = 0.0243 ± 80.90%, 36/37Ca = 0.000239 ± 8.17%, 39/37Ca = 0.000655 ± 3.50%												
4 amu discrimination = 1.0527 ± 0.41% (13-17)												
Crystal	T (C)	t (min.)	36Ar	37Ar	38Ar	39Ar	40Ar	%40Ar*	Ca/K	40Ar*/39ArK	Age (Ma)	1s.d.
1	1600	2	0.149	0.039	0.181	11.169	117.87	70.1	0.3845913	80.9455	237.47	4.50
2	1600	2	0.358	0.046	1.545	112.723	12146.60	99.3	0.0448902	108.3380	311.23	5.43
3	1600	2	0.296	0.054	1.282	88.465	11515.50	99.4	0.0671476	131.0268	370.13	6.91
4	1600	2	0.537	0.236	0.184	4.764	777.630	82.2	5.4565217	135.8397	382.38	6.87
5	1600	2	0.182	0.174	0.049	1.013	185.17	76.3	19.004043	140.2692	393.58	6.76
6	1600	2	0.425	0.033	0.475	29.197	4336.61	97.5	0.124334	146.6907	409.70	6.97
7	1600	2	0.939	0.035	0.675	37.500	5916.46	95.8	0.1026712	153.0261	425.46	7.22
8	1600	2	0.152	0.037	0.813	59.880	9724.31	99.7	0.0679717	163.9656	452.35	7.59
9	1600	2	0.741	0.037	0.934	60.079	9974.47	98.0	0.0677466	164.8751	454.57	7.96
10	1600	2	0.063	0.098	0.022	0.541	99.75	89.7	20.046767	164.9371	454.72	7.80
11	1600	2	0.091	0.342	0.042	1.573	276.810	95.2	24.056122	169.8550	466.66	8.01
12	1600	2	0.554	0.306	0.172	4.528	915.187	84.4	7.4473208	172.9384	474.11	8.27
13	1600	2	0.164	0.032	0.741	53.844	9599.68	99.6	0.0653764	179.9453	490.93	8.15
14	1600	2	0.265	0.365	0.084	2.171	459.38	86.5	18.57749	185.9198	505.14	9.75
15	1600	2	0.214	0.397	0.069	1.726	373.70	87.2	25.458029	192.1394	519.82	8.88
note: isotope beams in mV rlsd = released, error in age includes J error, all errors 1 sigma										Mean ± s.d. =	423.22	73.27
(36Ar through 40Ar are measured beam intensities, corrected for decay in age calculations)										No Wtd mean age		
										No isochron		

Table 15: Sample DRT-24 Single Crystal Sanidine Data

APPENDIX B: PALEONTOLOGICAL TABLES AND FIGURES

Table 1

Upper Dentition							
Specimen number		MD	MW	DW	PH	PaH	PHV
<i>Meroëhyrax kyongoi</i>							
Nakwai, Kenya							
08-071 TOP 46	LM3	15.82*	13.37	10.4	6.46	12.07	1.93
09-076 TOP 46	RM1	13.46	10.66	*	5.56	9.63*	2.57
08-071 TOP 46	RM1	12.01	11.33	10.8	5.2	10.66	1.95
KNM-NW 22586 A	RM1	13.08	10.76	8.73	5.14*	9.24*	1.93
KNM-NW 22598 A	RM2	16.64*	14.73	10.76*	4.44*	*	1.87
07-112 TOP 15	RM3	19.08*	12.99*	11.08	4.51*	8.67*	2.3
<i>Paraplioxyrax ngororaensis</i>							
Ngorora, Kenya							
KNM-BN 208	LM1	17.75*	18.59	18.1	4.71	14.29*	1.59
KNM-BN 207	LM1	19.53	15.29	14.16	3.47	10.18	3.35
	LM2	19.98	15.87	14.87	4.18	11.67	2.38
	LM3	28.55	14.52	13.24	5.82*	12.26	*
KNM-BN 1701	LM3	26.7	16.24	14.13	7.34*	16.72*	2.19*
KNM-BN 1702	LM3	23.10*	19.58	17.12	4.04	17.81	2.75
KNM-BN 821	LM3	19.59	11.97	16.45	*	12.3	*
Lower Dentition							
Specimen number		MD	MW	DW	PH	MH	TB
<i>Meroëhyrax kyongoi</i>							
Nakwai, Kenya							
KNM-NW 22555	LM1	9.39*	5.12	5.44	3.03	3.22	1.39
KNM-NW 22558 A	LM1	11.49	6.17	5.99	5.88	5.24	1.97
07-030 TOP 1	LM1	11.1	5.25	5.46*	3.32	3.99	1.75
KNM-NW 22547	LM1	11.72	5.73	5.58	5.12	5.85	1.52
	LM2	12.19*	5.84	5.12*	9.66	7.15	*
KNM-NW 22554	LM1	11.03	5.56	6.26	4.82	4.65	1.97
	LM2	12.26*	6.74	6.55	5.95	5.24	1.83
08-210 TOP 64	LM2	13.15	6.24	6.6	10.01	8.79	2.09

08-298 TOP 69	LM2	12.26*	7.05	7.52	6.25	6.06*	2.03
08-071 TOP 46	LM2	13.74	7.57	7.79	5.06	4.65*	2.49
	LM3	18.18	7.73	7.58	8.4	6.99	2.79
08-071 TOP 46	RM1	12.04*	7.09	7.18	5.53	5.27	2.69
09-027 TOP 69	RM2	15.59*	7.96	6.48	6.36	5.71*	2.55
KNM-NW 54722 12-004	RM2	13.68	7.36	7.64	6.83	6.9	2.28
KNM-NW 54376 12-202	RM3	18.74	7.23	8.11	3.23	4.13	1.77
07-005 TOP1	RM3	17.16	6.94	6.57	3.5	4.51	1.69
KNM-NW 22558 C	RM3	18.1	8.09	7.85	7.75	7.19	1.84
KNM-NW 22554	RM3	14.66*	7.57	7.52	9.12*	9.35	2.20*
KNM-NW 54712 12-031	RM3	*	8.37	7.29	7.45	7.25	2.04
<i>Meroëhyrax bateae</i>							
Rusinga Island, Kenya							
KNM-RU 2384	LM1	10.22	6.55	7.44	6.06	5.41	3.37
	LM2	10.05	6.94	6.67	6.79	5.53*	3.64
KNM-RU 163	LM3	15.26	7.76	6.76	6.33	5.81	2.12
<i>Paraplioxyrax ngororaensis</i>							
Ngorora, Kenya							
KNM-BN 214	LM1	17.96*	8.89*	9.21*	9.55*	7.35*	*
KNM-BN 1033	LM2	17.72*	9.87	9.92	10.71	8.90*	2.66
KNM-BN 212 + 237	LM2	16.64	10.4	10.05	6.14	4.11*	3.5
	LM3	21.19	10.47	9.62	7.67	6.2	2.84
KNM-BN 236	RM1	16.05	8.68	9.67	7.16*	5.48*	2.3
KNM-BN 212 + 237	RM1	13.00*	8.59	9.31	4.04	2.75*	2.97
	RM2	16.74*	10.02	10.09	5.74	4.41	2.85
KNM-BN 1245	RM2	19.02	9.56	10.04	9.44	7.43*	3.03
KNM-BN 213	RM2	18.85	11.96	12.76	12.1	8.93	3.03
KNM-BN 802	RM3	26.74	10.34	9.86	12.14	10.65	3.04
KNM-BN 819	RM3	27.4	10.65	10.27	7.97	6.43	1.96

*Damage to specimen affected measurement or prevented measurement to be taken.

Table 1: Measurements were taken of permanent molars and are reported in millimeters. The measurements for the upper molars: mesiodistal length (MD), mesial width (MW), distal width (DW), protocone height (PH), paracone height (PaH), and the height of the protocone/hypocone valley (PHV). Lower molar measurements: mesiodistal length (MD), mesial width (MW), distal width (DW), protoconid height (PH), metaconid height (MH), and the height to the base of the talonid basin (TB).

Figure 1

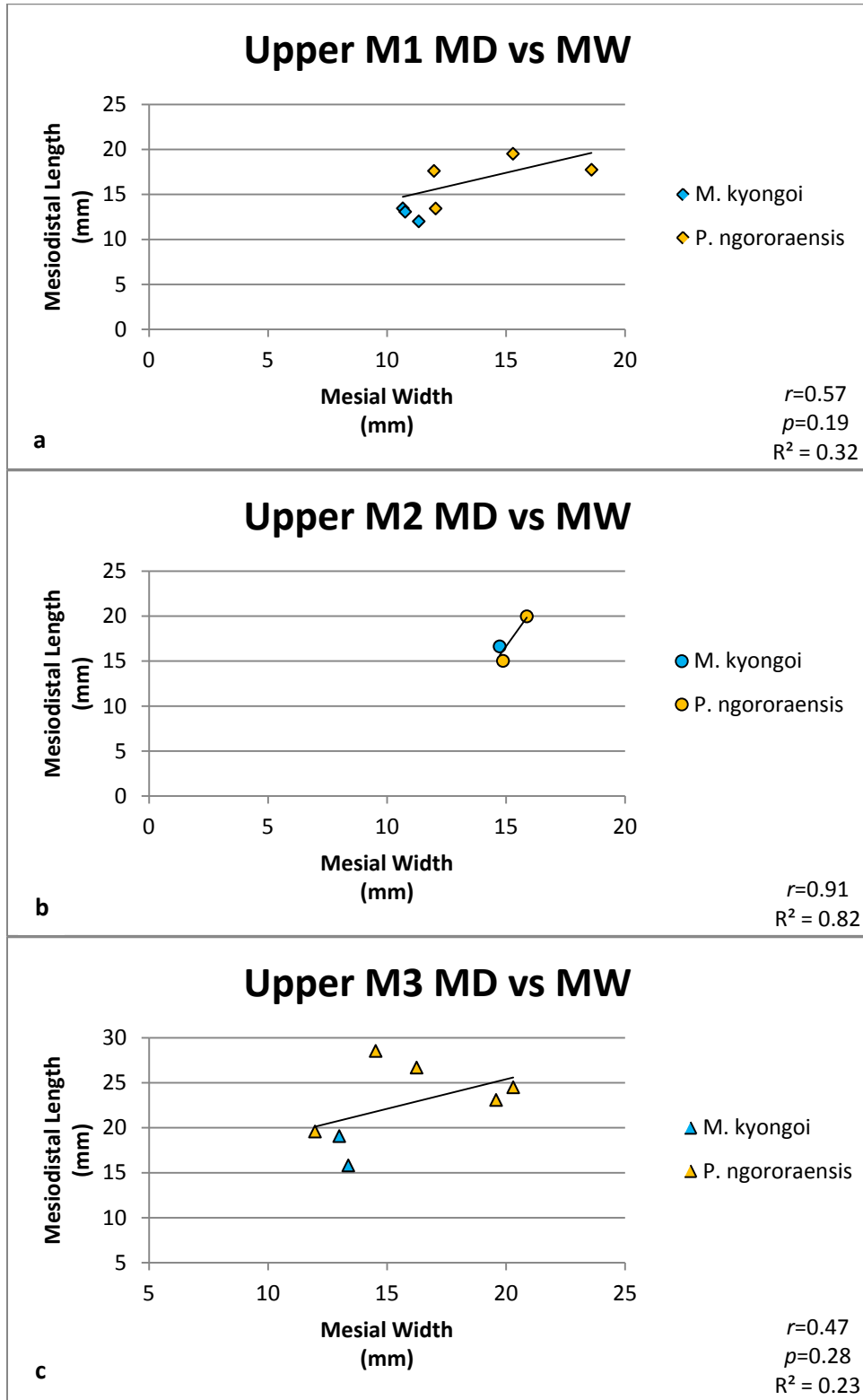


Figure 1 continued

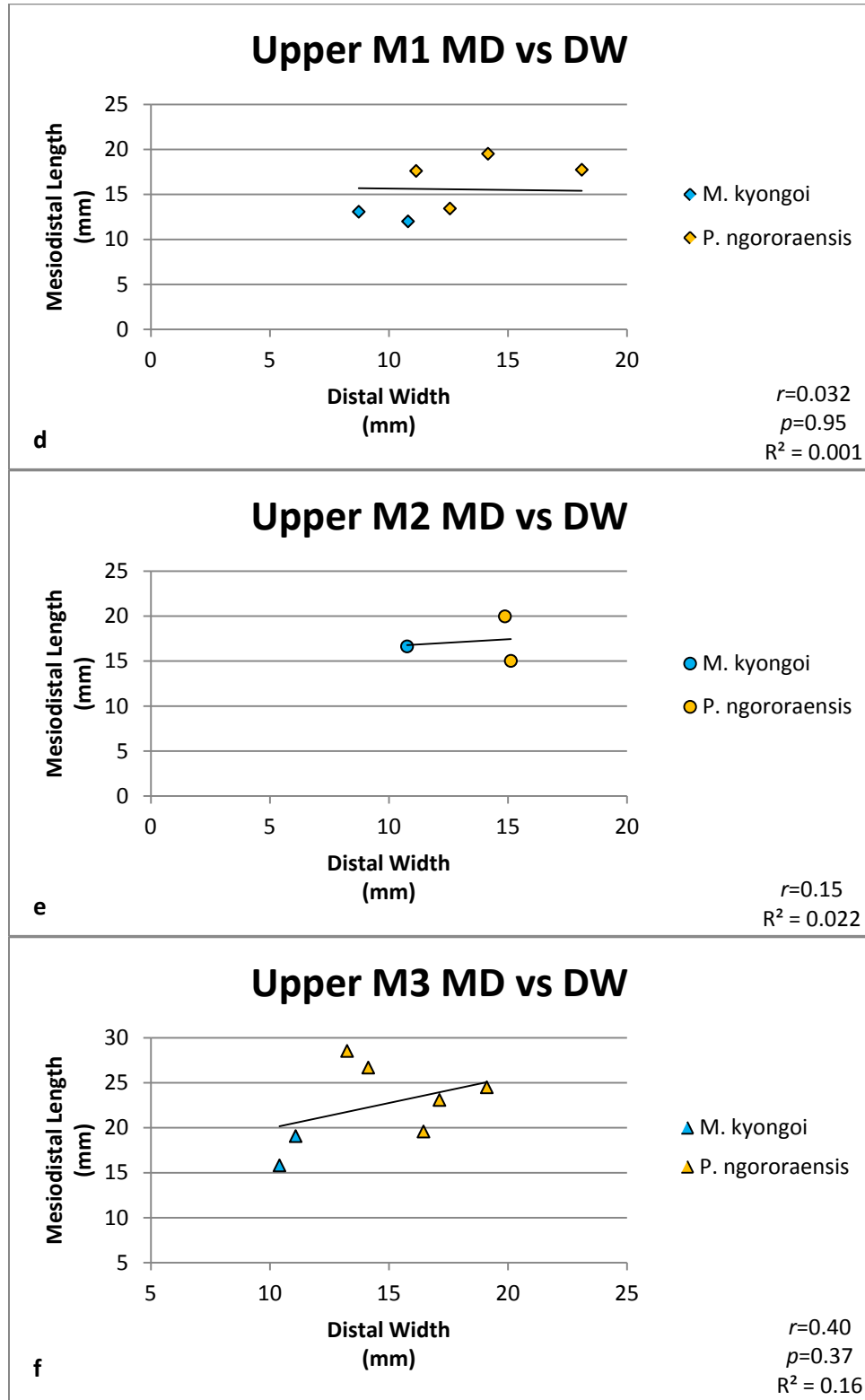


Figure 1 continued

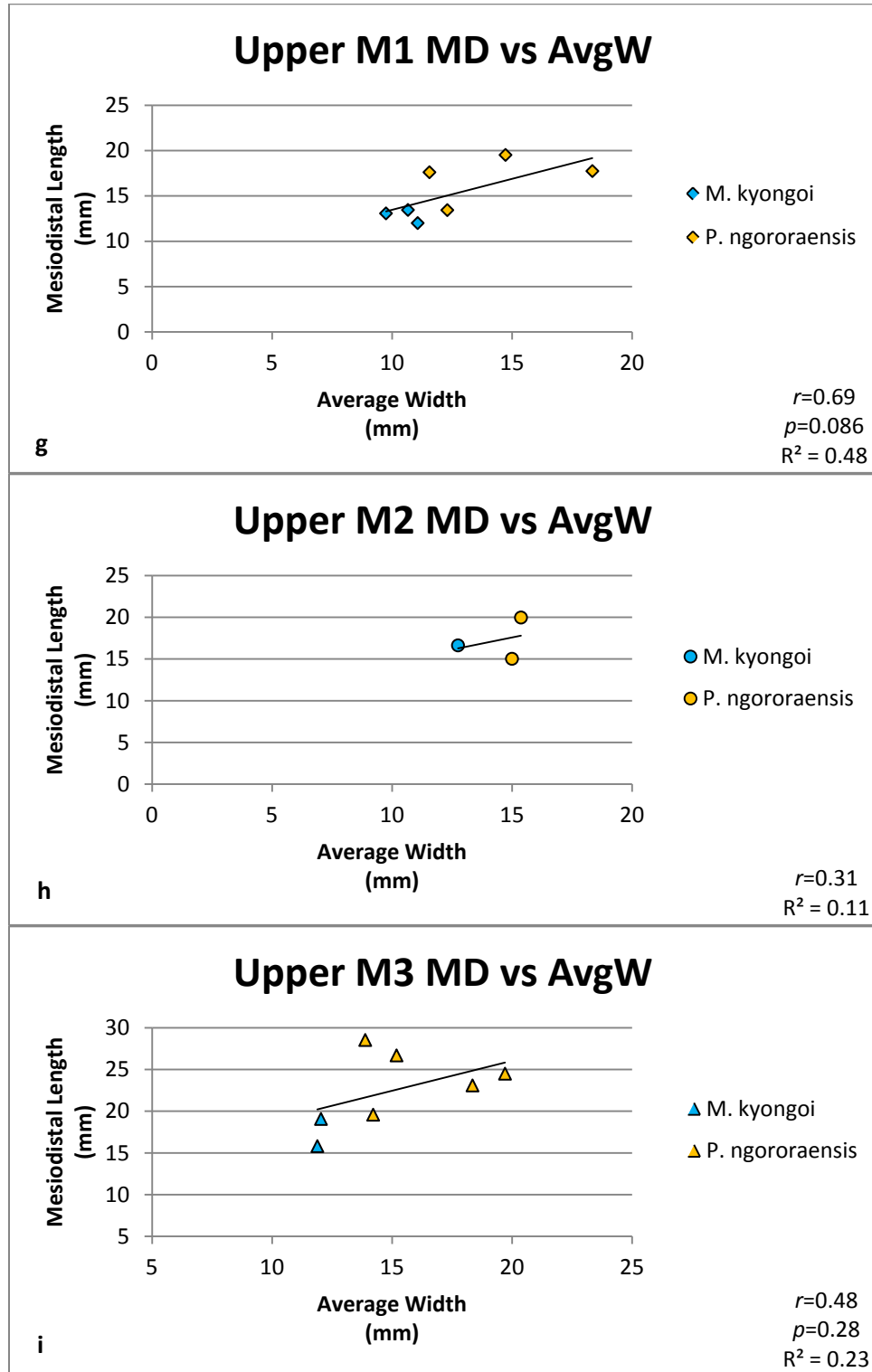


Figure 1: Upper mesiodistal length (MD) with mesial width (MW) of (a) first molar (M1), (b) second molar (M2), and (c) third molar (M3); distal width (DW) of (d) M1, (e) M2, and (f) M3; and average width (AvgW) of (g) M1, (h) M2, and (i) M3 from *Meroëhyrax kyongoi* (Mer. k, blue marker) and *Paraplioxyrax ngororaensis* (Para. n, yellow marker). The line represents the linear regression of the measurements within the graph.

Figure 2

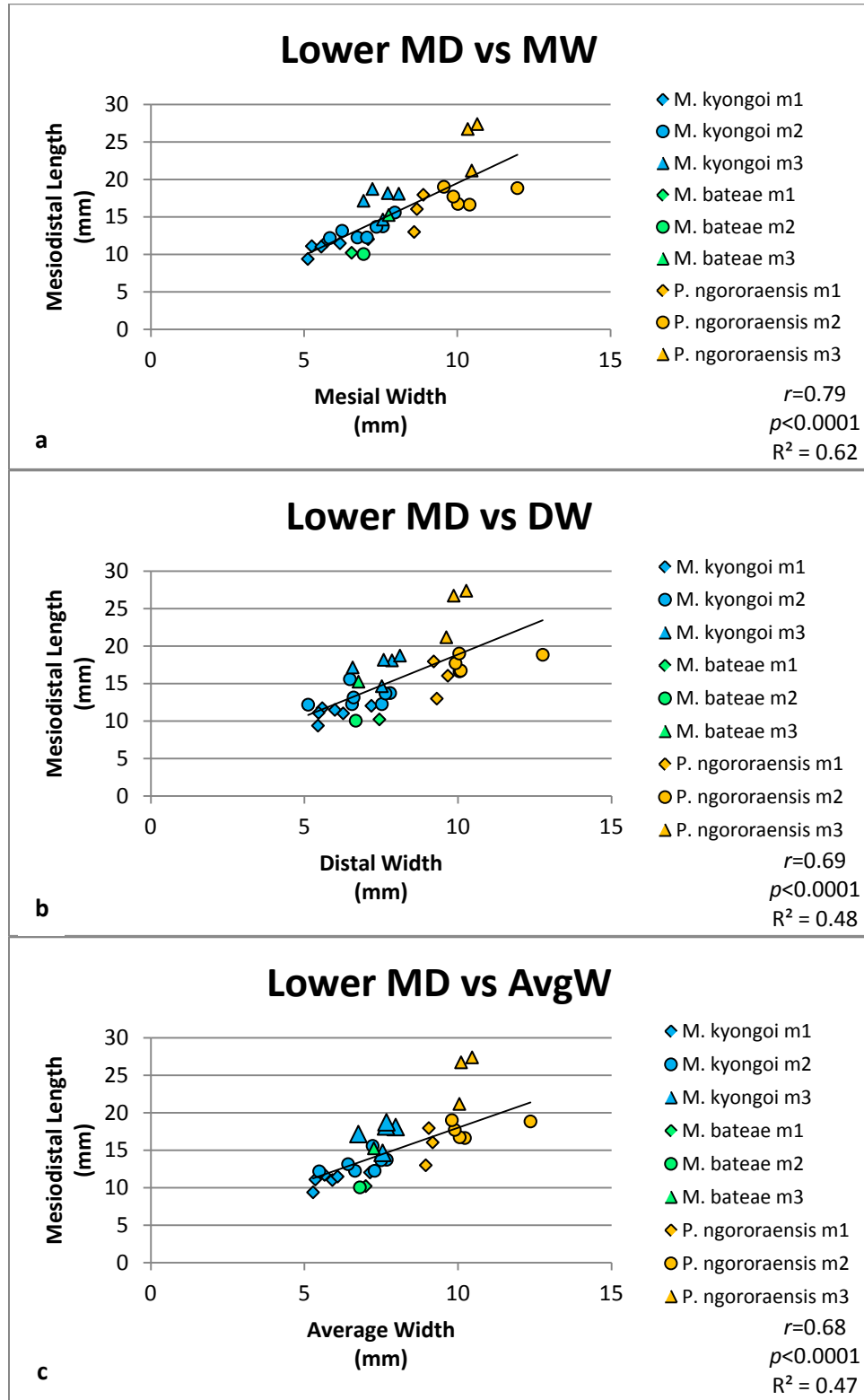


Figure 2 continued

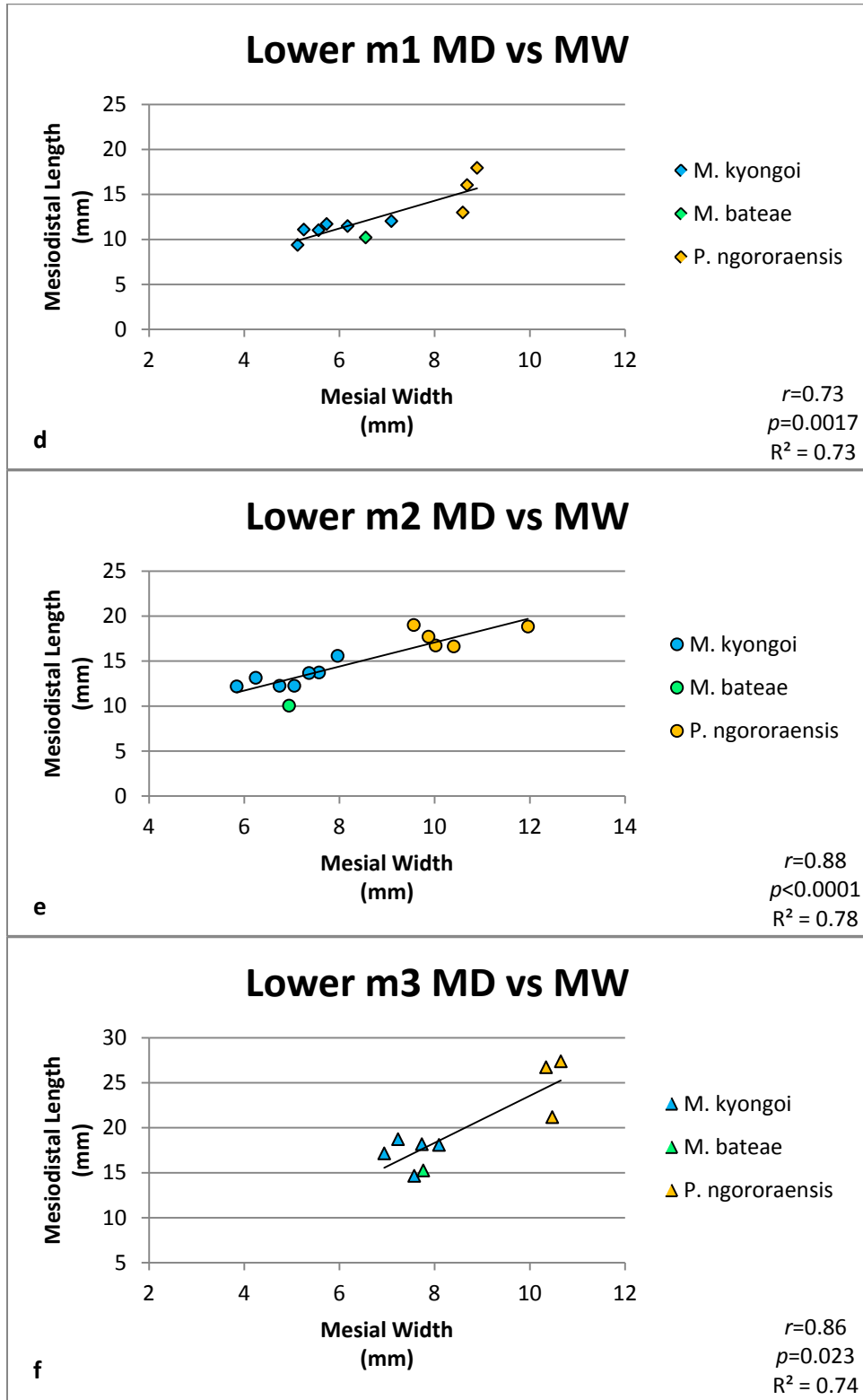


Figure 2 continued

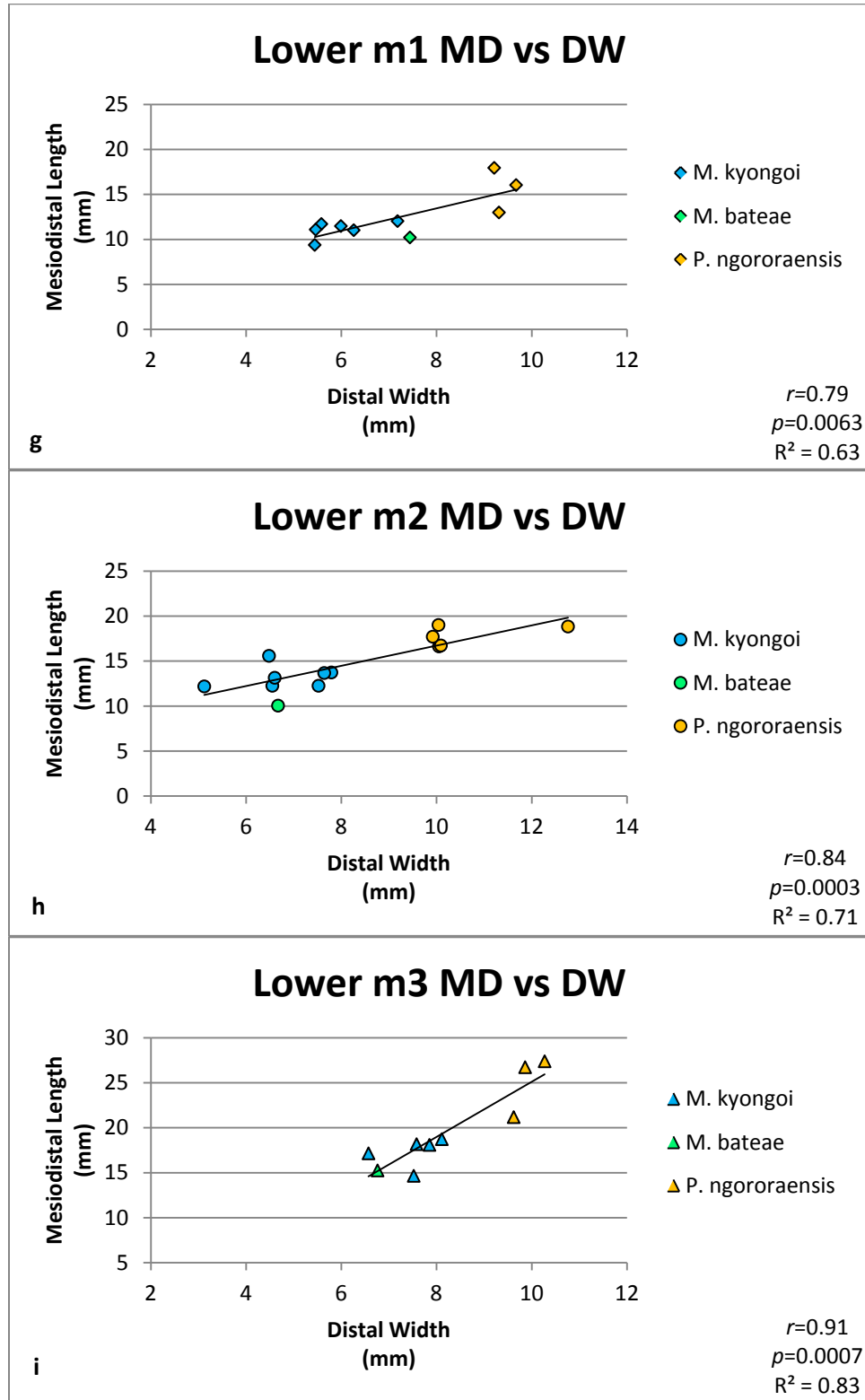


Figure 2 continued

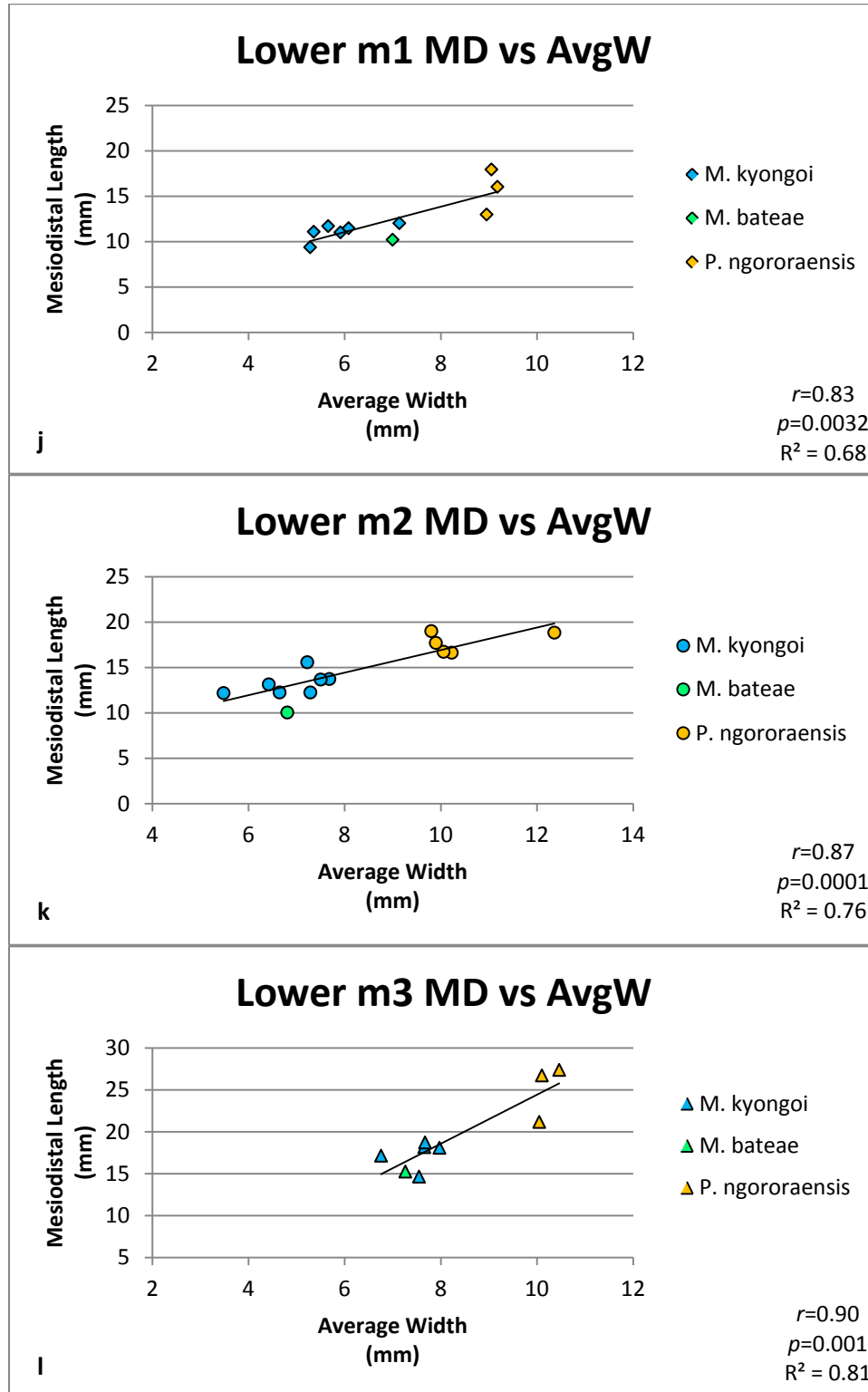


Figure 2: Lower mesiodistal length (MD) with (a) mesial width (MW), (b) distal width (DW), and (c) average width (AvgW) from *M. kyongoi* (blue marker), *M. bateae* (green marker), and *P. ngororaensis* (yellow marker). These comparison were then broken down by tooth number; MD with MW of (d) first molar (m1, diamonds), (e) second molar (m2, circles), and (f) third molar (m3, triangles); DW of (g) m1, (h) m2, and (i) m3; and AvgW of (j) m1, (k) m2, and (l) m3. The line represents the linear regression of the measurements within the graph.

Figure 3

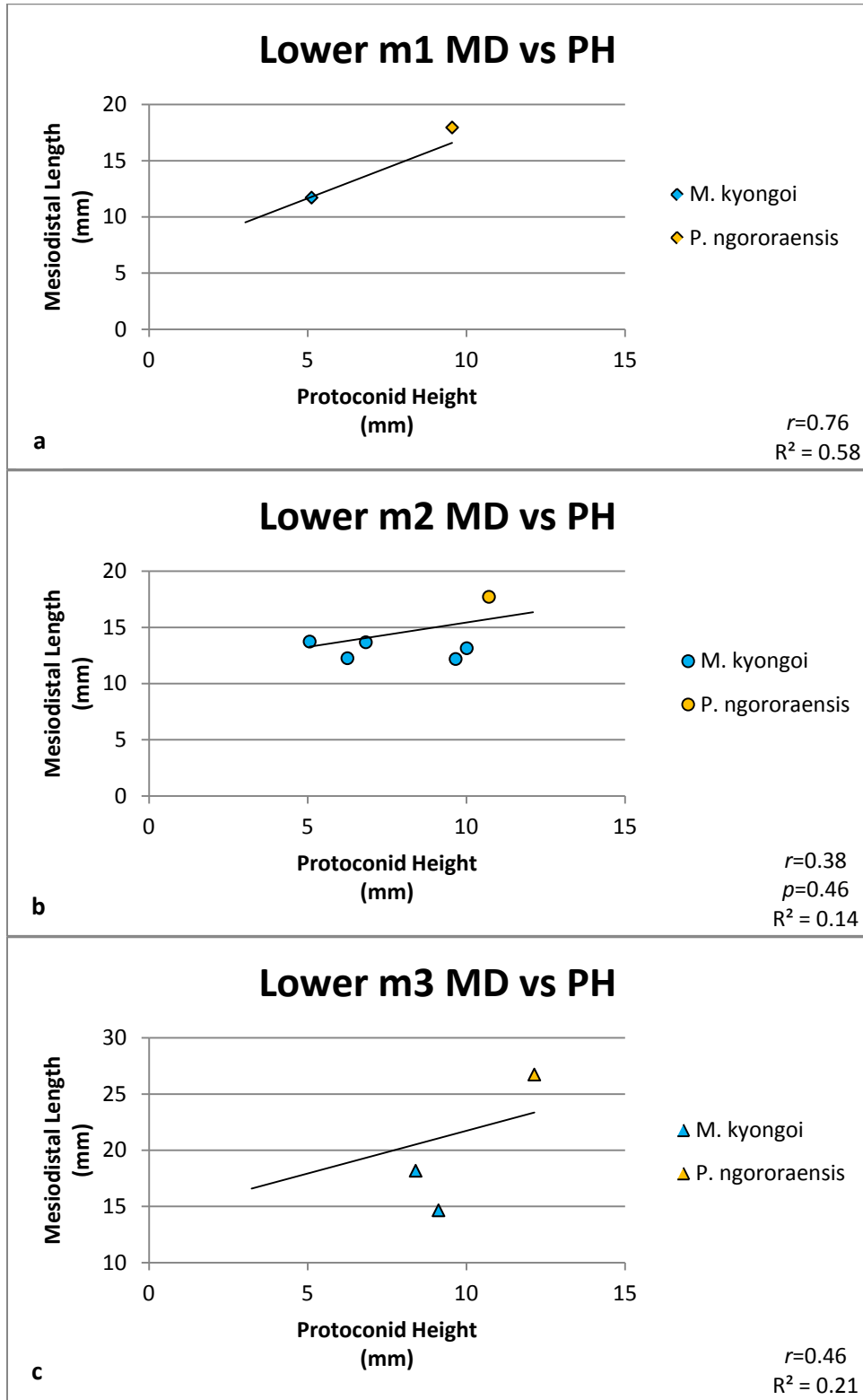


Figure 3 continued

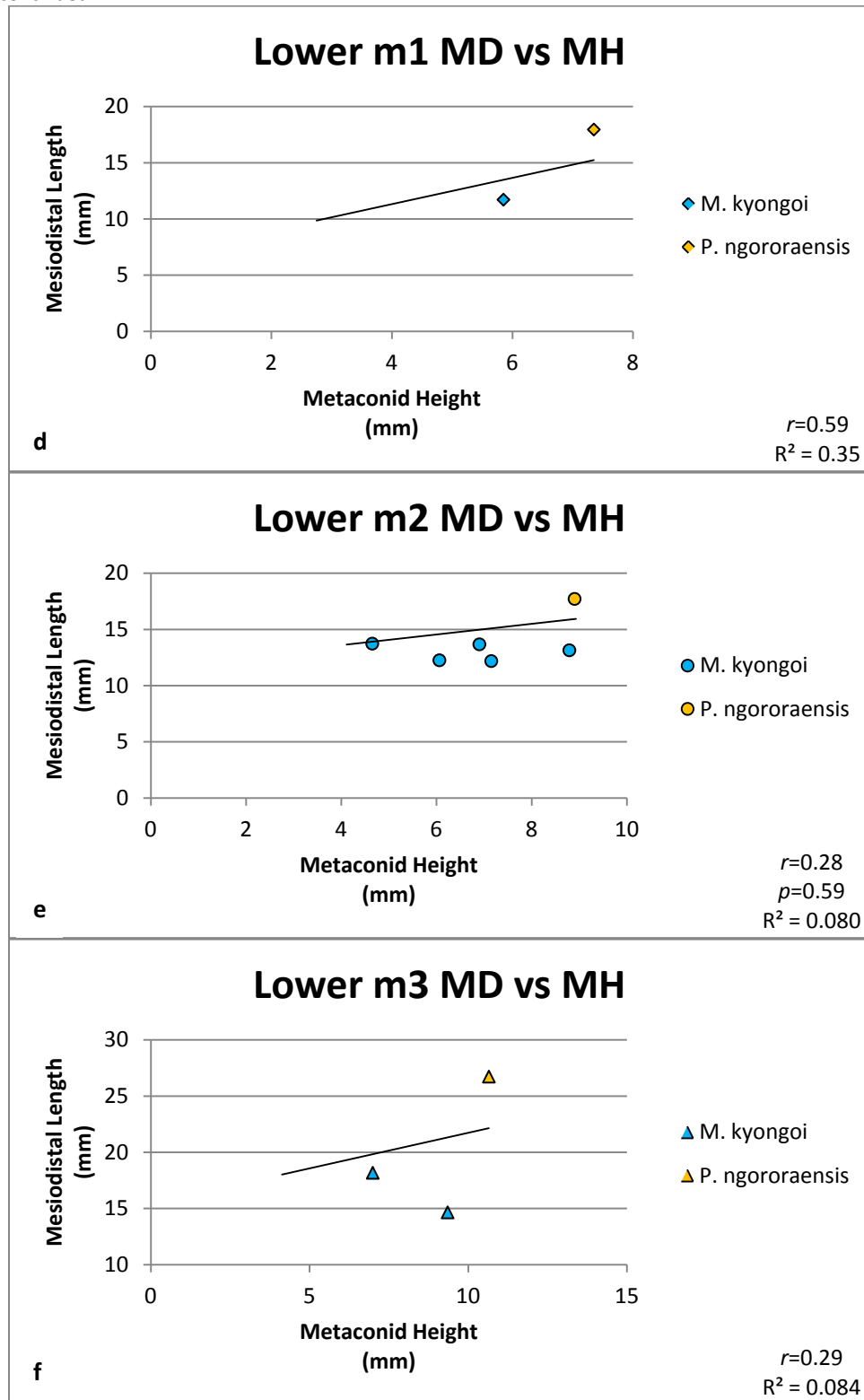


Figure 3 continued

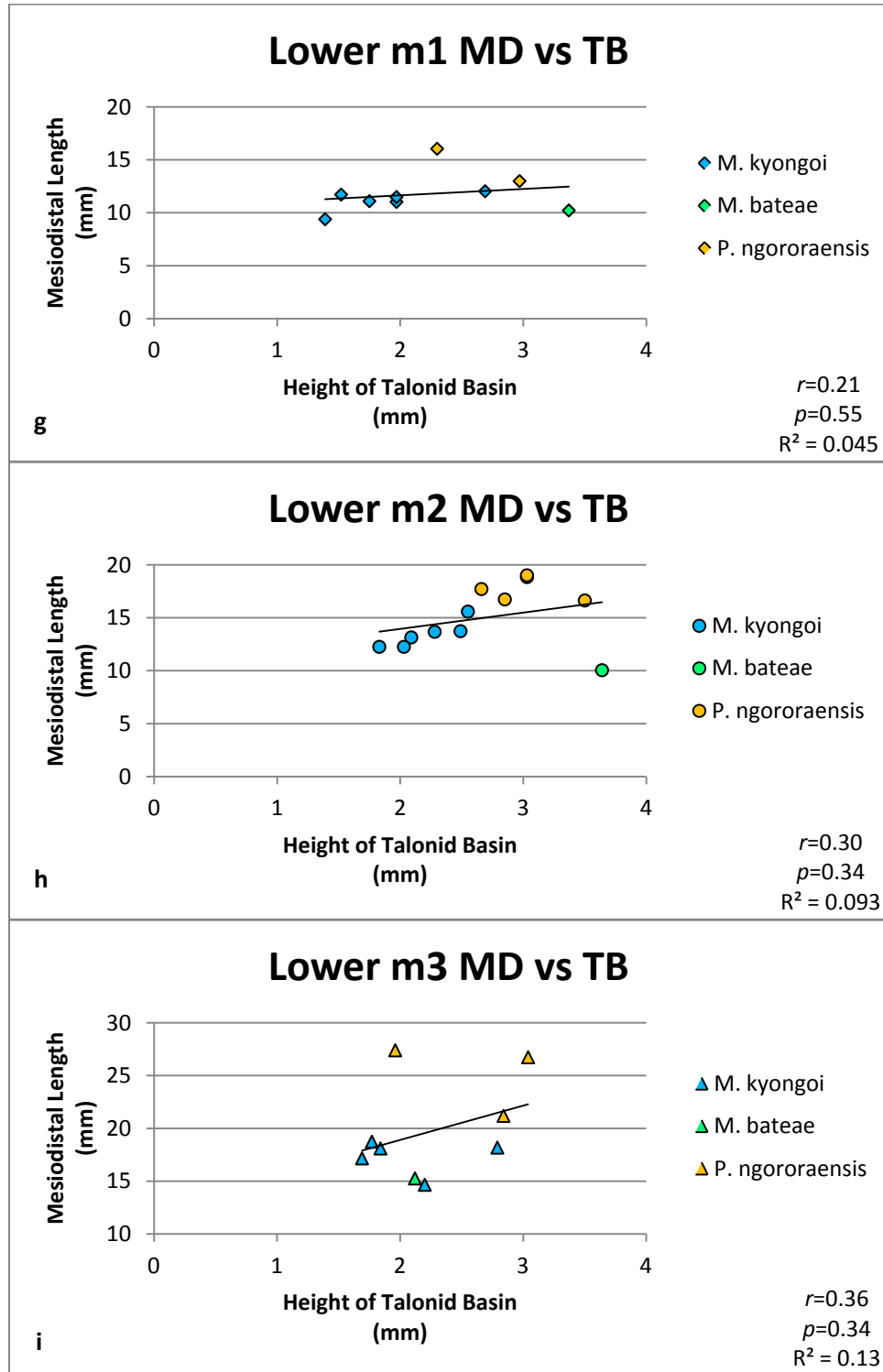


Figure 3: Comparisons between mesiodistal length (MD) and the three crown height measurements separated by tooth number: protoconid height (PH) of the (a) m1, (b) m2, and (c) m3; metaconid height (MH) of the (d) m1, (e) m2, and (f) m3; and the height of the talonid basin (TB) on the (g) m1, (h) m2, and (i) m3. Comparisons were made between *M. kyongoi* (blue marker), *M. bateae* (green marker), and *P. ngororaensis* (yellow marker). The line represents the linear regression of the measurements within the graph.

REFERENCES

- Baker, B.H., Williams, L.A.J., Miller, J.A., and Fitch, F.J. (1971). Sequence and Geochronology of the Kenya Rift Volcanics. *Tectonophysics*, 11, 191-215.
- Bargo, M.S., De Iuliis, G., and Vizcaíno, S.F. (2006). Hypsodonty in Pleistocene ground sloths. *Acta Palaeontologica Polonica*, 51(1), 53–61.
- Bobe, R. (2006). The evolution of arid ecosystems in eastern Africa. *Journal of arid Environments*, 66, 564-584.
- Boschetto, H.B., Brown, F.H., and McDougall, I. (1992). Stratigraphy of the Lothidok Range, northern Kenya, and K/Ar ages of its Miocene primates. *Journal of Human Evolution*, 22, 47-71.
- Brown, F.H., and McDougall, I. (2011). Geochronology of the Turkana Depression of Northern Kenya and Southern Ethiopia. *Evolutionary Anthropology*, 20, 217-227.
- Cooke, H.B.S. (1958). The Fossil Mammal Fauna of Africa. *The Quarterly Review of Biology*, 43(3), 234-264.
- Ducrocq, S., Boisserie, J.-R., Tiercelin, J.-J., Delmer, C., Garcia, G., Kyalo, M.F., Leakey, M.G., Marivaux, L., Otero, O., Peigne, S., Tassy, P., and Lihoreau, F. (2010). New Oligocene vertebrate localities from Northern Kenya (Turkana Basin). *Journal of Vertebrate Paleontology*, 30(1), 293-299.
- Feibel, C.S. (2011). A Geological History of the Turkana Basin. *Evolutionary Anthropology*, 20, 206-216.
- Feldhamer, G. A. (2007). *Mammalogy: adaptation, diversity, ecology*. JHU Press.
- Fortelius, M., Eronen, J., Liu, L., Pushkina, D., Tesakov, A., Vislobokova, I., and Zhang, Z. (2006). Late Miocene and Pliocene large land mammals and climatic changes in Eurasia. *Palaeogeography, Palaeoclimatology, Palaeoecology*, 238, 219–227.

- Gutierrez, M. (2011). Taxonomic and Ecological Characterization of a Late Oligocene Mammalian Fauna from Kenya [Ph.D. Dissertation] Washington University in St. Louis, St. Louis, Missouri.
- Hofmann, C. et al. (1997). Timing of the Ethiopian flood basalt event and implications for plume birth and global change. *Nature*, 389, 838–841.
- Janis, C.M. (1979). Mastication in the Hyrax and its Relevance to Ungulate Dental Evolution. *Paleobiology*, 5(1), 50-59.
- Janis, C.M. (1988). An Estimation of Tooth Volume and Hypsodonty Indices in Ungulate Mammals, and the Correlation of these Factors with Dietary Preference. In: Teeth Revisited: Proceedings of the VIIth International Symposium on Dental Morphology, Paris 1986, Russell DE, Santoro J-P, and Sigogncau-Russell D. (Eds.), *Mémoires de Musée d'Histoire Naturelle, Paris (series C)*, 53, 367-387.
- Janis, C.M. (1993). Tertiary Mammal Evolution in the Context of Changing Climates, Vegetation, and Tectonic Events. *Annual Review of Ecology and Systematics*, 24, 467-500.
- Kappelman, J., et.al. (2003). Oligocene mammals from Ethiopia and faunal exchange between Afro-Arabia and Eurasia. *Nature*, 426, 549-552.
- Koenigswald, W.v. (2011). Diversity of hypsodont teeth in mammalian dentitions – construction and classification. *Palaeontographica, Abt. A: Palaeozoology – Stratigraphy*, 294(1–3), 63–94.
- Leakey, M., Grossman, A., Gutierrez, M., and Fleagle, J.G. (2011). Faunal Change in the Turkana Basin During the Late Oligocene and Miocene. *Evolutionary Anthropology*, 20, 238-253.
- Pickford, M., and Fischer, M.S. (1987). Parapliohyrax ngororaensis, a new hyracoid from the Miocene of Kenya, with an outline of the classification of Neogene Hyracoidea. *Neues Jahrbuch für Geologie and Paläontologie, Abhandlungen*, 175, 207-234.

- Rasmussen, D.T., and Gutierrez, M. (2009). A Mammalian Fauna from the Late Oligocene of Northwest Kenya. *Palaeontographica Abt. A*, 288, 1-52.
- Rasmussen, D. T., and Gutierrez, M. (2010). Hyracoidea. In L. Werdelin and W.J. Sanders (Eds.), *Cenozoic Mammals of Africa* (pp. 123-145). Berkeley: University of California. Print.
- Rasmussen, T.D., and Simons, E.L. (1988). New Oligocene Hyracoids from Egypt. *Journal of Vertebrate Paleontology*, 8(1), 67-83.
- Rasmussen, D.T., and Simons, E.L. (2000). Ecomorphological diversity among Paleogene hyracoids (Mammalia): a new cursorial browser from the Fayum, Egypt. *Journal of Vertebrate Paleontology*, 20(1), 167-176.
- Renne, P.R., Swisher, C.C, Deino, A.L., Karner, D.B., Owens, T.L., DePaolo, D.J. (1998). Intercalibration of standards, absolute ages and uncertainties in $^{40}\text{Ar}/^{39}\text{Ar}$ dating. *Chemical Geology*, 145, 117-152.
- Sánchez, I. M., Quiralte, V., Morales, J. & Pickford, M. (2010). A new genus of tragulid ruminant from the early Miocene of Kenya. *Acta Palaeontologica Polonica*, 55, 177–187.
- Sanders, W.J., Kappelman, J., and Rasmussen, D.T. (2004). New large-bodied mammals from the late Oligocene site of Chilga, Ethiopia. *Acta Paleontologica Polonica*, 49(3), 365-392.
- Seiffert, E.R. (2007). Evolution and Extinction of Afro-Arabian Primates Near the Eocene-Oligocene Boundary. *Folia Primatol*, 78, 314-327.
- Simons, E.L., and Gingerich, P.D. (1974). New Carnivorous Mammals from the Oligocene of Egypt. *Animals of the Geological Survey of Egypt*, 4, 157-166.
- Strömberg, C.E. (2006). Evolution of hypsodonty in equids: testing a hypothesis of adaptation. *Paleobiology*, 32(2), 236-258.
- Wendt, I., and Carl, C. (1991). The statistical distribution of the mean squared weighted deviation. *Chemical Geology*, 86, 275-285.

Werdelin, L. (2010). Chronology of Neogene mammal localities. In L. Werdelin and W.J. Sanders (Eds.), *Cenozoic Mammals of Africa* (pp. 123-145). Berkeley: University of California.

Print.

Williams, S.H., and Kay, R.F. (2001). A Comparative Test of Adaptive Explanations for Hypsodonty in Ungulates and Rodents. *Journal of Mammalian Evolution*, 8(3), 207-229.

Dawn E. Reynoso
Department of Geoscience
University of Nevada-Las Vegas
4505 S. Maryland Parkway
Las Vegas, NV 89154-4010
(702) 232-1905
pape@unlv.nevada.edu

Education:

Graduate **Masters of Science in Geology**
University of Nevada-Las Vegas, Department of Geosciences
Committee Chair: Terry L. Spell Ph.D.
Degree expected: 12/14

Undergraduate **Bachelor of Science in Earth Science**
University of Nevada-Las Vegas, Department of Geosciences
Degree conferred: 08/11

High School **High School Diploma**
Centennial High School
Las Vegas, NV
Graduation: 06/01

Awards: Best Teaching Assistant 2012 Department of Geosciences UNLV
Outstanding Mineralogist 2009 Department of Geosciences UNLV
National Dean's List

Experience:

09/10-Present **Paleontological Field Manager**
-Assisted with paleontological survey, excavation, managing and
training volunteers in Tule Springs
Supervisor: Joshua Bonde

01/13-05/14 **Geoscience Department Graduate Outreach Coordinator**
-Organize interactions between the UNLV Geoscience Department
and local public schools, community colleges, and local boy/girl
scouts

- 07/13-07/13 **Applied EarthWorks**
 Staff Paleontologist
 -Conducted paleontological surveys and monitored active construction for paleontological resources which involved writing lithology descriptions and specimen collection and preparation
- 08/12-05/13 **Graduate Teaching Assistant**
 -Teaching Assistant for GEOL 220L Mineralogy in Fall 2012 and Teaching Assistant for GEOL 101L Introduction to Geology in Spring 2013
- 07/12-01/13 **Masters Field Work**
 -Field work in West Turkana, Kenya including: paleontological survey, fossil collection and $^{40}\text{Ar}/^{39}\text{Ar}$ dating sample collection, work in the Nairobi National Museum including: sorting through collections and identifying specimens for measurements and descriptions
- 01/12-05/12 **Graduate Research Assistant**
 - Lab tech work, some secretarial duties, diagram construction and preparation of resources for online course
 Supervisor: Pamela Burnley
- 05/11-05/12 **Gibler Geotechnical Consulting Inc.**
 -Lab Tech, data processing and billing
 Supervisor: Kati Gibler
- 12/11-01/12 **Nevada Isotope Geochronology Laboratory**
 -Mineral separation
 Supervisor: Terry Spell and Kathy Zanetti
- 08/11-06/12 **Student Volunteer**
 -Assisted with molding Jurassic trackway in Valley of Fire State Park
 Supervisor: Steve Rowland
- 01/10-01/12 **Student Worker**
 -Lab tech work, and some secretarial responsibilities
 Supervisor: Pamela Burnley
- 09/07-02/10 **Clark County School District Guest Teacher**
 -Filled in for regular contracted teachers in their absence

11/99-07/11

In-N-Out Burger (Level 7 Associate)

-Cook and supervised associates to allow management their breaks
Supervisor: Jason Slane

Professional Affiliations:

Geological Society of America
Geological Society of Nevada
Society of Vertebrate Paleontology

Professional Presentations:

Reynoso, D.E., and Spell, T.L., Evolution of dentition in *Meroëhyrax* from the Late Oligocene of Kenya: Paleontological analysis and $^{40}\text{Ar}/^{39}\text{Ar}$ dating, *Journal of Vertebrate Paleontology*, Program and Abstracts, 2013, p. 33.

Reynoso, D.E., and Spell, T.L., 2013, Evolution of Dentition in *Meroëhyrax* from the Late Oligocene in Kenya: Paleontological Analysis and $^{40}\text{Ar}/^{39}\text{Ar}$ Dating, UNLV Geosymposium.

Pape, D.E., Spell, T.L., and Kappelman, J., 2012, The African Faunal Transition in Kenya Following Geological Contact with Eurasia: $^{40}\text{Ar}/^{39}\text{Ar}$ Dating and Paleontological Study, UNLV Geosymposium.

Pape, D.E. " $^{40}\text{Ar}/^{39}\text{Ar}$ isotopic Dates for the Fossiliferous Willow Tank Formation (Cretaceous) in Valley of Fire State Park, Nevada." AEG Las Vegas Chapter. McCormick & Schmicks' Restaurant, Las Vegas, NV. 10 April 2012. Student Night Lecture.

Pape, D.E., Spell, T., Bonde, J.W., 2011, $^{40}\text{Ar}/^{39}\text{Ar}$ Isotopic Dates For The Fossiliferous Willow Tank Formation (Cretaceous) In Valley Of Fire State Park, Nevada, GSA Abstracts with Programs Vol. 43, No. 5.

Reynoso, D.E., Fish, B., Bruner, J., 2011, Radiometric Age Dating of Ash from the Willow Tank Formation, Valley of Fire State Park, Nevada, UNLV Geosymposium.

Sas, M., Reynoso, D.E., Erickson, B.K., Burnley, P.C., and Thomas, S-M., 2011, In-situ Synchrotron X-ray Diffraction Study of Quartz Deformation Using the D-DIA Apparatus, UNLV Geosymposium.

References:

Terry Spell PhD
702-895-1171
Terry.Spell@unlv.edu

Joshua Bonde PhD
702-895-1774
Joshua.Bonde@unlv.edu

Steve Rowland PhD
702-895-3625
Steve.Rowland@unlv.edu